

Abschlussbericht des Vorhabens 03G0192C „MANGO“

Zuwendungsempfänger:	Leibniz-Institut für Meereswissenschaften (IFM-GEOMAR) Wischhofstr. 1-3 24148 Kiel
Förderkennzeichen:	03G0192C
Projektleiter:	Prof. Dr. Heidrun Kopp (IFM-GEOMAR)
Vorhabenbezeichnung:	SO 192 MANGO Marine Geoscientific Investigation on the Input and Output of the Kermadec Subduction Zone
Laufzeit des Vorhabens:	01.01.2007 bis 30.04.2009
Berichtszeitraum:	01.01.2007 bis 31.10.2009

1. Aufgabenstellung

Im Rahmen des Forschungsprojektes MANGO (Marine Geowissenschaftliche Untersuchungen zum In- und Output der Kermadec Subduktionszone) wurden marin-geophysikalische Untersuchungen mit FS SONNE entlang der Kermadec Subduktionszone, zwischen der Nordinsel Neuseelands und Raoul Island durchgeführt. Während der Fahrt SO 192-1 wurden - neben bathymetrischen und Magnetfeldmessungen – refraktionsseismische und reflexionsseismische Daten mit dem Ziel gewonnen, strukturelle Wechselwirkungen zwischen Unter- und Oberplatte zu untersuchen.

2. Voraussetzungen

Die SONNE-Fahrt SO192-1 wurde im Zeitraum vom 24.03. bis zum 22.04.2007 planmäßig und erfolgreich durchgeführt. Ergänzend zur Expedition des FS SONNE wurden von den neuseeländischen Projektpartnern ein paar Monate später hochauflösende reflexionsseismische Daten deckungsgleich mit dem südlichsten MANGO-Profil akquiriert. Ein regelmäßiger Austausch zwischen den Arbeitsgruppen in Kiel (IFM-GEOMAR) und den neuseeländischen Projektpartnern in Wellington (GNS Science) bildete die Grundlage für den erfolgreichen Abschluss der wissenschaftlichen Arbeiten, die in den unten aufgeführten Publikationen detailliert dargestellt sind. Die parallel ablaufenden Arbeiten der Datenbearbeitung und Dateninterpretationen auf die beiden Standorte Wellington und Kiel setzte einen koordinierten wissenschaftlichen Austausch voraus, der aufgrund der guten Kooperation der Arbeitsgruppen erfolgreich und effektiv umgesetzt werden konnte.

3. Planung und Ablauf

Der vorgelegte Zeitplan wurde eingehalten.

4. Wissenschaftlich-technischer Stand

Der wissenschaftlich-technische Stand ist im Antrag ausführlich dargelegt.

5. Zusammenarbeit mit anderen Stellen

Neben den Projektmitarbeitern des Verbundprojektes MANGO waren weitere Wissenschaftler aus Kiel (Christian-Albrechts-Universität) und Neuseeland (GNS Science und Victoria University of Wellington) an der Ausfahrt beteiligt.

Die Arbeiten des Vorhabens profitierten maßgeblich von einem Austausch mit laufenden sowie abgeschlossenen Projekten basierend auf FS SONNE-Fahrten entlang des gesamten Hikurangi-Kermadec-Tonga-Bogens (SO191, SO194 und SO195), so dass die Ergebnisse nicht nur im Hinblick auf das Untersuchungsgebiet, sondern im Rahmen des plattentektonischen Systems einzuordnen sind.

Die im MANGO Projekt aufgezeichneten magnetischen Daten sind in die neuseeländische

Datenbank sämtlicher aeromagnetischen und von Schiffen gesammelten Daten aufgenommen, welche wiederum auch dem MANGO Projekt zur Verfügung gestellt wurden.

6. Eingehende Darstellung der wissenschaftlichen Ergebnisse

Geophysikalische Untersuchungen der nördlichen Hikurangi Subduktionszone nordöstlich von Neuseeland mit den MANGO-Daten bilden den Forearc und die umgebenden lithosphärischen Strukturen ab. Ein seismisches Geschwindigkeitsfeld (V_p) wurde mit seismischen Weitwinkeldaten bestimmt, und die strukturelle Interpretation wurde unterstützt von seismischer Mehrkanal-Reflexionsstratigraphie sowie Schwere- und Magnetik-Modellierungen. Dabei stellte sich heraus, dass das subduzierende Hikurangi Plateau eine 2-km mächtige Sedimentschicht über einer 2-km mächtigen Schicht aus vulkanischen Klasten, losem Kalkstein und Kies trägt. Die obere Plateaukruste hat eine seismische Geschwindigkeit von 4.9-6.7 km/s über einer unteren Kruste mit $V_p > 7.1$ km/s. Die Schweremodellierung ergibt eine Plateau-Mächtigkeit von ca. 10 km. Das reaktivierte Raukumara-Forearc-Becken ist über 10 km tief auf einer 5-10 km mächtigen australischen Kruste. Der Forearc-Mantel, mit $V_p > 8$ km/s, erscheint unbeeinflusst durch Subduktions-Hydrierungs-Prozesse. Unter dem East Cape Rücken (Forearc-Hoch) liegt bei 3.5 km Tiefe eine stark magnetische Hochgeschwindigkeitszone, die als Teil des an Land befindlichen vulkanischen Matakaoa-Allochthon und/oder als aufgeschobenes Raukumarabecken-Grundgebirge von wahrscheinlich ozeanischen Krustenursprungs interpretiert wurde. Unter der Tiefseegrabensteigung befindet sich Material mit langsamen seismischen Geschwindigkeiten, hoher Wellendämpfung und niedriger Dichte, was als akkretiertes und recyceltes Material interpretiert wurde und andeutet, dass Underplating und Hebung den East Cape Rücken destabilisieren und Hangrutschungen nach zwei Seiten auslöst. Eine Massenbilanz zeigt, dass das akkretierte und recycelte Material 25-100% des gesamten reinkommenden Sediments ausmacht, wovon der Rest durch Erosion von älterem akkretierten Material in die umliegenden Becken erklärt werden kann. Dadurch würde sich ergeben, dass der Abtrag von kontinentalem Material in den Mantel an Subduktionszonen erheblich überschätzt wurde, weil Underplating unter Forearc-Hochs bislang nicht angemessen berücksichtigt wurde. Eine detaillierte Darstellung der Ergebnisse ist im Manuskript von Scherwath et al., 2009, JGR zusammengefasst.

Die seismischen Refraktionsdaten des MANGO Projekts sind zusammen mit seismischen Reflexionsdaten genutzt worden, um Krustenstrukturen zu bestimmen, ein Forearc-Becken mit 12 km mächtigen Sedimenten zu kartieren, und einen Subduktions-Thrust bis in 35 km Tiefe abzubilden. Seismische Reflexionsmegasequenzen innerhalb des Beckens korrelieren mit der Geologie an Land: Megasequenz X, marine passive Kontinentalrandsedimente der späten Kreide und des Paläogen; Megasequenz Y, eine 10000 kubik-km Meeresbodenrutschung während der Initiierung der Subduktion vor 22 Ma; und Megasequenz Z, eine Subduktionszonenrandsequenz aus dem Neogen. Die Moho liegt bei 17 km Tiefe unter dem Zentralbecken und bei 35 km Tiefe am südlichen Rand. Unterhalb des westlichen Beckenrandes liegen vermutlich reflektive Einheiten der Gondwana-Forearc-Sedimente, die während der Kreide über die 7-km mächtige ozeanische Kruste geschoben wurden. Das Raukumara Becken zeigt Abschiebungen am westlichen Rand und ist entlang seines östlichen und südlichen Randes gehoben. Das Raukumara Becken stellt einen rigiden Forearc-Block von >150 km Länge dar, der den weit verbreiteten Störungen und Rotationen des Neogen im Süden entgegensteht. Die Feinstrukturen der allochthonen Megasequenz Y entsprechen eher einer westwärts oder nordwestwärts gerichteten Ablagerung, und widersprechen damit der vorgeschlagenen Südwestwärtsbewegung des entsprechenden Allochthons an Land. Die räumliche Korrelation zwischen den Gesteinshebungen der östlichen und südlichen Beckenränder und dem Schnittpunkt von Moho und der subduzierten Lithosphärenplatte deutet darauf hin, dass krustales Underplating durch die Forearc-Krustenmächtigkeit angepasst wird. Die Tiefseegrabenhang hat viele kleine Dehnungsstörungen und keine kohärenten internen Reflektoren, was auf Abbrechen von verhärteten Gestein hinweist, an Stelle einer Akkretion von >1 km mächtigen Sedimenten der reinkommenden Platte. Fehlende vulkanische Einschlüsse östlich des aktiven Arcs und der

stratigraphische Nachweis der Erweiterung des Forearcs mit der Zeit deuten auf Forearc-Akkretion seit 22 Ma hin. Es wird ein Kreislauf der Forearc-Kinematik vorgeschlagen, in dem das Gestein durch den Subduktionskanal in die Nähe der Krustenbasis transportiert wird, wo Underplating zu Gesteinhebung führt, der Tiefseeegrabenhang zu steil wird und Richtung Graben und Subduktionskanal kollabiert. Dieser Gesteinspartikelkreislauf führt zu stetiger Senkung des Tiefseeegrabenhanges während der Akkretion. Globale Schätzungen von Forearc-Verlust sind systematisch zu hoch, da sie nur von vertikalen Partikelbewegungen ausgehen. Weitere Details sind in der Veröffentlichung Sutherland et al., 2009, Tectonics, aufgeführt.

Seismische Weitwinkeldaten von der zentralen Tonga-Kermadec-Subduktionszone bestimmen die Strukturen der reinkommenden pazifischen Platte und dem überliegenden australischen Arc in der Nähe des aktiven Arc-Vulkans Raoul Island bei 29° Süd. Die subduzierende pazifische Platte ist 5-6 km mächtig mit Geschwindigkeiten von 5.2-6.9 km/s sowie isolierten Zonen verringerter Geschwindigkeiten und ist bedeckt mit bis zu 100 m mächtigen Sedimentpaketen. Der darunter liegende pazifische Mantel hat eine seismische Geschwindigkeit von 7.4 km/s. Diese allgemein niedrigen Geschwindigkeiten in Kruste und Mantel zeigen eine erhebliche Veränderung der rauen und gebrochenen reinkommenden Platte, welche somit wahrscheinlich einen höheren Anteil von freiem Wasser in die Subduktionszone einbringt. Die Arc-Kruste ist ungefähr 12 km mächtig mit Geschwindigkeiten von 4.2-7.0 km/s und einer 40-km weiten Region verringerter Geschwindigkeiten direkt über der Kontaktzone mit der subduzierten Kruste. Die Sedimente auf dem Arc sind durchschnittlich ca. 1 km mächtig und bilden ein bis zu 3 km tiefes und 90 km breites Forearc-Becken. Der Mantelkeil hat eine seismische Geschwindigkeit von 7.5-7.7 km/s, was niedriger als typischer Arc-Mantel ist. Diese niedrigen Geschwindigkeiten werden als Ergebnis von Serpentinisierung des vorderen Arc-Mantels angesehen, verursacht durch die hohe Menge an reinkommendem freiem Wasser. Diese Ergebnisse demonstrieren die Möglichkeit, dass auch in Regionen ohne viel subduzierendes Sediment relativ viel freies Wasser in Subduktionszonen eingeführt werden kann. Eine detaillierte Darstellung der Ergebnisse ist im Manuskript von Scherwath et al., 2009, EPSL zusammengefasst.

Um 34.5° und um 33° Süd befinden sich zwei weitere Datenprofile des MANGO Projekts. Diese beiden Profile der zentralen Kermadec-Subduktionszone decken den australischen Arc zu beiden Seiten des Kermadec-Rückens ab. Trotz der relativen Nähe dieser beiden Profile zeigen die Ergebnisse einige Unterschiede auf. Im Back-Arc-Bereich ist die Kruste am nördlichen Profil deutlich verdünnt, was auf eine durch Rifting gestreckte Kruste schließen lässt. Auch die Wassertiefen sind größer als beim südlichen Profil, wo auch die Back-Arc-Kruste deutlich mächtiger ist. Dieser südlichere Teil weist auch verringerte seismische Geschwindigkeiten im oberen Mantel auf (7.6 km/s statt 7.9 km/s wie im Fore-Arc-Bereich), was eventuell auf thermische Streckung hinweist, die mit einer Veränderung des Arc-Vulkanismus einhergeht. Details zu diesen Ergebnissen wurden in einem erweiterten Abstrakt von Scherwath et al., 2009, beschrieben und werden in einem umfassenderen Manuskript zur Publikation vorbereitet.

7. Fortschreibung des Verwertungsplans

- Es sind keine Erfindungen/Schutzrechtsanmeldungen gemacht oder Schutzrechte erteilt worden.
- Wirtschaftliche Verwertungskonzepte sind derzeit nicht konkret.
- Wissenschaftliche Ergebnisse wurden in Publikationen und auf nationalen und internationalen Tagungen mit Kurzfassungen von Postern und Vorträgen verwertet. Diese sind Ansatzpunkte für zukünftige Forschungsarbeiten und eröffnen bzw. vertiefen unsere internationale wissenschaftliche Zusammenarbeit in der marinen Geophysik (aktive Kontinentalränder). Bisher erschienene und eingereichte Publikationen sind im Anhang gelistet. Publikationen mit peer-review Verfahren finden sich in Kopie im Anhang.

- Wissenschaftliche Anschlussfähigkeit für eine mögliche nächste Phase: Eine weitergehende Untersuchung des Messgebietes, die Lücken schließt und offene Fragen angeht, soll in Form eines SONNE-Fahrtvorschlages im März 2010 beantragt werden.

8. Ergebnisse von dritter Seite mit Relevanz zum laufenden Projekt

- Wir stehen in engem Austausch mit internationalen Gruppen, die sich mit der Systemforschung an aktiven Kontinenträndern befassen und haben laufend Ergebnisse von dritter Seite in unsere Arbeiten integriert (z.B. neue Untersuchungen der Hikurangi-Zone des GNS Neuseeland (S. Henrys, R. Sutherland), die viele Korrelationen mit dem Äußeren Hoch im SINDBAD-Arbeitsgebiet (SO190) aufweisen.

9. Publikationen

Begutachtete Publikationen:

Sutherland, R., Stagpoole, V., Uruski, C., Henrys, S., Field, B., Toulmin, S., Barker, D., Bannister, S., Davey, F., Kennedy, C., Bassett, D., Stern, T., Scherwath, M., Flueh, E., Kopp, H., Reactivation of tectonics, crustal underplating and uplift after 60 Myr of passive subsidence, Raukumara Basin, Hikurangi-Kermadec forearc, New Zealand: implications for global growth and recycling of continents, accepted in *Tectonics* in 2009.

Scherwath, M., Kopp, H., Flueh, E.R., Henrys, S.A., Sutherland, R., Stagpoole, V.M., Barker, D.H.N., Reyners, M.E., Bassett, D.G., Planert, L., Dannowski, A., Forearc deformation and underplating at the northern Hikurangi margin, New Zealand, *J. Geophys. Res.* in review, 2009.

Scherwath, M., Kopp, H., Flueh, E.R., Henrys, S.A., Central Tonga-Kermadec subduction zone structures - evidence for strong upper mantle anomalies from seismic wide-angle data, to be submitted to *Earth and Planetary Science Letters* in Nov. 2009.

Publikationen in Vorbereitung:

Scherwath, M., Kopp, H., Flueh, E.R., Henrys, S.A., Lateral differences in subduction zone structures along the Kermadec arc, to be submitted in Feb. 2010.

Vorträge / Poster:

EGU-Jahrestagung, Wien, 19.-24. April 2009

Scherwath, M., Kopp, H., Flueh, E.R., Henrys, S.A. and Sutherland R., Fore- and Back-Arc Structures along the Hikurangi-Kermadec Subduction zone, POSTER.

DGG-Jahrestagung, Kiel, 23.-26. March 2009

Scherwath, M., Kopp, H., Flueh, E.R., Henrys, S.A., Sutherland R., and Stagpoole, V., Geophysical imaging of the fore-arc deformation at the northern Hikurangi margin, New Zealand, VORTRAG.

SONNE Statusseminar, Bremerhaven, 12.-13. Feb. 2009

Scherwath, M., Kopp, H., Flueh, E.R., Henrys, S.A. und Sutherland R., Struktur der Hikurangi-Kermadec Subduktionszone vor Neuseeland - Ergebnisse von der MANGO Ausfahrt SO-192-1, POSTER.

AGU-Jahrestagung, San Francisco, 15.-19. Dec. 2008:

Scherwath, M., Kopp, H., Flueh, E.R., Henrys, S.A. and Sutherland R., Structure and deformation of the Hikurangi-Kermadec subduction zone - transitions revealed by seismic wide-angle data, POSTER.

Sutherland, R., Stagpoole, V., Uruski, C., Henrys, S., Field, B., Toulmin, S., Barker, D., Bannister, S., Davey, F., Kennedy, C., Bassett, D., Stern, T., Scherwath, M., Flueh, E.R. and Kopp, H., Crustal erosion and accretion processes leading to forearc uplift of Raukumara Basin, Hikurangi-Kermadec subduction zone, northeastern New Zealand, POSTER

Geosciences'08 Joint Annual Conference of the GSNZ, NZGS and NZGEMS, Wellington, 23.- 26. Nov. 2008:

Scherwath, M., Kopp, H., Flueh, E.R., Henrys, S.A. and Sutherland R., Lateral variations of subduction zone structures along the Hikurangi-Kermadec trench between 29°S and 38°S, POSTER

EGU-Jahrestagung, Wien, 13.-18. April. 2008:

Scherwath, M., Kopp, H., Flueh, E.R., Henrys, S.A., Subduction and backarc spreading structures along the Kermadec Trench from wide-angle seismic data, POSTER

AGU-Jahrestagung, San Francisco, 10.-14. Dec. 2007:

Scherwath, M., Kopp, H., Flueh, E.R., Henrys, S.A., Subduction in central Kermadec: Crustal Structures from the incoming plate and the arc-backarc region from wide-angle seismics, POSTER

1 **Forearc deformation and underplating at the northern Hikurangi margin, New Zealand**

2
3 Scherwath, M.*, Kopp, H., Flueh, E.R.,

4 *Leibniz Institute of Marine Sciences, IFM-GEOMAR, Wischhofstr. 1-3, 24148 Kiel, Germany*

5
6 Henrys, S.A., Sutherland, R., Stagpoole, V.M., Barker, D.H.N., Reyners, M.E.,

7 *GNS Science, PO Box 30-368, Lower Hutt, New Zealand*

8
9 Bassett, D.G.,

10 *Victoria University of Wellington, PO Box 600, Wellington, New Zealand*

11
12 Planert, L., Dannowski, A.

13 *Leibniz Institute of Marine Sciences, IFM-GEOMAR, Wischhofstr. 1-3, 24148 Kiel, Germany*

14
15 * corresponding author:

16 Martin Scherwath, Leibniz Institute of Marine Sciences, IFM-GEOMAR, Wischhofstr. 1-3, 24148

17 Kiel, Germany, phone: +49-431-600-2333, fax: +49-431-600-2333, e-mail: mscherwath@ifm-

18 geomar.de

19
20 submitted to *J. Geophys. Res.* on 25 May 2009.

21
22 **Abstract**

23
24 Geophysical investigations of the northern Hikurangi subduction zone northeast of New Zealand,

25 image forearc and surrounding upper lithospheric structures. A seismic velocity (V_p) field is

26 determined from seismic wide-angle data, and our structural interpretation is supported by multi-

27 channel seismic reflection stratigraphy and gravity and magnetic modeling. We found that the

28 subducting Hikurangi Plateau carries about 2 km of sediments above a 2 km mixed layer of

29 volcanics, limestone and chert. The upper plateau crust is characterized by $V_p=4.9-6.7$ km/s

30 overlying the lower crust with $V_p>7.1$ km/s. Gravity modeling yields a plateau thickness around 10

31 km. The reactivated Raukumara forearc basin is >10 km deep, deposited on 5-10 km thick
32 Australian crust. The forearc mantle of $V_p > 8$ km/s appears unaffected by subduction hydration
33 processes. The East Cape Ridge forearc high is underlain by a 3.5 km deep highly magnetic high-
34 velocity zone, interpreted as part of the onshore Matakaoa volcanic allochthon and/or uplifted
35 Raukumara Basin basement of probable oceanic crustal origin. Beneath the trench slope, we
36 interpret low-seismic-velocity, high-attenuation, low-density forearc material as accreted and
37 recycled, suggesting that underplating and uplift destabilizes East Cape Ridge, triggering two-sided
38 mass wastings. A mass balance calculation indicates that the proposed accreted and recycled
39 material represents 25-100% of all incoming sediment, and any remainder could be accounted for
40 through erosion of older accreted material into surrounding basins. We suggest that continental
41 mass flux into the mantle at subduction zones may be significantly overestimated because crustal
42 underplating beneath forearc highs have not properly been accounted for.

43

44 Index Terms: 8170 Subduction zone processes (1031, 3060, 3613, 8413); 3025 Marine seismics
45 (0935, 7294); 7218 Lithosphere (1236); 3040 Plate tectonics (8150, 8155, 8157, 8158); 8015 Local
46 crustal structure.

47 Keywords: subduction accretion and erosion; underplating; subduction mass balance; forearc basin;
48 Hikurangi Margin.

49

50 **1. Introduction**

51

52 Understanding and quantifying how mass transfer processes vary in space and time at subduction
53 zones is essential to address questions surrounding the long-term growth of continents [e.g. *Rudnick*
54 *and Fountain*, 1995]. The balance of sediment accretion, subduction erosion, and addition of
55 mantle-derived material in the magmatic arc determines if a convergent margin is a site of net

56 crustal growth or destruction. The structure of accretionary wedges and erosional margins is now
57 well imaged in classic reflection seismic lines [e.g. *Davey et al.*, 1986; *Ye et al.*, 1997; *Park et al.*,
58 2002; *Kopp and Kukowski*, 2003; *von Huene et al.*, 2004], and many analogue and numerical
59 simulations dedicated to convergent margin processes have focused on both the growth and erosion
60 of convergent margins [e.g. *Davis et al.*, 1983; *Gutscher et al.*, 1998; *Upton et al.*, 2003; *Litchfield*
61 *et al.*, 2007]. Based on such data and models, the global fluxes of subducted sediment and
62 continental material have been estimated [*von Huene and Scholl*, 1991; *Clift and Vannucchi*, 2004],
63 but large uncertainties remain. In this paper, we present new geophysical data from the northern
64 Hikurangi margin, New Zealand, and challenge some of the assumptions that underpin estimates of
65 global crustal fluxes in subduction zones.

66

67 The processes of forearc crustal accretion or erosion are causally related to the behavior of the
68 subduction thrust and faults within both the footwall and hanging wall, so our results have
69 significance for understanding seismic hazard. Subduction zones typically show significant along-
70 strike variability and it is clear that deep forearc basins point to significant regional tectonic controls
71 on processes occurring at the plate interface, with implications for the nucleation and propagation of
72 large-magnitude subduction earthquakes [*Song and Simons*, 2003; *Wells et al.*, 2003]. For most
73 subduction zones, the details of the spatial and temporal relationships between subduction
74 accretion, erosion processes, forearc basin subsidence, and regional uplift patterns remain largely
75 unresolved. However, it has been suggested that there is a correlation between the locations of large
76 earthquakes, forearc basins, and gravity lows; and permanent interseismic subsidence is inferred to
77 have been caused by plate coupling and long-term subduction erosion in those regions [*Song and*
78 *Simons*, 2003; *Wells et al.*, 2003].

79

80 The northern Hikurangi margin and Raukumara Peninsula of New Zealand (Figure 1) provide an

81 ideal setting to examine these along-strike processes, because a broad range of complimentary data
82 types are available and marked differences in morphology and geological structure along and across
83 the margin point to significant changes in subduction mechanics. The Hikurangi Plateau, a
84 Cretaceous Large Igneous Province of the Pacific Plate [Davy and Wood, 1994; Mortimer and
85 Parkinson, 1996], is subducting westward at c. 60 mm/yr relative to the forearc, causing active
86 uplift of Raukumara Peninsula [Litchfield et al., 2007; Wilson et al., 2007], but farther to the east
87 the outer trench slope is steep and subject to basal tectonic erosion [Collot et al. 1996; Davey et al.,
88 1997; Barker et al., 2009]. Along-strike towards the north, Raukumara Peninsula is replaced by a
89 deep (>12 km) sedimentary basin coincident with a prominent -140 mgal gravity low, and is
90 bounded to the east by a protuberant outer forearc high and a steep frontal margin wedge.

91

92 Recently, Sutherland et al. [2009] presented an overview of new seismic reflection and refraction
93 data where the large-scale structure and stratigraphy of Raukumara Basin were mapped out,
94 suggesting a new kinematic model of the forearc that involved frontal subduction erosion and basal
95 accretion of the eroded material into the lower crust of the hanging wall. In this paper, we present a
96 detailed analysis of seismic wide-angle reflection and refraction data collected along a dip profile
97 through the basin and across the subduction zone to the footwall. Our seismic velocity image is
98 combined with stratigraphy from multi-channel seismic reflection profiles and ship-born gravity
99 and magnetic data to yield structural constraints that allow us to more precisely identify and
100 quantify subduction processes within the upper 20 km, which in this case of relatively thin hanging-
101 wall crust includes the Moho, crust, and the accreted forearc material.

102

103 **2. Tectonic Setting**

104

105 The region immediately northeast of the North Island of New Zealand (Figure 1), marks a transition

106 from the Tonga-Kermadec to the Hikurangi subduction zone. The region includes a north-to-south
107 transition on the downgoing Pacific plate from typical oceanic crust to anomalously-thick oceanic
108 crust of the Hikurangi Plateau (Rapuhia scarp, Figure 1) [Davy and Collot, 2000], and on the over-
109 riding plate from thin crust of possible oceanic type to continental crust of 30-40 km thickness
110 [Reyners *et al.*, 1999; Reyners *et al.*, 2006; Sutherland *et al.*, 2009]. The Cretaceous Hikurangi
111 Plateau [Mortimer and Parkinson, 1996] has a crustal thickness of about 10-15 km to the east of
112 Raukumara Peninsula [Davy and Wood, 1994]. The anomalous nature of this subducting plateau is
113 implicated in models for uplift of the East Coast of the North Island and exposure of the forearc
114 [Litchfield *et al.*, 2007]. Geodetic measurements and active faulting indicate that the eastern part of
115 the peninsula is currently extending normal to the plate margin [Thornley, 1996] and experienced
116 up to 6 km of extension since the Pliocene [Nicol *et al.*, 2007].

117

118 In the region of the northern Hikurangi margin, the Pacific and Australian plates are converging
119 obliquely at about 45 mm/yr [DeMets *et al.* 1994] (Figure 1), but back-arc spreading in the Havre
120 Trough and central North Island result in almost orthogonal convergence across the subduction
121 thrust at c. 60 mm/yr in our study region [Wallace *et al.* 2004]. The general shape of the subducted
122 plate has been revealed by compilations of seismicity from the IRIS Data Management Center, the
123 New Zealand national seismograph network, and deployment of a dense network of portable
124 seismographs [Reyners *et al.*, 1999]. The continental crust is ~20 km thick beneath the northern
125 Raukumara Peninsula and thickens to greater than 35 km to the south, as inferred from crustal
126 seismic P-wave velocity (V_p) estimates of 5.5-6.5 km/s [Reyners *et al.*, 1999; Reyners *et al.*, 2006;
127 Sutherland *et al.*, 2009]. Earthquake hypocenters cluster within the upper part of the subducting
128 plate at 15 km depth, and in the crust between the east coast of Raukumara Peninsula and the
129 subduction front. The uppermost c. 10 km of the mantle of the subducted slab consistently has V_p
130 >8.5 km/s, and reduces to more normal mantle velocities of c. $V_p=8.2$ km/s beneath [Reyners *et al.*,

131 1999]. Earthquake focal mechanisms indicate down-dip tensional strain within the subducting plate,
132 and NNW-SSE extensional strain within the shallow part of the upper plate [*Reyners and McGinty,*
133 1999], consistent with geological and geodetic observations [*Árnadóttir et al., 1999*].

134

135 Onshore, Raukumara Peninsula can be divided into distinct geological units [*Mazengarb and*
136 *Harris, 1994; Field et al., 1997; Mazengarb and Speden, 2000*] (Figure 1) that can also be
137 recognized offshore as seismic-reflection megasequences [*Sutherland et al., 2009*]: (1) a western
138 unit of Early Cretaceous greywacke basement in the Raukumara Range; (2) Late Cretaceous and
139 Paleogene marine passive margin sediments (megasequence X); (3) the East Coast Allochthon
140 (megasequence Y), a belt of Late Cretaceous and Early Tertiary rocks that were thrust towards the
141 southwest over units 1 and 2 during the earliest Miocene. The East Coast allochthon, together with
142 the enigmatic Matakaoa volcanic rocks, are considered concomitant with the emplacement of the
143 Northland ophiolite terrane of northern New Zealand [*Whattam et al., 2004*] and emplacement at
144 about 25-22 Ma was immediately followed by the onset of arc volcanism in Northland [*Rait et al.,*
145 1991; *Herzer, 1995*]; (4) an eastern unit consisting of Neogene marine sedimentary rocks
146 (megasequence Z) that overlie the allochthon in the east and is faulted against it in the west. Along
147 the Raukumara Range broad Quaternary antiformal uplift up to 4 mm/yr [*Litchfield et al., 2007;*
148 *Wilson et al., 2007*] (Figure 1) has been interpreted as being due to sediment subduction and
149 underplating at the base of the crust of the Australian plate [*Walcott, 1987; Reyners et al., 1999*].

150

151 It is clear from the geometry of the toe of the frontal wedge today that the subducting margin is
152 undergoing tectonic erosion and subduction of material from the front of the wedge. Multibeam
153 bathymetry, side-scan sonar and seismic reflection studies [*Collot et al., 1996*] indicate that the toe
154 of the margin is indented by 10-25 km to the east of Raukumara Peninsula, relative to regions to the
155 northeast and southwest. This is inferred to be the result of repeated impacts of the large seamounts

156 that are abundant on the northern Hikurangi Plateau. The two most recent impacts have left the
157 major Ruatoria and Poverty indentations [Lewis *et al.*, 1998; Collot *et al.*, 2001] in the margin east
158 of Raukumara Peninsula (Figure 1). Also, immediately to the north of Raukumara Peninsula
159 additional northward traveling debris avalanches have been mapped (Matakaoa Submarine
160 Instability Complex, off Matakaoa Scarp, as part of the Raukumara Plain in Figure 1) where ~3200
161 km³ of sediment has accumulated in the last 5 Ma [Lamarche *et al.*, 2008]. These mass-transport
162 deposits are likely to be the result of slope oversteepening associated with peninsula uplift and
163 Raukumara Basin subsidence.

164

165 **3. Seismic Wide-angle Data and Modeling**

166

167 In March 2007, seismic wide-angle data were acquired onboard R/V Sonne as part of the MANGO
168 (Marine Geoscientific Investigations on the Input and Output of the Kermadec Subduction Zone)
169 project [Flueh and Kopp, 2007]. A total of 29 Ocean Bottom Seismometers and Hydrophones
170 (hereinafter referred to as OBS/H) were deployed from about 40 km east of the subduction front on
171 the Hikurangi Plateau, across the deformation front and East Cape Ridge, and covering the eastern
172 part of the Raukumara forearc basin (MANGO-1 in Figure 1). Airgun shots from a 64 liter G-gun
173 cluster, spaced nominally at 150 m, covered the line of OBS/H stations and extended across the
174 entire Raukumara Basin and ending on the Kermadec Ridge near Whakatane volcano. Adverse
175 weather conditions led to the occasional interruption of the shooting when the ship had to leave
176 track to sail into the wind. The data quality generally is moderate, with signals recorded at offsets
177 up to 30-50 km, and to 70 km in Raukumara Basin.

178

179 The seismic wide-angle data were used to generate a two-dimensional (2D) P-wave velocity model
180 of the crust and uppermost mantle using the ray-tracing and travelttime inversion method of Zelt and

181 *Smith* [1992]. This method calculates arrival times through forward ray-tracing in a model that
182 consists of nodes for layer depth and velocities at the top and bottom of each layer. The calculated
183 arrival times are compared to the observed ones and the misfit is reduced either by automatic least-
184 square inversion or by manually adjusting the model. A resolution matrix is calculated to assess the
185 model uncertainty [*Zelt and Smith*, 1992].

186

187 Bathymetry data and structure and interval velocities from the coincident seismic reflection profile
188 RAU07-05 (see below) provide prior information and were used to determine the shallow structure
189 for a suitable starting model. The final model was determined from the top down, adding seismic
190 phases with longer offsets from deeper structures. This strategy prevents smearing effects of
191 possibly inaccurate shallow structures into deeper parts of the model. As our preferred final model
192 should only consist of structures derived from the data plus the prior information, the final model is
193 a "minimum-parameter/prior structure" model as defined by *Zelt* [1999]. Our modeling involved
194 both automatic inversion and manual model adjustments at complex model regions or limited data
195 coverage where inversion proved difficult.

196

197 Examples of the wide-angle data are shown in Figures 2a to f. Arrival times for several seismic
198 phases were picked: (1) refracted arrivals from the sediments (P_{sed}) (e.g. Figure 2a), upper and
199 lower crust (P_g) (e.g. Figure 2b), and upper-most Australian mantle (P_n) (Figures 2e and f); and (2)
200 later arrivals corresponding to reflected waves from intermittent boundaries such as from the
201 presumed decollement (P_{dP}) (Figure 2c), mid-sedimentary reflection from Raukumara Basin
202 (P_{sedP}) (Figure 2f), and finally deeper reflections from Australian crust (P_{cP}) and Moho (P_{mP})
203 (Figure 2f). We were unable to detect deeper phases from the incoming Pacific plate, and neither
204 could we pick reflections off the downgoing slab beneath Raukumara Basin as these arrivals were
205 masked by the water column multiple (Figure 2f). In total 4400 arrivals were picked and modeled.

206

207 Figure 3 shows our preferred final model which consists of a water layer, up to five sedimentary
208 layers to accommodate the structures within Raukumara Basin, one intermediate velocity layer
209 above the Hikurangi Plateau crust and below the sediments, three crustal layers for the Hikurangi
210 Plateau of which the uppermost layer only marks a change in the velocity gradient of the shallow
211 crust, and finally two crustal and one mantle layer for the overriding Australian arc. Note that the
212 Moho shown below the Hikurangi Plateau is based on the gravity modeling (below) and is not
213 resolved by the seismic data. Details of the model features are discussed below.

214

215 The data examples in Figures 2a-f also show predicted arrival times from our preferred final model.
216 The central panels of Figures 2a-f show all predicted P-waves plotted on top of the recorded data,
217 whereas the bottom panel shows rays that correspond only to the picked arrivals to indicate model
218 coverage. The average RMS misfit of the predicted arrivals is 70 ms which, taking into account the
219 relatively large data uncertainty from the reduced data quality, corresponds to a normalized chi-
220 square value of just below 1.

221

222 Model resolution and coverage are shown in Figure 4, using only the seismic wide-angle reflection
223 and refraction data without taking into account available multi-channel seismic (MCS) data (see
224 below). Resolution values between 0.0 (small symbols) and 1.0 (large symbols) indicate how well
225 each model parameter is resolved with respect to the relative number of rays. *Zelt and Smith* [1992]
226 found that a node with a resolution value greater 0.5 is considered well resolved. Evaluating model
227 resolution together with the ray paths, Figure 4 shows that the shallow structures of the Hikurangi
228 Plateau are well resolved. In the central part, below East Cape Ridge, only few rays could be traced
229 and used for determining the deeper structure, yet the shallow structures again appear well resolved.
230 Raukumara Basin in the west is well resolved in its central part down to the arc mantle at 19 km

231 depth, although its western part is increasingly less resolved by the wide-angle data. The structures
232 of the western Raukumara Basin are entirely based on the MCS data as shown below, and no
233 modeling emphasis has been placed to this region outside the OBS/H station distribution. The MCS
234 data are also the basis for modeling the shallow sedimentary structures and therefore the resolution
235 of the high number of model nodes is not shown here. Similarly, the subducting slab is manifest as a
236 clear reflector in the MCS data and was used to determine the slab dip below Raukumara Basin but
237 is not obviously apparent in the wide-angle data.

238

239 Considering model coverage, node resolution, data uncertainties and manually adjusting model
240 parameters to test alternative structures, the following model uncertainties are estimated (larger
241 estimates in brackets are for deeper or less resolved structures): Depth to sediments: +/- 80 (300) m;
242 depth to crust: +/- 100 (500) m, depth to mantle: +/- 500 (1000) m; velocity of sediments: +/- 100
243 (300) m/s; velocity of crust 80 (400) m/s; velocity of mantle: +/- 150 m/s.

244

245 **4. Coincident Seismic Reflection Profile**

246

247 The wide-angle reflection and refraction line MANGO-1 was co-located with the MCS line
248 RAU07-05, which was recorded also in 2007 a few months after the MANGO-1 deployment
249 [*Sutherland et al.*, 2009]. Data for RAU07-05 were acquired using a 86.5 l (5280 cu in) source and
250 7.3 km streamer, with 50 m shotpoint spacing and 15.3 s record length. Details of data processing
251 applied are given elsewhere [*Fugro Seismic Imaging*, 2007].

252

253 Line RAU07-05 (Figure 5) provides a clear image of Raukumara Basin, the underlying Australian
254 crust, and a clear reflection band off the subducting slab down to 15 s two-way travel time (TWT).

255 Figure 5 shows the wide-angle model drawn as reflections in TWT on top.

256

257 Following the interpretation of *Sutherland et al.* [2009], the reflection strata can be divided into
258 three sedimentary megasequences, X, Y and Z (Figure 5). Starting from the top, megasequence Z
259 comprises recent slumps and slides including the Matakaoa Submarine Instability Complex across
260 the Raukumara Plain [*Lamarche et al.*, 2008] as well as the downslope collapse structures east of
261 East Cape Ridge. The bottom of megasequence Z is marked in our model as the bottom of the
262 second sedimentary layer, reaching down to 4.5 km depth (2.5 km below seafloor) around model-
263 km 185, the depocenter of the more recent arc volcanic input. The base consists of mostly
264 continuous reflectors.

265

266 Megasequence Y is a thin unit (0-1.6 km thick) extending between East Cape Ridge and the center
267 of Raukumara Basin where it pinches out. Due to its small size, however, we did not include a small
268 additional layer in our model (Figure 3) but combined this unit with our sedimentary layer 3.
269 Megasequence Y is interpreted to represent a single large Cenozoic allochthonous slope failure
270 originating from East Cape Ridge.

271

272 The underlying megasequence X is up to 8 km thick in the deepest part of Raukumara Basin. The
273 sedimentary strata is interpreted to be Cretaceous in age and appears to be remarkably little
274 deformed considering its age and the tectonic history of the region [*Sutherland et al.*, 2009].

275

276 Below the sedimentary megasequences there appear clear reflections from the top of the Australian
277 crust and the Moho, indicating the thinning of the crust around model-km 110. The strong sub-
278 Moho reflection at 15 s TWT around model-km 130 is interpreted and modeled as the top of the
279 downgoing slab.

280

281 In contrast to the relatively deep reflectivity within and beneath the Raukumara forearc basin, the
282 profile reveals a relatively unreflective outer forearc high (East Cape Ridge), indicating intensive
283 forearc deformation potentially destroying coherent reflectivity here. The interpreted decollement
284 reflection that appears on the seismic wide-angle data (PdP on Figure 2c) would be predicted on the
285 MCS data around model-km 25 at about 5.5 s TWT but does not appear as strong reflection here.
286 Furthermore, the incoming Hikurangi Plateau appears also relatively unreflective, probably due to
287 its rough, scattering crust or its weakly reflective internal composition. Further discussion is given
288 below.

289

290 **5. Gravity and Magnetic Data and Modeling**

291

292 Potential field data from ship measurements along our profile were used to verify and improve the
293 seismically derived structural model as well as to constrain seismically unresolved sections of the
294 model. In particular, gravity data helped to estimate the thickness of the incoming Hikurangi
295 Plateau, where no deep mantle phases could be identified in the seismic data. The magnetic
296 anomalies yielded information on the occurrence of volcanic rock type and origin.

297

298 For an overview, Figure 6 shows a 3D view of gravity and magnetic anomalies draped over the
299 bathymetry. The 3D gravity anomalies stem from satellite data [*Sandwell and Smith, 1997*]. The
300 magnetic grid is a compilation of aeromagnetic data [*Malahoff et al., 1982*] and all available ship
301 data from the region, including newly collected data from the seismic cruises in 2007, leveled to a
302 common surface.

303

304 The most notable feature in the gravity data is the -140 mgal gravity low at the southern part of
305 Raukumara Basin. This gravity low is associated with both the deep basin as well as the southward

306 thickening of the Australian Plate during its transition from island arc to continental character.

307

308 The magnetic field exhibits distinct positive (>150 nT) anomalies extending from the Matakaoa
309 volcanic anomaly onshore northeastward along East Cape Ridge (Figure 6). This corroborates the
310 suggestion by *Davey et al.* [1997] that the magnetic anomalies along East Cape Ridge are
311 associated with the same allochthonous material as observed onshore.

312

313 Gravity and magnetic data were also acquired along with the seismic reflection data of line RAU07-
314 05. The potential field data were modeled in a 2.5D sense using our previously derived velocity
315 structures to provide layer depths and to estimate densities and magnetizations. The result of our
316 forward model is shown in Figure 7.

317

318 Note that the lateral extent in and out of the model plane of the deeper parts of Raukumara Basin
319 were limited to 50 km on either side in accordance with the seismic reflection data [*Sutherland et*
320 *al.*, 2009]. Furthermore, below the base of the reference lithosphere (at 70 km depth) a density
321 anomaly was inserted to model the subducting plate lithosphere sinking into the asthenosphere.

322

323 The density model produces anomalies that are in good agreement with the observed data. The
324 densities used here are also consistent with previous models [*Gillies*, 1984; *Davey et al.*, 1997;
325 *Davy et al.*, 2008], though compared with *Sutherland et al.* [2009] they are about 5-10% denser in
326 the lower parts (except the mantle) but up to 5% lighter in the shallower parts of the model. The
327 latter discrepancy can readily be explained by the simplicity of *Sutherland et al.*'s [2009] density
328 model which only aimed at indicating a consistency between the general structural interpretation
329 and the observed densities without taking into account the accuracy of our new seismically derived
330 crustal model.

331

332 The magnetic anomalies proved more difficult to be modeled in 2D and we expect much of the
333 existing misfit to be due to 3D effects. Our main aim here was to determine the cause of the two
334 major positive anomalies; one at the western edge of the model, coincident with the Whakatane
335 volcano, and the second being the East Cape Ridge anomaly at model-km 65. Both can be modeled
336 by highly magnetized uppermost crust. The highest magnetic susceptibilities used were 0.085 to 0.1
337 and convert to magnetizations of 3.3 to 3.9 A/m. These values are larger than the largest
338 magnetizations of up to 3.3 A/m used by *Davey et al.* [1997], but in the range of magnetizations
339 (1.0 to 4.5 A/m) used by *Gillies* [1984], who had a more localized distribution of magnetic sources.
340 By placing smaller magnetizations into the remaining layers (magnetic susceptibility 0.002-0.05,
341 magnetization 0.1-2.0), magnetic anomalies of similar magnitudes and wavelength as the observed
342 anomalies are produced, but they do not exactly match the observed locations. A more localized
343 distribution of magnetic sources [*Gillies*, 1984; *Davey et al.*, 1997] and, moreover, 3D modeling
344 may be attempted but would go beyond the purpose of our interpretation as discussed below.

345

346 A second magnetic model was produced using 2D Euler deconvolution [*Durrheim and Cooper*,
347 1998; *Cooper*, 2002; *Cooper*, 2004]. Figure 8 shows the most likely distribution of magnetic
348 sources along the model. The result matches the East Cape Ridge anomaly relatively well but fails
349 to focus magnetic sources at the western model edge (Whakatane volcano) where the deconvolution
350 window cannot capture the full wavelength of the associated magnetic anomaly. Another interesting
351 area of magnetic sources occurs around model-km 100, at about 3.5 km depth. The source coincides
352 with the thinned frontal edge of part of the offshore allochthon (Megasequence Y) as interpreted by
353 *Sutherland et al.* [2009]. The implications are discussed below.

354

355 **6. Discussion**

356

357 **6.1 Structure and Sediment Cover of the Subducting Hikurangi Plateau**

358

359 When plateaus enter subduction zones, their role in the subduction processes is manifold. Plateaus
360 such as the Hikurangi Plateau carry a significant amount of water into the subduction zone,
361 potentially leading to voluminous arc volcanism [*de Ronde et al.*, 2007]. Furthermore, plateau crust
362 is usually more buoyant than normal oceanic crust and may therefore cause either subduction
363 erosion [*von Huene and Scholl*, 1991] or enhanced uplift of the forearc [*Collot and Davy*, 1998;
364 *Kopp et al.*, 2006]. If its thickness is too buoyant for subduction it may halt volcanism [*McGeary et*
365 *al.*, 1985] or actually stall subduction entirely [*Cloos*, 1993; *Mann and Taira*, 2004; *Davy et al.*,
366 2008]. Our results place some new constraints on the geometry of the subducting Hikurangi
367 Plateau.

368

369 The northern Hikurangi Plateau is modeled as a 10 (+/-1) km thick crust ($V_p > 4.9$ km/s) that is
370 overlain by up to 4 km of seismically slow (< 4.0 km/s) material (Figure 3). We interpret the
371 topmost 2.2 (+/-0.1) km of sediments with seismic velocities increasing from 1.6 to 3.5 km/s to
372 consist of predominantly coarse debris sourced by the collapsing frontal slope (e.g. Ruatoria Slide,
373 Figure 1). Below that lies a 2 (+/-0.2) km thick layer with seismic velocities of 3.8-4.0 km/s which,
374 following the recent description of the Hikurangi Plateau by *Davy et al.* [2008], is a mixed layer of
375 volcanoclastics, limestone, and chert (Figures 5 and 9). This interpretation is based on the seismic
376 velocities (too slow for basaltic or gabbroic crust) which are near the faster limit of volcanoclastics,
377 dredged from adjacent to the survey area [*Hoernle et al.*, 2004], and limestone and chert as sampled
378 by drill cores from similar oceanic plateaus in the southwest Pacific [*Davy et al.*, 2008].

379

380 Where the plateau enters the forearc, strong reflections are observed on OBS 12 around 4.5 s

381 (Figure 2c), and these also appear on the two surrounding OBS. Strong reflections above the
382 downgoing plate typically stem from the decollement with elevated pore fluid pressures in the
383 subduction channel below [von Huene *et al.*, 2004]. Our model predicts a suitable reflection off a
384 simple continuation of the mixed layer of volcanoclastics, limestone, and chert that produced clear
385 first arrival refractions on the seismic record from the Hikurangi Plateau (Figures 2a and b).
386 However, we cannot exclude the possibility that some of the overlying sediments are carried within
387 this subduction channel. In any case, if our interpretation for these strong reflections is correct, we
388 can infer a subduction thrust at about 20-40 km from the deformation front occurs at about 7-8 km
389 depth, below a 5-7 km thick hanging wall (Figure 9).

390

391 The underlying plateau crust is divided into two layers. The upper 4-5 km thick layer displays
392 seismic velocities of 4.9-6.7 km/s, around the typical average of 5.5 km/s for flood basalts normal
393 for the upper plateau crust [Coffin and Eldholm, 1994]. The lower crust could only be detected by a
394 few refractions of a velocity >7.1 km/s, again typical for lower plateau crust that presumably
395 consists of gabbroic to ultramafic material [Coffin and Eldholm, 1994]. As no refractions could be
396 detected from the bottom of the plateau, its thickness could only be estimated using gravity data. In
397 our model, the depth of the Moho increases from 16 km in the east to 22 km below East Cape
398 Ridge, yielding a plateau thickness of roughly 10 km. This value appears to be a relatively thin
399 compared internationally to other Large Igneous Provinces (LIPs) with typical thicknesses of 20-40
400 km [Coffin and Eldholm, 1994]. Even compared to previous Hikurangi Plateau estimates of up 23
401 km thickness for the southern area [Davy *et al.*, 2008] it seems relatively thin, but is in good
402 agreement with other estimates from the central and northern part of the plateau [Henry *et al.*,
403 2006; Davy and Wood, 1994], and is sufficiently thin to subduct [Cloos, 1993].

404

405 Subduction of the Hikurangi Plateau occurs at a relatively shallow dip angle of a few degrees up to

406 East Cape Ridge and then appears to steepen downdip. Reflections off the slab as recorded on MCS
407 line RAU07-05 (Figure 5) suggest that the slab dips at around 20 degrees below Raukumara Basin,
408 about 120 km from the deformation front, and deep seismicity indicates an angle of almost 50
409 degrees further downdip toward the arc.

410

411 No direct evidence has been found for the down-dip extent of the Hikurangi Plateau, below which
412 the Pacific Plate subducts as normal oceanic crust. Our gravity model (Figure 7) requires less
413 negative density anomalies below the well-imaged Raukumara Basin; as a result we reduced the
414 thickness of the downgoing Pacific plate in this region. This complies with previous notions from
415 tomographic results from Raukumara Peninsula [Reyners *et al.*, 2006] or geometrical considerations
416 regarding the possible common history of the Hikurangi and the Manihiki and Ontong-Java
417 Plateaus [Davy *et al.*, 2008].

418

419 **6.2 Arc and Forearc Raukumara Basin**

420

421 The basin stratigraphy of line RAU07-05 has been described briefly above and in length by
422 *Sutherland et al.* [2009] and is shown in Figures 5 and 9. We generally note a good correlation
423 between what has been interpreted as Cretaceous sedimentary units and relatively fast (3.7-4.9
424 km/s) seismic velocities at depths between 6.0 km and 12.5 km. With an assigned density optimum
425 of 2.6 g/cm³ these basal sediments are considered to be highly consolidated and weakly
426 metamorphosed. Whakatane volcano of the active Kermadec arc is imaged at model 220 km
427 (Figures 1, 3, 5, 7, 8, and 9), at the western margin of Raukumara Basin.

428

429 With a sedimentary infill of more than 10 km, Raukumara Basin is one of the deepest known
430 forearc basins at an active margin. A comparable forearc basin is found at the Middle American

431 subduction zone, Sandino Basin offshore Nicaragua with an infill of up to 16 km [*Ranero et al.*,
432 2000; *McIntosh et al.*, 2007]. For Sandino Basin it has been suggested that it was created when a
433 new subduction zone developed seaward of the previous (Jurassic/Cretaceous) subduction zone
434 [*Walther et al.*, 2000]. This is strikingly similar to the interpretation in our study area [*Sutherland et*
435 *al.*, 2009], and perhaps the only mechanism that allows for the development of such super-deep
436 forearc basins.

437

438 A correlation exists between the thickest and deepest part of Raukumara Basin and the thinnest part
439 of the underlying crust. Below Raukumara Basin, the crustal thickness varies between up to 10 km
440 in the west and as thin as 5 km toward the central and eastern part of the basin (Figure 3). Isostasy
441 would have caused a natural depression at the thinnest part of the crust where sedimentation
442 commenced at the Gondwana margin. With the eastern margin of the basin tilted upwards at East
443 Cape Ridge, it is unclear what the eastern basin geometry was like before the onset of Neogene
444 distortion.

445

446 We speculate that the initiation of subduction in this location at 25-22 Ma was near the thinnest part
447 of the crust, based upon the correlation between the thickness of the upper plate and the location of
448 the plate edge near East Cape Ridge (Figures 3 and 9).

449

450 Below the forearc crust, we measured an upper mantle V_p of 8.05 ± 0.15 km which is typical for
451 normal, unaltered mantle without serpentinization induced by hydration [*Carlson and Miller,*
452 2003]. *Bostock et al.* [2002] speculate that all mantle wedges would be serpentinized, and this
453 would inhibit subduction zone thrust earthquakes to rupture below the Moho interception [*Tichelaar*
454 *and Ruff*, 1993]. Our measurements, however, imply a non-serpentinized mantle wedge at the Moho
455 interception, and so the northern Hikurangi margin may have a different mega-thrust earthquake

456 potential than otherwise assumed.

457

458 **6.3 East Cape Ridge Volcanics**

459

460 We detected relatively high seismic velocities (about 5.8 km/s) at 3.5 km depth below the seafloor
461 at East Cape Ridge (Figure 3). We also model a source region for the observed magnetic anomaly
462 that approximately coincides with this seismic anomaly (Figures 7 and 8). We interpret the high-
463 velocity magnetic material to be volcanic and consider possibilities that the source material is: a
464 seamount that was subducted and accreted; or part of allochthonous unit Y within the basin
465 [*Sutherland et al.* 2009] and a correlative to the Matakaoa Volcanic unit mapped onshore
466 [*Mazengarb and Speden*, 2000]; or that it represents basement to Raukumara Basin that has been
467 uplifted.

468

469 Forearc accretion of seamounts from the Hikurangi Plateau may be likely in this region [*Davey et*
470 *al.*, 1997; *Henrys et al.*, 2006; *Pecher et al.*, 2005], because the subducting Hikurangi Plateau has
471 numerous seamounts visible in the bathymetry (Figure 1) [*Wood and Davy*, 1994]. It has been
472 speculated that in the vicinity of our study area subducted seamounts are required to explain
473 localized uplift, erosion and basin evolution [*Collot et al.*, 2001; *Lewis et al.*, 2004]. Consideration
474 of the model location and dimension of the specific anomaly, which lies 10 km above the
475 subduction interface at East Cape Ridge, requires a detached and uplifted seamount. If a seamount
476 of 1-2 km elevation, which is the average for the Hikurangi Plateau, was subducted and detached
477 from the downgoing plate, then it has experienced an uplift of 8-9 km from the subduction interface
478 and has attained that height against its negative buoyancy. The large rock uplift value suggests that
479 it was accreted from the downgoing plate and has since undergone a long history of further
480 subduction and basal accretion. Although this scenario would explain the lack of any detectable scar

481 at the trench, we consider it unlikely that such a scenario is mechanically feasible. However, we
482 have not made any mechanical model to simulate this process and retain it as a hypothesis.

483

484 There are several magnetic anomalies associated with East Cape Ridge that have similar amplitude
485 and wavelength and are aligned parallel to the ridge (Figure 6). The most southwestern anomaly
486 corresponds to where the Matakaoa Volcanics unit is mapped onshore as part of an allochthonous
487 unit emplaced at 25-22 Ma [*Mazengarb and Speden, 2000*]. Based upon our Euler deconvolution
488 analysis (Figure 8), we note a correlation between seismic-reflection megasequence Y (Figure 9),
489 which is a correlative of the onshore allochthon [*Sutherland et al., 2009*], and model sources of
490 magnetization (Figure 8). As this unit is supposed to represent a slump from the southeast, now the
491 region of East Cape Ridge, the magnetization indicates that the highly magnetic high velocity
492 anomaly below East Cape Ridge could either be a correlative of the unit, or could be the slump
493 source (large dashed arrow in Figure 9). Therefore, we conclude that we have very likely detected
494 an offshore part of the Matakaoa volcanics within allochthonous megasequence Y, and our results
495 support the conclusion by *Davey et al. [1997]* that the onshore allochthon volcanic geology extends
496 further northeast along East Cape Ridge.

497

498 The seismic velocity of the anomaly beneath East Cape Ridge (c. 5.8 km/s) is relatively similar to
499 that of the adjacent upper Australian crust beneath Raukumara Basin (5.4-5.8 km/s) and faster than
500 that of the upper Hikurangi Plateau crust (4.9 km/s). Thus, the origin of the seismic and magnetic
501 anomaly beneath East Cape Ridge could be from uplifted basement of Raukumara Basin, which in
502 turn may be the source of allochthonous material that was emplaced into the basin during
503 subduction initiation as the Matakaoa Volcanics and seismic-reflection megasequence Y. *Cassidy*
504 [*1993*] reports magnetizations of up to 5.5 A/m from similar allochthonous units in Northland that
505 were also emplaced at 25-22 Ma, so our estimate of 3.3-3.9 A/m seems reasonable and may imply a

506 common origin of the material.

507

508 **6.4 Tectonic Erosion and Accretion Between East Cape Ridge and the Trench**

509

510 We interpret the region from East Cape Ridge to the Hikurangi Trench as the dynamic frontal 100
511 km of the forearc that is actively deforming. Our structural model (Figures 3 and 5) has a frontal
512 zone of relatively slow seismic velocities and high attenuation to the east of the high-velocity
513 anomaly that lies beneath East Cape Ridge (above). Figure 9 shows our structural interpretation of
514 the dip-profile from trench to forearc basin.

515

516 The slope of the seafloor near the deformation front is relatively steep at ~11 degrees over a
517 distance of 13 km in water depths of 3600 to 1100 m. High-resolution bathymetry and seismic data
518 reveal a highly-faulted slope of acoustically-reflective indurated material, apparently indicative of
519 collapse and subduction erosion [*Collot and Davy, 1998*]. Oversteepening of trench slopes by
520 subduction erosion can lead to dramatic, possibly tsunamogenic avalanches, highlighting the
521 importance of these observations [*von Huene et al., 1989*].

522

523 To classify margin types, however, wavelengths above 50 km need to be examined, and the frontal
524 forearc slope of our profile is around 3 degrees from East Cape Ridge to the trench. This is steeper
525 than observed globally at accretive margins and could, therefore, be considered as evidence for an
526 erosive subduction margin [*Clift and Vannucchi, 2004*]. However, allowing for the shallow
527 subduction angle of the plateau crust (~4 degrees within 70 km of the deformation front), the taper
528 angle is relatively shallow (7 degrees). In global comparison, this low taper angle is not clearly
529 erosive, and taking into account the trench sediment supply of about 2 km and the orthogonal plate
530 convergence rate of 60 km/Myr, the northern Hikurangi margin exhibits characteristics more

531 consistent with an accretive margin setting [*Clift and Vannucchi, 2004*].

532

533 Another argument against net subduction erosion at the margin is given by *Sutherland et al.* [2009].

534 They argue that tectonic erosion of the forearc would lead to trench retreat over geologic time and

535 hence the Hikurangi volcanic arc would have moved westward with time, relative to Raukumara

536 Basin, to preserve the distance between the deformation front and the arc volcanoes [*Lallemand,*

537 1995]. However, they present evidence that extinct arc volcanoes are not present within the basin

538 and hence suggest little or no net tectonic erosion of the forearc since 22 Ma.

539

540 An alternative mechanism to consider is that of lower-crustal underplating and hence forearc uplift

541 caused by continuity of volume. Rather than being accreted at the toe of the forearc wedge,

542 incoming sedimentary material enters a subduction channel and then, because it is too buoyant and

543 weak to penetrate beneath the overriding mantle wedge, it is transferred across the subduction thrust

544 and is underplated to the forearc crust to form the root of the outer forearc high. This mechanism

545 was first suggested for Raukumara Peninsula by *Walcott* [1987], and was developed by *Sutherland*

546 *et al.* [2009] to include both subducted sediment and material derived from frontal subduction

547 erosion to explain the geometry and uplift of East Cape Ridge.

548

549 We are able to test and quantify the forearc kinematic model of *Sutherland et al.* [2009]. The region

550 between the trench and East Cape Ridge consists of material of relatively low seismic velocities

551 (3.3 km/s at 6 km below the seafloor) and low sedimentary densities (<2.3 g/ccm), as indicated by

552 the depression of the sedimentary bodies at model-km 40 in Figures 3 and 7. In addition, we infer

553 high seismic attenuation east of model-km 100 based upon weak refracted signals and the

554 incoherent seismic-reflection character of MCS data (Figures 2b-e and 5). We attribute these

555 seismic and density characteristics to the considerable internal deformation of the accreted and

556 recycled forearc. Similar observations were made at the forearc high of the Sunda-Banda arc
557 transition [Shulgin *et al.*, 2009], where the source of the material is attributed to basal accretion
558 based on numerical modeling [Selzer *et al.*, 2008].

559

560 Our identification in cross-section of the material that is being recycled or actively accreted to the
561 forearc allows us to perform simplified calculations of mass fluxes at the subduction zone since 22
562 Ma. The total convergence at the subduction zone at this location since 22 Ma is assumed to be the
563 sum of the plate motion of 880 km, as computed from the rotations of *Cande and Stock* [2004], and
564 the back-arc opening in the Havre Trough of c. 120 km. The input of the subduction zone that is
565 available for accretion is the sediment thickness on the downgoing plate, and any volcanics (e.g.
566 seamounts) that could detach, integrated over the 22 Myr history of convergence. We identify 4 km
567 of material currently entering the subduction system on our cross-section, of which 2.2 km is
568 inferred to have collapsed off the adjacent trench slope, and some basal volcanoclastics may be
569 classified as part of the oceanic crust. The proximity of our profile to the Ruatoria Debris Avalanche
570 [Collot *et al.*, 2001] results in an overestimation of how much material is added on average from
571 outside the system. About 1 km less trench fill is observed today on seismic lines north and south of
572 the Ruatoria Debris Avalanche. In general, the sediment thickness found on the Hikurangi Plateau
573 away from the active trench is <1 km [Davy *et al.*, 2008], and so we estimate the total input to be
574 1000+/-500 km². The total volume of accreted and recycled forearc material beneath the trench
575 slope is estimated from our cross-section to be 500+/-50 km², so our best estimate is that half of the
576 incoming material has been accreted to the margin, though the possible range is 25-100%. Crustal
577 material may leave the forearc through erosion into sedimentary basins to the east or west, or may
578 be subducted into the mantle. The volumes of Neogene basins surrounding East Cape Ridge are
579 large, but the sedimentary fill is mostly composed of clasts transported from onshore New Zealand
580 and minor volcanoclastic input. Therefore, we cannot determine the proportion that is eroded from

581 East Cape Ridge, but we can identify a large enough reservoir to potentially account for all of the
582 remaining deficit in mass flux.

583

584 A similar suggestion of close to zero net-balance of subduction zone material transfer is made for
585 the eastern Sunda Arc region [*Lueschen et al.*, submitted manuscript] that may extend as far as east
586 of Sumba Island in the east [*Shulgin et al.*, 2009] and Java Island in the west [*Kopp et al.*, 2006].

587 Another recycling system is described for the paleo-accretionary wedge in south-central Chile
588 [*Glodny et al.*, 2004] though only an uplift and erosion balance is estimated without considering the
589 total mass budget. And another area of pronounced uplift of the outer forearc high but subsidence
590 and collapse of the trench slope is reported at the Tonga trench [*Clift et al.*, 1998], where we
591 propose that underplating of the forearc crust may have been partly overlooked due to a lack of
592 data. The steep slopes in these regions indicate a relatively high basal friction and may have higher
593 input than output to form a pronounced outer forearc high [*Gutscher et al.*, 1998].

594

595 Of particular interest for global models of crustal growth is the flux of material with a continental
596 chemistry that is transported back into the mantle at subduction zones, because it is widely believed
597 that this must be in approximate balance with the rate of production of new continental crust at
598 volcanic arcs [e.g. *von Huene and Scholl*, 1991; *Clift and Vannucchi*, 2004; *Hawkesworth and*
599 *Kemp*, 2006]. It has been widely assumed that margins with evidence for subsidence and collapse of
600 the trench slope are regions of trench retreat and long-term recycling of forearc crust into the mantle
601 [e.g. *Clift and Vannucchi*, 2004], but we challenge the underlying assumption used to estimate
602 these rates. According to the model suggested by *Sutherland et al.* [2009] and our determination of
603 the volume of accreted material at East Cape Ridge, past estimates of the rate of crustal recycling
604 into the mantle could be much greater than the true value because the significance of underplating at
605 the base of the crust may not have been fully recognized. Our observations may go a long way

606 towards explaining the discrepancy between independent estimates of crustal growth at arcs
607 [*Reymer and Schubert*, 1984] and crustal destruction at subduction zones [*Clift and Vannucchi*,
608 2004].

609

610 **7. Conclusions**

611

612 Seismic wide-angle and vertical reflection data together with gravity and magnetic anomalies have
613 been used to determine lithospheric structures of the northern Hikurangi margin, where the
614 Hikurangi Plateau subducts beneath the Raukumara forearc basin. A combination of seismic ray-
615 tracing modeling, seismic stratigraphy, gravity and magnetic modeling reveal the structure and
616 deformation of the subduction zone as well as the origin and possible age of certain rock units.

617

618 The shallow structure of the Hikurangi Plateau as determined by seismic wide-angle data consists at
619 the Hikurangi trench of up to 2 km sediments with seismic velocities up to 3.5 km/s above a unit of
620 about 2 km of seismically faster (>3.8 km/s) volcanoclastic, limestone and chert material. The
621 underlying crust is composed of an upper, 4 km thick layer with velocities of 4.9-6.7 km/s above the
622 lower crust which is characterized by velocities >7.1 km/s. The Moho depth was estimated by
623 gravity modeling and could not be verified by the seismic data. The thickness of the plateau is
624 approximately 10 km.

625

626 The Raukumara forearc basin represents one of the deepest known (> 10 km thick) forearc basins,
627 and formed initially during the Mesozoic Gondwana subduction episode, but was reactivated during
628 the Neogene Hikurangi subduction [*Sutherland et al.* 2009]. This reactivation process may be the only
629 mechanism that creates such super-deep forearc basins. Raukumara Basin developed on a 5-10 km
630 thick crust. Up to 6 km of Cretaceous and Paleogene sediment was deposited over the thinnest part

631 of the crust, which was then overlain by an allochthon that was emplaced at 25-22 Ma. We infer
632 sourced Matakaoa volcanic material from uplifted basement exposed on a precursor to East Cape
633 Ridge, where a high velocity, highly magnetized anomaly points to Matakaoa volcanics exposed
634 onshore. Neogene sediments up to 3 km thick were then deposited on top of this allochthon
635 [*Sutherland et al.*, 2009]. Refractions from the forearc mantle indicate seismic velocities above 8
636 km/s, implying that outside the region of arc volcanism the mantle material appears unaltered.
637 Below Raukumara Basin, seismic reflections off the subducting slab indicate that the inclination of
638 the initially low-angled slab dip steepens to over 10 degrees, and, according to seismicity, steepens
639 further to almost 50 degrees below the arc.

640

641 The East Cape Ridge to the trench is a 100 km wide region that is experiencing uplift due to
642 underplating of relatively low-seismic-velocity and low density crust from a subduction channel.
643 The limited depth penetration of seismic data indicates high seismic attenuation attributed to
644 significant internal deformation related to material recycling within the hanging-wall wedge. Uplift
645 of the forearc causes over-steepening of the frontal taper, and material collapses and enters into the
646 subduction channel from which it can become underplated and uplifted again.

647

648 A mass balance calculation indicates that the low-seismic-velocity, high-attenuation, low-density
649 forearc crust that we image beneath the trench slope and interpret to be accreted and recycled
650 material represents 25-100% of the incoming sediment from the downgoing plate, and that the
651 remainder could be accounted for through erosion of older accreted material into surrounding
652 sedimentary basins. We suggest that previous estimates of continental mass flux into the mantle at
653 subduction zones may be overestimated because they have not properly accounted for crustal
654 underplating beneath forearc highs.

655

656 **Acknowledgments**

657

658 We thank Captain Mallon and the crew of R/V Sonne for a smooth and efficient acquisition of the
659 seismic wide-angle data, the New Zealand National Institute of Water and Atmospheric Research
660 (NIWA) for providing high-resolution bathymetry of the research area, and the German Ministry for
661 Education and Research (BMBF), the German Research foundation (DFG), the New Zealand
662 Foundation for Research Science and Technology (FRST), the New Zealand Ministry for Economic
663 Development (MED) for funding various aspects of this research. Most figures were made with
664 GMT [*Wessel and Smith*, 1998].

665

666 **References**

667

668 Ārnadóttir, T., S. Thornley, F. F. Pollitz, and D. J. Darby (1999), Spatial and temporal strain rate
669 variations at the northern Hikurangi margin, New Zealand, *J. Geophys. Res.*, 104(B3), 4931-4944.

670

671 Barker D. H. N., R. Sutherland, S. Henrys, and S. Bannister (2009), Geometry of the Hikurangi
672 subduction thrust and upper plate, North Island, New Zealand, *Geochem. Geophys. Geosyst.*, 10,
673 Q02007, doi:10.1029/2008GC002153.

674

675 Bostock M. G., R. D. Hyndman, S. Rondenay, and S. M. Peacock (2002), An inverted continental
676 Moho and serpentinization of the forearc mantle, *Nature*, 417, 536-538.

677

678 Carlson R. L., and D. J. Miller, 2003, Mantle wedge water contents estimated from seismic
679 velocities in partially serpentinized peridotites, *Geophys. Res. Lett.*, 30(5), 1250,
680 doi:10.1029/2002GL016600.

681

682 Cassidy, J. (1993), Tectonic implications of paleomagnetic data from the Northland Ophiolite, New
683 Zealand, *Tectonophys.*, 223(3-4), 199-211.

684

685 Clift, P. D., and P. Vannucchi (2004), Controls on tectonic accretion versus erosion in subduction
686 zones: Implications for the origin and recycling of the continental crust, *Rev. Geophys.*, 42,
687 RG2001, doi:2010.1029/2003RG000127.

688

689 Clift P. D., C. J. MacLeod, D. R. Tappin, D. J. Wright, and S. H. Bloomer (1998), Tectonic controls
690 on sedimentation and diagenesis in the Tonga Trench and forearc, southwest Pacific, *Geol. Soc. Am.*
691 *Bul.*, 110(4), 483-496.

692

693 Cloos, M. (1993), Lithospheric buoyancy and collisional orogenesis: subduction of oceanic
694 plateaus, continental margins, island arcs, spreading ridges, and seamounts, *Geol. Soc. Am. Bul.*,
695 105, 715-737.

696

697 Coffin M. F., and O. Eldholm (1994), Large igneous provinces - Crustal structure, dimensions, and
698 external consequences, *Rev. Geophys.* 32(1), 1-36.

699

700 Collot, J.-Y., J. Delteil, K. B. Lewis, B. Davy, G. Lamarche, J. C. Audru, P. Barnes, F. Chanier, E.
701 Chaumillon, S. Lallemand, B. M. de Lepinay, A. Orpin, B. Pelletier, M. Sosson, B. Toussaint, and
702 C. Uruski (1996), From subduction to intra-continental transpression: structures of the Southern
703 Kermadec-Hikurangi margin from multibeam bathymetry, side-scan sonar, and seismic reflection,
704 *Marine Geophys. Res.*, 18, 357-381.

705

706 Collot, J.-Y., and B. Davy (1998), Forearc structures and tectonic regimes at the oblique subduction
707 zone between the Hikurangi Plateau and the southern Kermadec margin, *J. Geophys. Res.*, 103(B1),
708 623-650.
709

710 Collot, J.-Y., K. B. Lewis, G. Lamarche, and S. Lallemand (2001), The giant Ruatoria debris
711 avalanche on the Northern Hikurangi Margin, New Zealand: Result of oblique seamount
712 subduction, *J. Geophys. Res.*, 106(B9), 19,271-19,297.
713

714 Cooper, G. R. J. (2002), An improved algorithm for the Euler deconvolution of potential field data,
715 *The Leading Edge*, 21(12), 1197-1198.
716

717 Cooper, G. R. J. (2004), A semi-automatic procedure for the interpretation of geophysical data,
718 *Explor. Geophys.*, 35, 180-185.
719

720 Davey, F. J., M. Hampton, J. Childs, M. A. Fisher, K. Lewis, and J. R. Pettinga (1986), Structure of
721 a growing accretionary prism, Hikurangi margin, New Zealand, *Geology*, 14, 663-666.
722

723 Davey, F. J., S. Henrys, and E. Lodolo (1997), A seismic crustal section across the East Cape
724 convergent margin, New Zealand, *Tectonophys.*, 269, 199-215.
725

726 Davis, D. M., J. Suppe, and F. A. Dahlen (1983), Mechanics of fold-and-thrust belts and
727 accretionary wedges, *J. Geophys. Res.*, 88, 1153-1172.
728

729 Davy, B. W., and J.-Y. Collot (2000), The Rapuhia Scarp (northern Hikurangi Plateau): its nature
730 and subduction effects on the Kermadec Trench, *Tectonophys.*, 328, 269-295.

731

732 Davy, B., and R. Wood (1994), Gravity and magnetic modeling of the Hikurangi Plateau, *Mar.*
733 *Geol.*, 118(1-2), 139-151.

734

735 Davy, B., K. Hoernle, and R. Werner (2008), Hikurangi Plateau: Crustal structure, rifted formation,
736 and Gondwana subduction history, *Geochem. Geophys. Geosyst.*, 9, Q07004,
737 doi:10.1029/2007GC001855.

738

739 de Ronde, C., E. Baker, G. Massoth, J. Lupton, I. Wright, R. Sparks, S. Bannister, M. Reyners, S.
740 Walker, R. Greene, J. Ishibashi, K. Faure, J. Resing, and G. Lebon (2007), Submarine hydrothermal
741 activity along the mid-Kermadec Arc, New Zealand: Large scale effects on venting, *Geochem.*
742 *Geophys. Geosyst.*, 8, Q07007, doi:891 10.1029/2006GC001495.

743

744 DeMets, C., R. G. Gordon, D. F. Argus, and S. Stein (1994), Effect of recent revisions to the
745 geomagnetic time scale on estimates of current plate motions, *Geophys. Res. Lett.*, 21, 2191-2194.

746

747 Durrheim, R. J., and G. R. J. Cooper (1998), Euldep: A program for the Euler deconvolution of
748 magnetic and gravity data, *Computers & Geosciences*, 24, 545-550.

749

750 Field, B. D., C. Uruski, and others (1997), Cretaceous-Cenozoic geology and petroleum systems of
751 the east coast region, New Zealand, Institute of Geological and Nuclear Sciences, *Geological*
752 *Monograph*, 19, 301.

753

754 Flueh, E. R., and H. Kopp (2007), FS Sonne Fahrtbericht/Cruise Report SO192 MANGO: Marine
755 Geoscientific Investigations on the Input and Output of the Kermadec Subduction Zone, IFM-

756 GEOMAR Report No. 11, pp. 127.

757

758 Fugro Seismic Imaging (2007), Raukumara Basin 2D Seismic Survey - RAU07, New Zealand,
759 Unpublished Openfile Petroleum Report, 1-37 pp, Ministry of Economic Development, Crown
760 Minerals, Wellington, New Zealand.

761

762 Gillies, P. N. (1984), A Marine Geophysical Study of the Junction of the Kermadec and Hikurangi
763 Subduction Systems, PhD Thesis (Unpubl.), Univ. Auckland, New Zealand.

764

765 Glodny, J., J. Lohrmann, H. Echtler, K. Gräfe, W. Seifert, S. Collao, and O. Figueroa, (2004),
766 Internal dynamics of a paleoaccretionary wedge: insights from combined isotope tectonochronology
767 and sandbox modelling of the South-Central Chilean forearc, *Earth Planet. Sci. Lett.*, 231(1-2), 23-
768 39.

769

770 Gutscher, M.-A., N. Kukowski, J. Malavieille, S. Lallemand (1998), Material transfer in
771 accretionary wedges from analysis of a systematic series of analog experiments, *J. Struct. Geol.*,
772 20(4), 407-416.

773

774 Hawkesworth, C. J., and A. I. S. Kemp (2006), Evolution of the continental crust, *Nature*, 443, 811-
775 817.

776

777 Henrys, S. A., M. Reyners, I. Pecher, S. Bannister, Y. Nishimura, and G. Maslen (2006), Kinking of
778 the subducting slab by escalator normal faulting beneath the North Island of New Zealand,
779 *Geology*, 34(9), 777-780, doi: 710.1130/G22594.22591.

780

781 Herzer, R. H. (1995), Seismic stratigraphy of a buried volcanic arc, Northland, New Zealand and
782 implications for Neogene subduction, *Marine and Petroleum Geology*, 12(5), 511-531.
783

784 Hoernle, K., F. Hauff, R. Werner, and N. Mortimer (2004), New insights into the origin and
785 evolution of the Hikurangi oceanic plateau, *Eos Trans. AGU*, 85(41), 401-416.
786

787 Kopp, H., E. R. Flueh, C. J. Petersen, W. Weinrebe, A. Wittwer, and Meramex Scientists (2006),
788 The Java margin revisited: Evidence for subduction erosion off Java, *Earth Planet. Sci. Lett.*, 242(1-
789 2), 130-142.
790

791 Kopp, H., and N. Kukowski (2003), Backstop geometry and accretionary mechanics of the Sunda
792 margin, *Tectonics*, 22(6), 1072, doi:10.1029/2002TC001420.
793

794 Lallemand, S. (1995), High-rates of arc consumption by subduction processes - some consequences,
795 *Geology*, 23(6), 551-554.
796

797 Lamarche, G., C. Joanne, and J.-Y. Collot (2008), Successive, large mass-transport deposits in the
798 south Kermadec fore-arc basin, New Zealand: The Matakaoa Submarine Instability Complex,
799 *Geochem. Geophys. Geosyst.*, 9, Q04001, doi:10.1029/2007GC001843.
800

801 Lewis, K. B., J.-Y. Collot, and S. E. Lallemand (1998), The dammed Hikurangi Trough: a channel-
802 fed trench blocked by subducting seamounts and their wake avalanches (New Zealand-France
803 GeodyNZ Project), *Basin Res.*, 10, 441-468.
804

805 Lewis, K. B., S. Lallemand, and L. Carter (2004), Collapse in a Quaternary shelf basin off East

806 Cape, New Zealand: Evidence for passage of a subducted seamount inboard of the Ruatoria giant
807 avalanche, *N. Z. J. Geol. Geophys.*, 47(3), 415-429.

808

809 Litchfield, N., S. Ellis, K. Berryman, and A. Nicol (2007), Insights into subduction-related uplift
810 along the Hikurangi Margin, New Zealand, using numerical modeling, *J. Geophys. Res.*, 112,
811 F02021, doi:10.1029/2006JF000535.

812

813 Lueschen E., C. Mueller, H. Kopp, M. Engels, R. Lutz, L. Planert, A. Shulgin, and Y. Djajadihardja
814 (submitted), Structure, evolution and tectonic activity of the eastern Sunda forearc, Indonesia, from
815 marine seismic investigations, *Tectonophys.*, submitted manuscript 2009.

816

817 Malahoff, A., R. H. Feden, and H. S. Fleming (1982), Magnetic Anomalies and Tectonic Fabric of
818 Marginal Basins North of New Zealand, *J. Geophys. Res.*, 87(B5), 4109-4125.

819

820 Mann, P., and A. Taira (2004), Global tectonic significance of the Solomon Islands and Ontong Java
821 Plateau convergent zone, *Tectonophys.*, 389(3-4), 137-190.

822

823 Mazengarb, C., and D. H. M. Harris (1994), Cretaceous stratigraphic and structural relationships of
824 Raukumara Peninsula, New Zealand; stratigraphic patterns associated with the migration of a thrust
825 system, *Annales Tectonicae*, 8(2), 100-118.

826

827 Mazengarb, C., and I. G. Speden (2000), Geology of the Raukumara area, in Institute of Geological
828 and Nuclear Sciences 1:250 000 geological map, vol. 6, pp. 60, Institute of Geological and Nuclear
829 Sciences Limited, Lower Hutt, New Zealand.

830

831 McGeary, S., A. Nur, and Z. Ben-Avraham (1985), Spatial gaps in arc volcanism: The effect of
832 collision or subduction of oceanic plateaus, *Tectonophys.* 119 195-221.
833

834 McIntosh, K. D., E. A. Silver, I. Ahmed, A. Berhorst, C. R. Ranero, R. K. Kelly, and E. R. Flueh
835 (2007), The Nicaragua Convergent Margin: Seismic Reflection Imaging of the Source of a Tsunami
836 Earthquake; in: The seismogenic zone of subduction subduction thrust faults, T. Dixon and J. C.
837 Moore (Eds.), Columbia University Press, New York, p. 257-287.
838

839 Mortimer, N., and D. Parkinson (1996), Hikurangi Plateau: a Cretaceous large igneous province in
840 the southwest Pacific Ocean, *J. Geophys. Res.*, 101, 687-696.
841

842 Nicol, A., C. Mazengarb, F. Chanier, G. Rait, C. Uruski, and L. Wallace (2007), Tectonic evolution
843 of the active Hikurangi subduction margin, New Zealand, since the Oligocene, *Tectonics*, 26,
844 TC4002, doi:10.1029/2006TC002090.
845

846 Park, J.-O., T. Tsuru, S. Kodaira, P. R. Cummins, and Y. Kaneda (2002), Splay fault branching along
847 the Nankai subduction zone, *Science*, 297, 1157-1160.
848

849 Pecher, I. A., S. A. Henrys, S. Ellis, S. M. Chiswell, and N. Kukowski (2005), Erosion of the
850 seafloor at the top of the gas hydrate stability zone on the Hikurangi Margin, New Zealand,
851 *Geophys. Res. Lett.*, 32, L24603, doi:10.1029/2005GL024687.
852

853 Rait, G., F. Chanier, and D. W. Waters (1991), Landward- and seaward-directed thrusting
854 accompanying the onset of subduction beneath New Zealand, *Geology*, 19(3), 230-233.
855

856 Ranero, C. R., R. von Huene, E. R. Flueh, M. Duarte, D. Baca, and K. McIntosh (2000), A cross
857 section of the convergent Pacific margin of Nicaragua; *Tectonics*, 19(2,) 335-357.
858

859 Reymer, A., and G. Schubert (1984), Phanerozoic addition rates to the continental crust and crustal
860 growth, *Tectonics*, 3(1), 63-77.
861

862 Reyners, M., D. Eberhart-Phillips, and G. Stuart (1999), A three-dimensional image of shallow
863 subduction: crustal structure of the Raukumara Peninsula, New Zealand, *Geophys. J. Int.*, 137(3),
864 873-890.
865

866 Reyners, M., and P. McGinty (1999), Shallow subduction tectonics in the Raukumara Peninsula,
867 New Zealand, as illuminated by earthquake focal mechanisms, *J. Geophys. Res.*, 104, 3025-3034.
868

869 Reyners, M., D. Eberhart-Phillips, G. Stuart, and Y. Nishimura (2006), Imaging subduction from the
870 trench to 300 km depth beneath the central North Island, New Zealand, with Vp and Vp/Vs,
871 *Geophys. J. Int.*, 165, 565-583, doi:10.1111/j.1365-246X.2006.02897.x.
872

873 Rudnick, R. L., and D. M. Fountain (1995), Nature and composition of the continental crust: A
874 lower crustal perspective, *Rev. Geophys.*, 33.
875

876 Sandwell, D. T. and W. H. F. Smith (1997), Marine gravity from Geosat and ERS-1 altimetry, *J.*
877 *Geophys. Res.*, 102, 10039-10054.
878

879 Shulgin A., H. Kopp, C. Mueller, E. Lueschen, L. Planert, M. Engels, E. R. Flueh, A. Krabbenhoft,
880 and Y. Djajadihardja (2009), Sunda-Banda arc transition: Incipient continent-island arc collision

881 (northwest Australia), *Geophys. Res. Lett.*, 36, accepted 2009.

882

883 Selzer, C., S. J. H. Buitter, and O. A. Pfiffner (2008), Numerical modeling of frontal and basal
884 accretion at collisional margins, *Tectonics*, 27, TC3001, doi:10.1029/2007TC002169.

885

886 Song, T. R. A., and M. Simons (2003), Large trenchparallel gravity variations predict seismogenic
887 behavior in subduction zones: *Science*, 301, 630-633, doi:10.1126/science.1085557.

888

889 Sutherland, R., V. Stagpoole, C. Uruski, S. Henrys, B. Field, S. Toulmin, D. Barker, S. Bannister, F.
890 Davey, C. Kennedy, D. Basset, T. Stern, M. Scherwath, E. Flueh, and H. Kopp (2009), Reactivation
891 of tectonics, crustal underplating and uplift after 60 Myr of passive subsidence, Raukumara Basin,
892 Hikurangi-Kermadec forearc, New Zealand: implications for global growth and recycling of
893 continents, *Tectonics*, accepted 2009.

894

895 Thornley, S. (1996), Neogene Tectonics of Raukumara Peninsula, Northern Hikurangi Margin, New
896 Zealand, PhD Thesis (Unpubl.), Victoria Univ. Wellington, New Zealand.

897

898 Tichelaar, B. W., and L. J. Ruff (1993), Depth of seismic coupling along subduction zones, *J.*
899 *Geophys. Res.*, 98(B2), 2017-2037.

900

901 Upton, P., P. O. Koons, and D. Eberhart-Phillips (2003), Extension and partitioning in an oblique
902 subduction zone, New Zealand: Constraints from three-dimensional numerical modeling, *Tectonics*,
903 22(6), 1068, doi:10.1029/2002TC001431.

904

905 Von Huene, R., and D. W. Scholl (1991), Observations at convergent margins concerning sediment

906 subduction, subduction erosion, and the growth of continental crust, *Rev. Geophys.*, 29, 279-316.
907

908 Von Huene, R., J. Bourgois, J. Miller, and G. Pautot (1989), A large tsunamogenic landslide and
909 debris flow along the Peru trench, *J. Geophys. Res.*, 94(B2), 1703-1714.
910

911 Von Huene, R., C. R. Ranero, and P. Vannucchi (2004), Generic model of subduction erosion,
912 *Geology*, 32(10), 913-916.
913

914 Walcott, R. I. (1987), Geodetic strain and the deformational history of the North Island of New
915 Zealand during the late Cainozoic, *Philosophical Transactions of the Royal Society of London*, 321,
916 163-181.
917

918 Wallace, L. M., J. Beavan, R. McCaffrey, and D. Darby (2004), Subduction zone coupling and
919 tectonic block rotations in the North Island, New Zealand, *J. Geophys. Res.*, 109, doi
920 10.1029/2004JB003241.
921

922 Walther, C. H. E., E. R. Flueh, C. R. Ranero, R. von Huene, and W. Strauch (2000), Crustal
923 structure across the Pacific margin of Nicaragua: evidence for ophiolitic basement and a shallow
924 mantle sliver, *Geophys. J. Int.*, 141, 759-777.
925

926 Wells, R. E., R. J. Blakely, Y. Sugiyama, D. W. Scholl, and P. A. Dinterman (2003), Basin-centered
927 asperities in great subduction zone earthquakes: A link between slip, subsidence, and subduction
928 erosion?, *J. Geophys. Res.*, 108(B10), 2507, doi:10.1029/2002JB002072.
929

930 Wessel, P., and W. H. S. Smith (1998), New version of generic mapping tools released, *Eos Trans.*

931 *AGU*, 79, 579.

932

933 Whattam, S. A., J. G. Malpas, J. R. Ali, I. E. M. Smith, C. H. Lo (2004), Origin of the Northland
934 Ophiolite, northern New Zealand: discussion of new data and reassessment of the model, *N. Z. J.*
935 *Geol. and Geophys.*, 47(3), 383-389.

936

937 Wilson, K., K. Berryman, U. Cochran, and T. Little (2007), Holocene coastal evolution and uplift
938 mechanisms of the northeastern Raukumara Peninsula, North Island, New Zealand, *Quaternary*
939 *Science Reviews*, 26(7-8), 1106-1128.

940

941 Wood, R., and B. Davy (1994), The Hikurangi Plateau, *Mar. Geol.*, 118(1-2), 153-173.

942

943 Ye, S., E. R. Flueh, D. Klaeschen, R. von Huene (1997), Crustal structure along the EDGE transect
944 beneath the Kodiak shelf off Alaska derived from OBH seismic refraction data, *Geophys. J. Int.*,
945 130(2), 283-302.

946

947 Zelt, C. A., and R. B. Smith (1992), Seismic travelt ime inversion for 2-D crustal velocity structure,
948 *Geophys. J. Int.*, 108, 16-34.

949

950 Zelt, C. A. (1999), Modelling strategies and model assessment for wide-angle seismic travelt ime
951 data, *Geophys. J. Int.*, 139, 183-204.

952

953 **Figure Captions**

954

955 **Figure 1.** Regional basemap, southwest Pacific, northeast of North Island, New Zealand. The Data

956 Profile corresponds to the seismic wide-angle data transect MANGO-1, seismic reflection line
957 RAU07-05 and available ship-born gravity and magnetic profiles. Yellow triangles mark locations
958 of mapped volcanoes, orange circles represent earthquakes larger magnitude 4.0 since 1990, scaled
959 according to size. Plate motion of the Pacific relative to the Australian plate after *DeMets et al.*
960 [1994]. Bottom panel shows onshore Raukumara Peninsula simplified geology (after *Mazengarb*
961 *and Speden* [2000]) and uplift (after *Lichtfield et al.* [2007]), and offshore locations of the ocean
962 bottom seismic receivers with those stations annotated whose data are shown in Figure 3.

963

964 **Figure 2.** Data examples and predicted arrivals of every 5th OBS/H. Locations of these example
965 stations are marked in Figure 2. Central panels show all predicted P-wave arrivals drawn on top of
966 the seismic data, bottom panels show, however, rays only for picked arrivals. Note the contrast in
967 data quality and offset range between western stations on Raukumara Basin (model distance >100
968 km) and the eastern station on the East Cape Ridge and the Hikurangi Plateau. Annotated seismic
969 phases correspond to: Psed(fast/slow)=refraction through (fast/slow) sediments; Pg(u/l)=refraction
970 through (upper/lower) crust; Pn=refraction through mantle; Pmv=refraction through shallow high-
971 velocity anomaly (interpreted as Matakaoa Volcanics); PdP=reflection from decollement;
972 PsP=reflection from sediments; PcP=reflection from mid-crust; PmP=reflection from Moho.

973

974 **Figure 3.** Final proposed velocity model derived from ray-tracing of the seismic wide-angle data.
975 Masked areas represent parts of the model without ray coverage, though seismic reflection data
976 from line RAU07-05 as well as gravity data were used to place some constraints on this model as
977 explained in the text. Also shown are earthquakes, circles from the global database with magnitudes
978 larger than 4 from within 50 km of either side of the model, and crosses are from the Raukumara
979 Peninsula network from *Reyners et al.* [1999] from up to 100 km to the south of our profile. Note
980 the increased concentration of hypocenters around the location where the incoming plate bends

981 most below the forearc.

982

983 **Figure 4.** (a) Model resolution, with depth nodes (squares) and velocity nodes (circles) drawn to
984 scale indicating node resolution; values larger than 0.5 are considered well resolved. (b) Model
985 coverage, demonstrating the shallow coverage of the incoming Hikurangi Plateau and comparably
986 good coverage of the Raukumara Basin structures. The gap in the center is due to relatively weak
987 seismic signals recorded to relatively narrow offsets, probably caused by high seismic attenuation
988 within the margin wedge of the fore-arc.

989

990 **Figure 5.** Seismic reflection data from line RAU07-05 with velocity model structures and
991 interpretation [*Sutherland et al.*, 2009] overlain. Triangles on seafloor mark OBS/H stations. West
992 of the stations, the velocity model does not predict the reflections well, as no modeling emphasis
993 was placed outside the region of wide-angle data coverage.

994

995 **Figure 6.** Gravity and magnetic data around the northern Hikurangi Margin, viewed from northeast.
996 Top: Gravity data reveal a prominent -140 mgal anomaly associated with Raukumara Basin.
997 Bottom: East Cape Ridge exhibits several large magnetic positive anomalies that can be traced
998 towards land to link up with the Matakaoa volcanics.

999

1000 **Figure 7.** Gravity and magnetic model from 2.5D modeling. Model layers extend practically
1001 indefinitely in all directions except the deep sedimentary layer in Raukumara Basin which was
1002 limited to 50 km in and out of the model plain. Densities are given for all layers, magnetic
1003 susceptibility (dimensionless number behind density) is given only for magnetized layers.

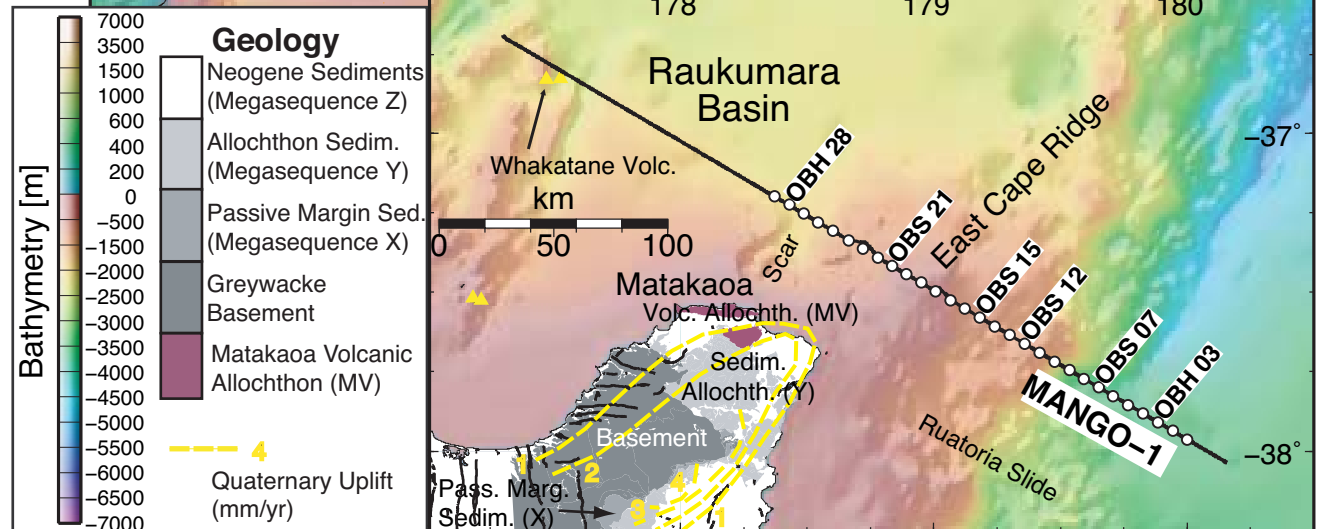
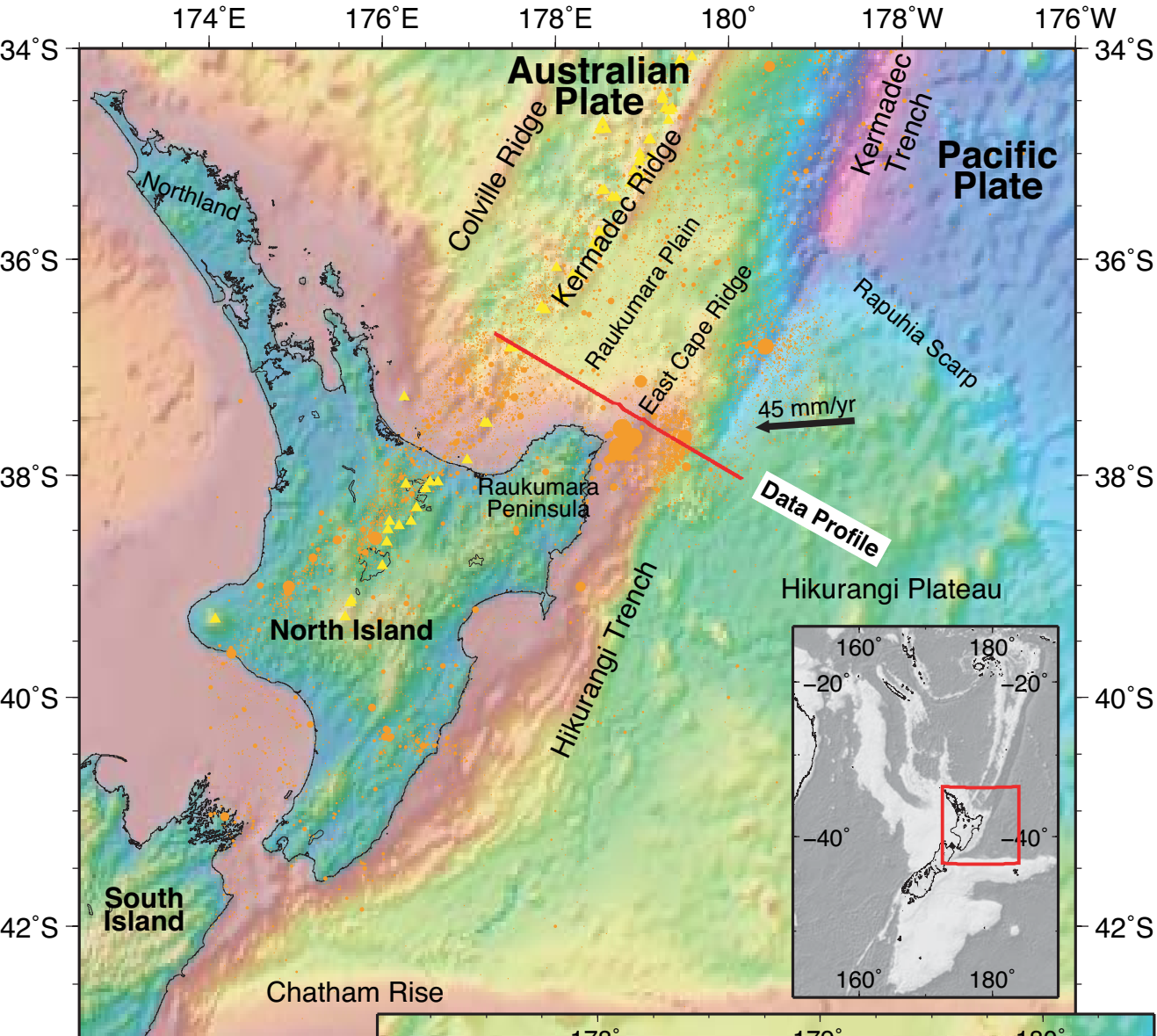
1004

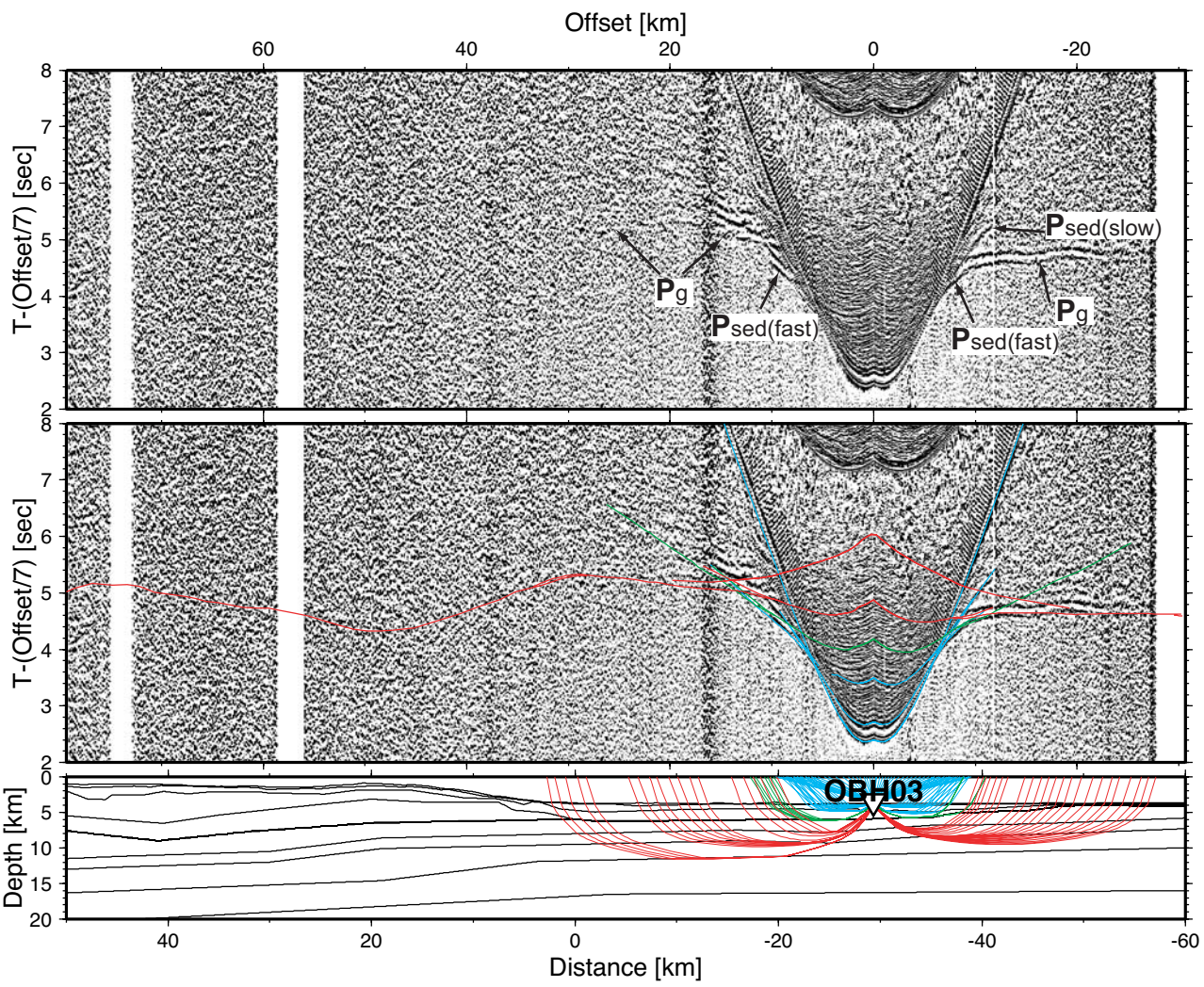
1005 **Figure 8.** Magnetic Euler deconvolution, indicating regions for likely magnetic sources: Red color

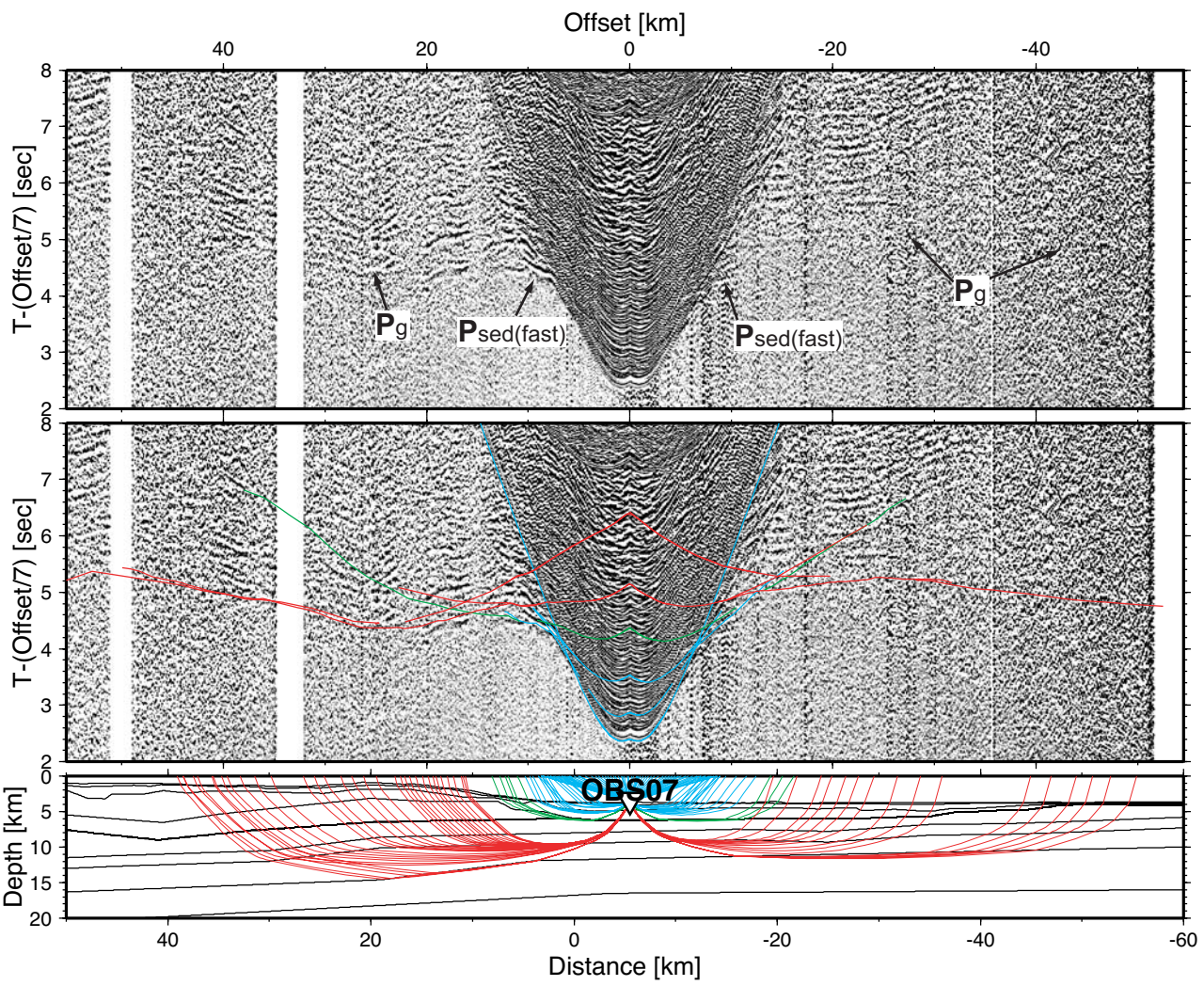
1006 marks most likely location, green likely, and blue unlikely locations for magnetic sources. Note the
1007 reasonably good correlation of the East Cape Ridge anomaly of the seismic velocity structure
1008 (drawn on top). Also remarkable are the shallow anomalies at the eastern edge of Raukumara Basin,
1009 which are associated with the large slump called Megasequence Y [*Sutherland et al.*, 2009],
1010 originating from the East Cape Ridge anomaly.

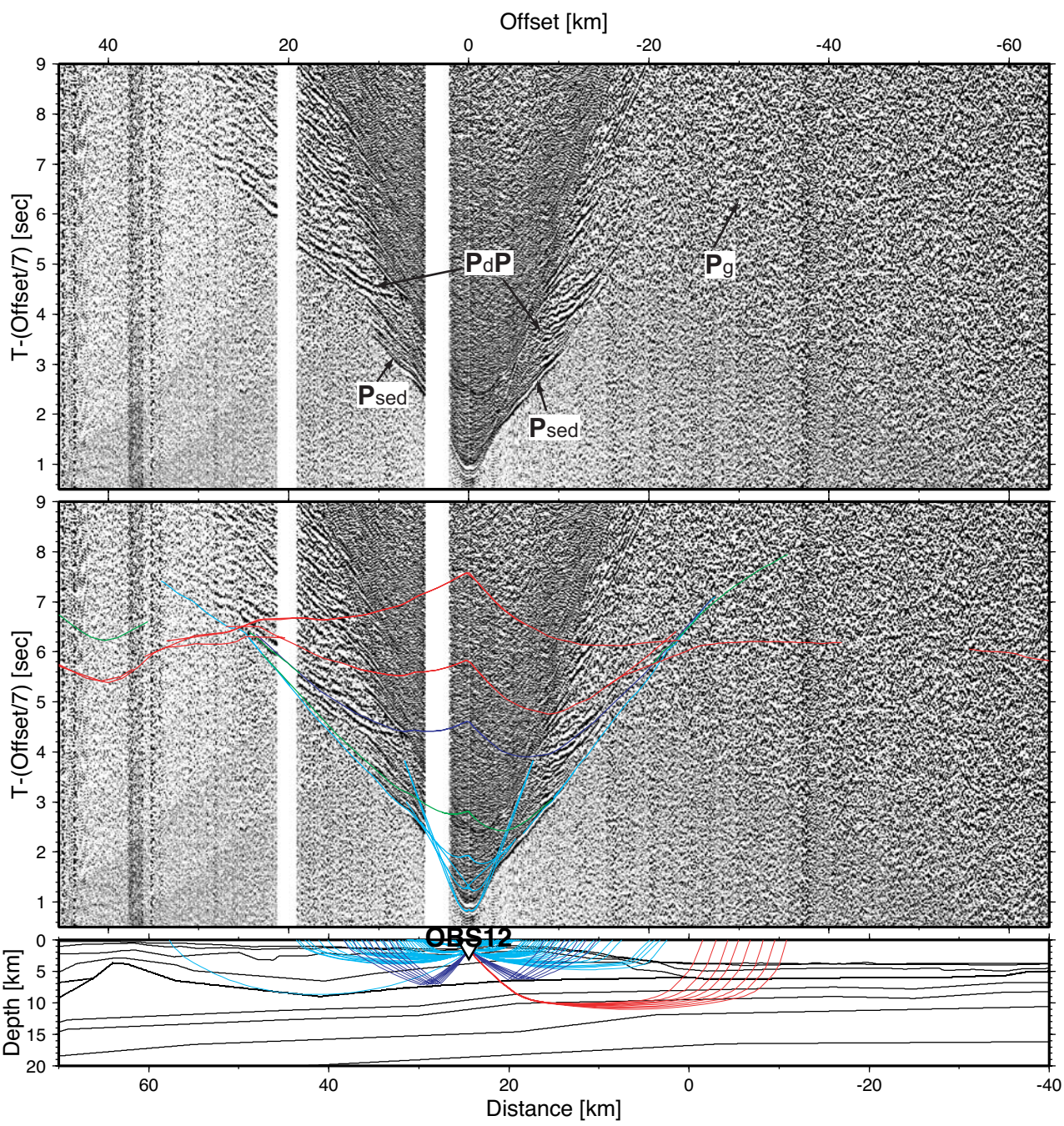
1011

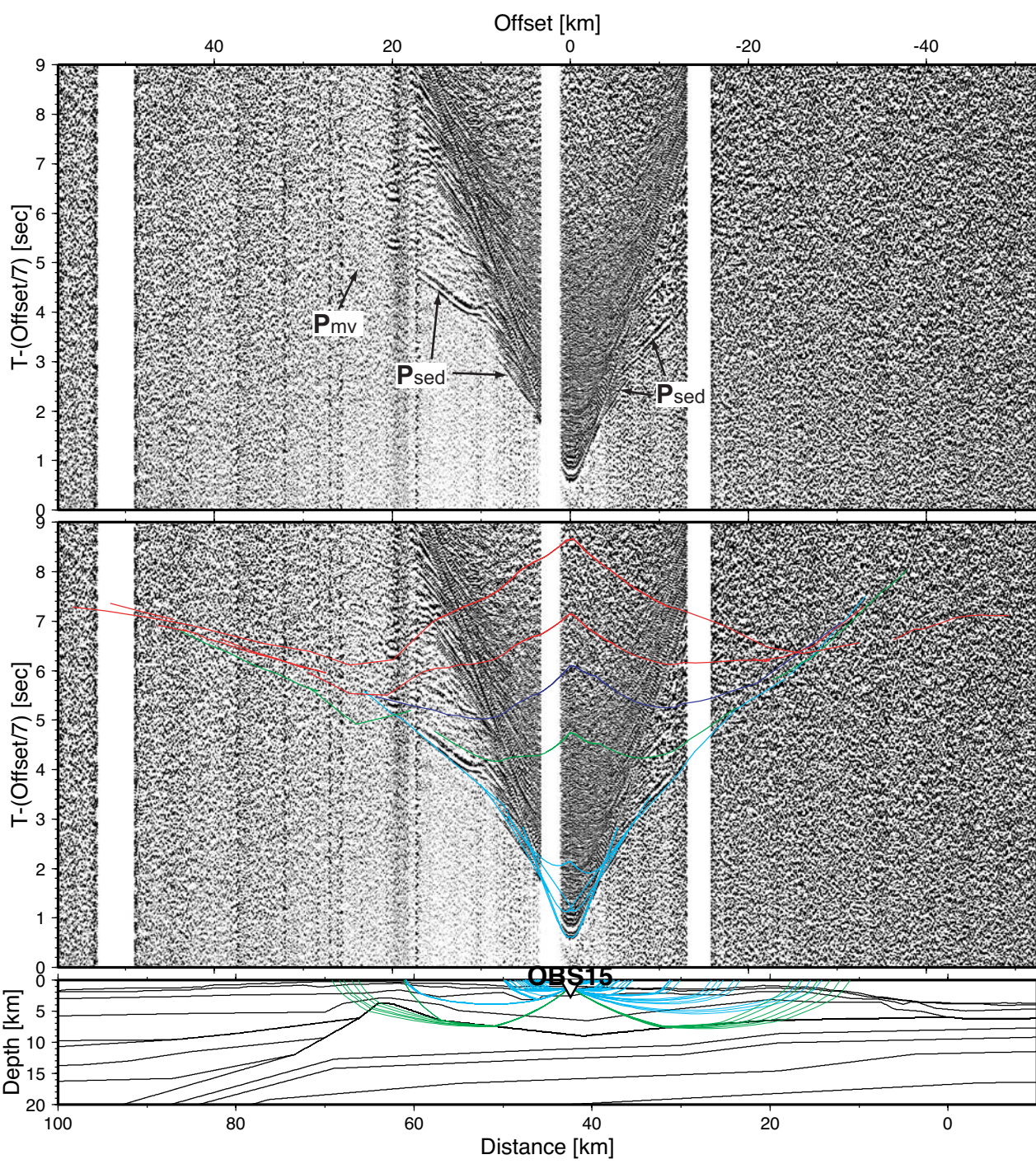
1012 **Figure 9.** Summary of structural interpretation, with concepts of material recycling within the
1013 subduction wedge (top right), uplift and mass wasting focused at the shallow East Cape Ridge near
1014 our data profile (bottom). Here, we also detected a strong shallow high velocity and strong magnetic
1015 anomalous rock (marked as "MV" in top panel) which is also interpreted as the source region for
1016 Megasequence Y, indicated by dashed arrow (center in top panel).

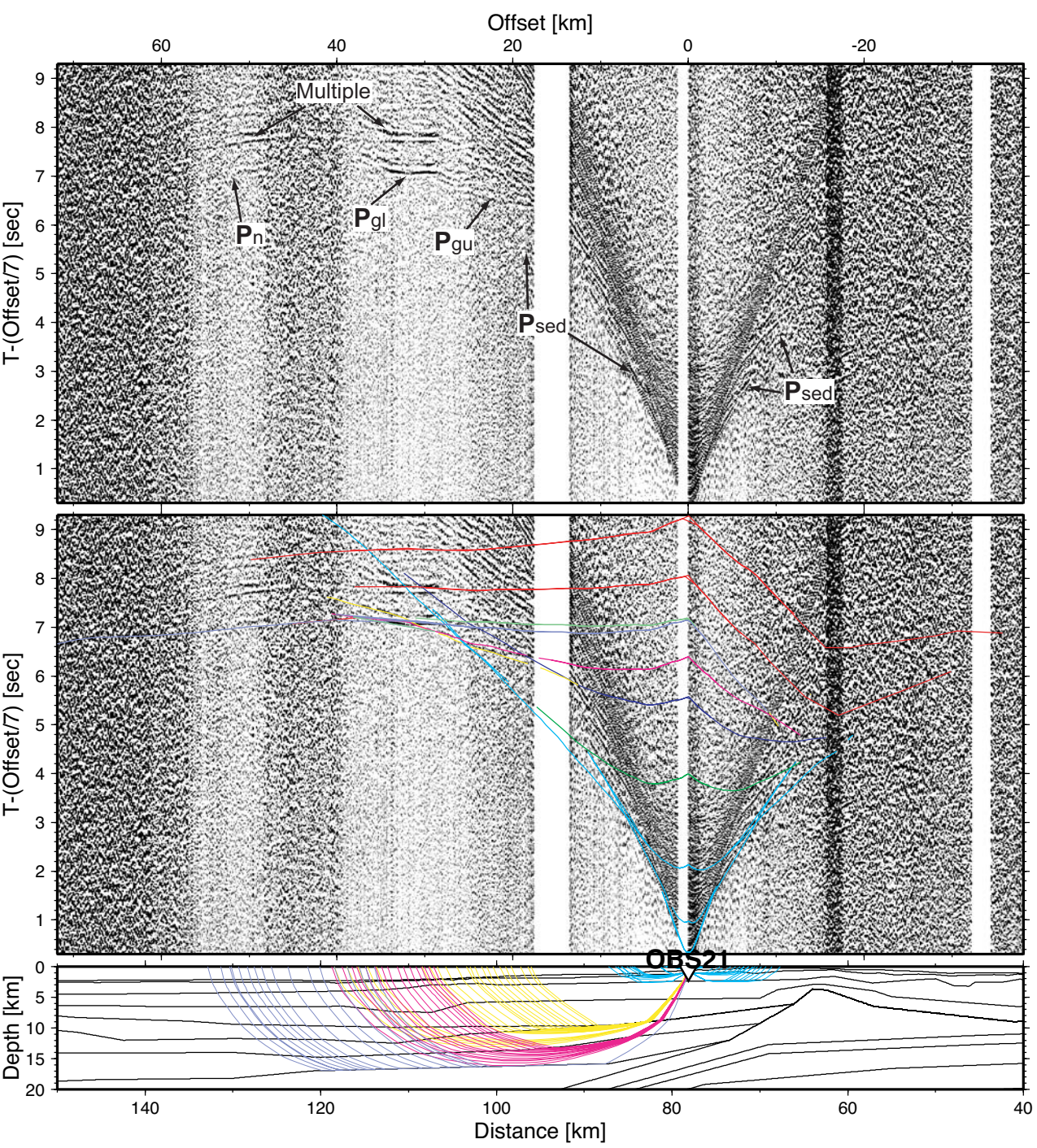


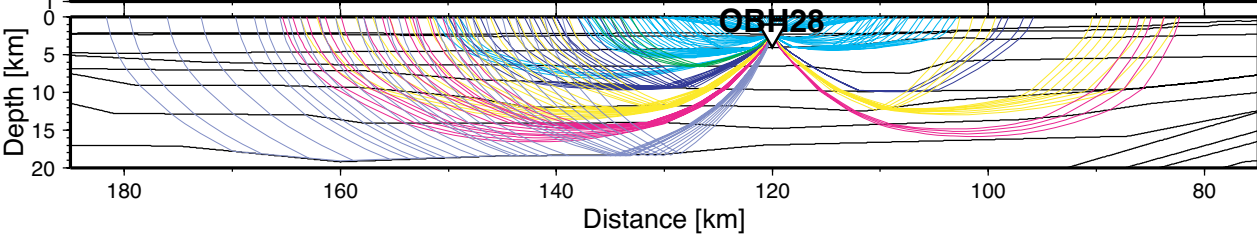
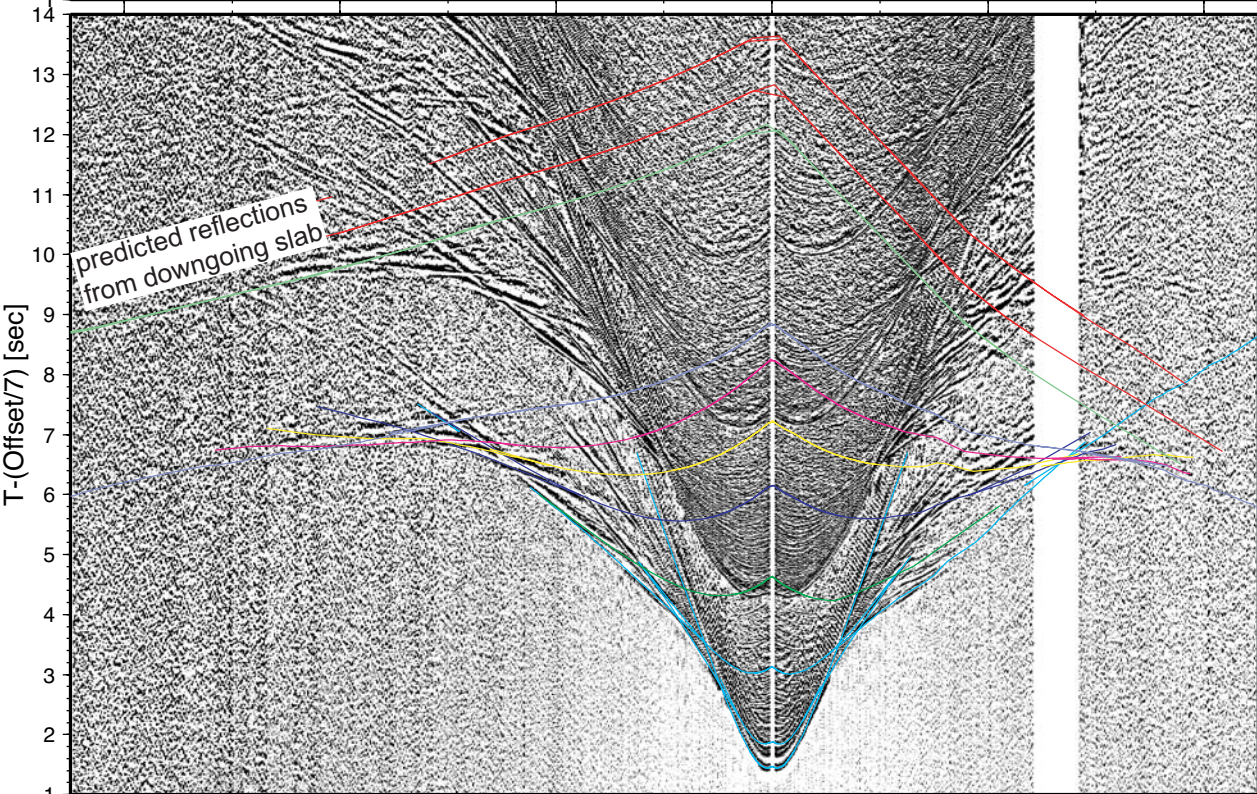
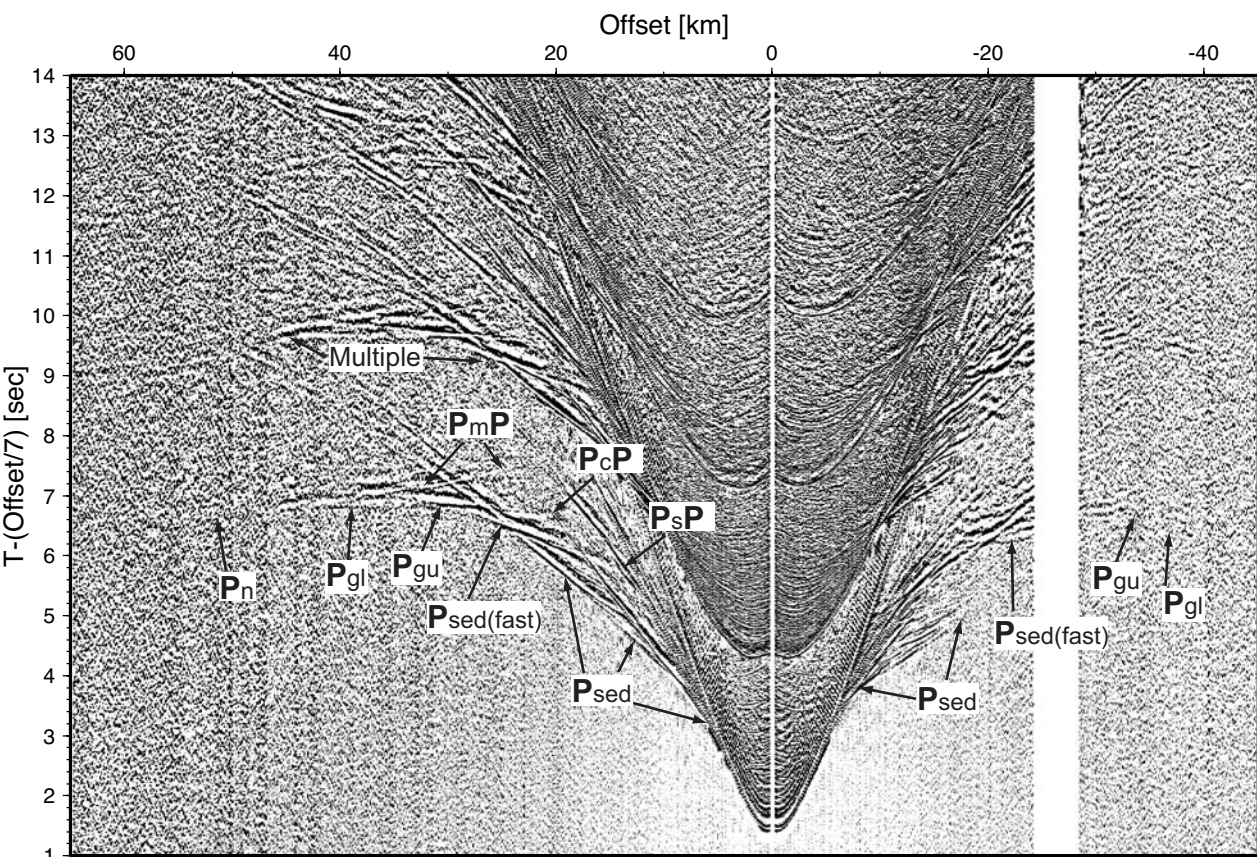


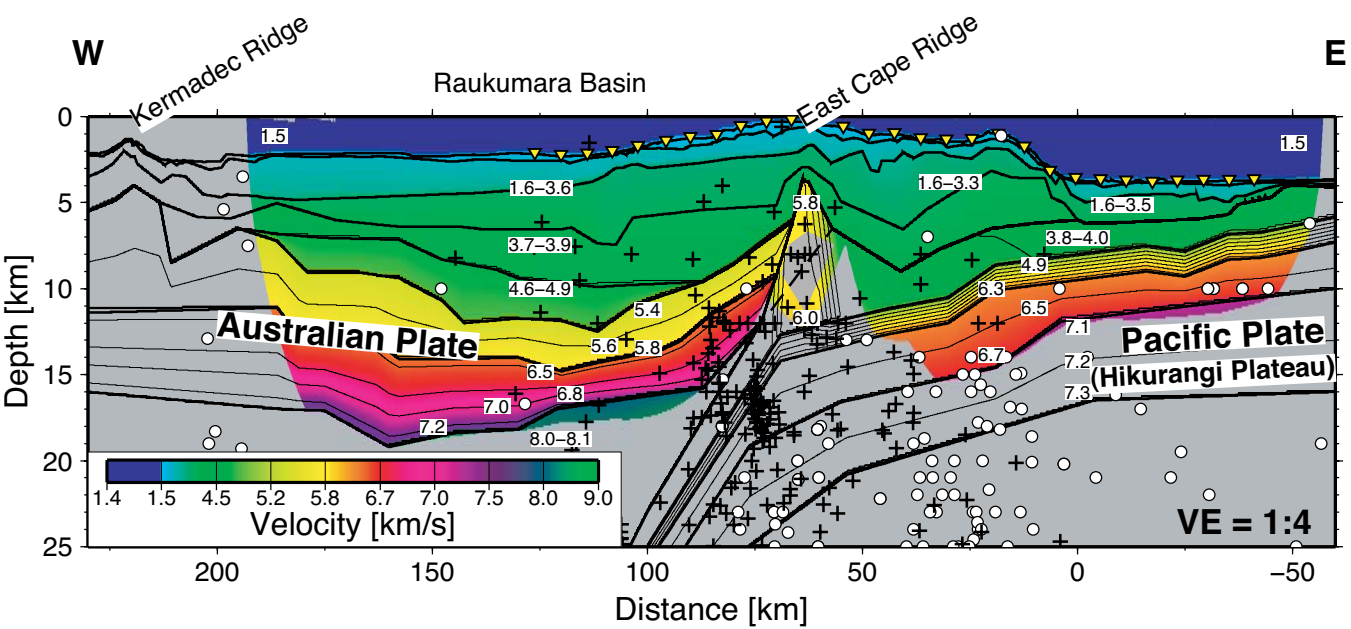


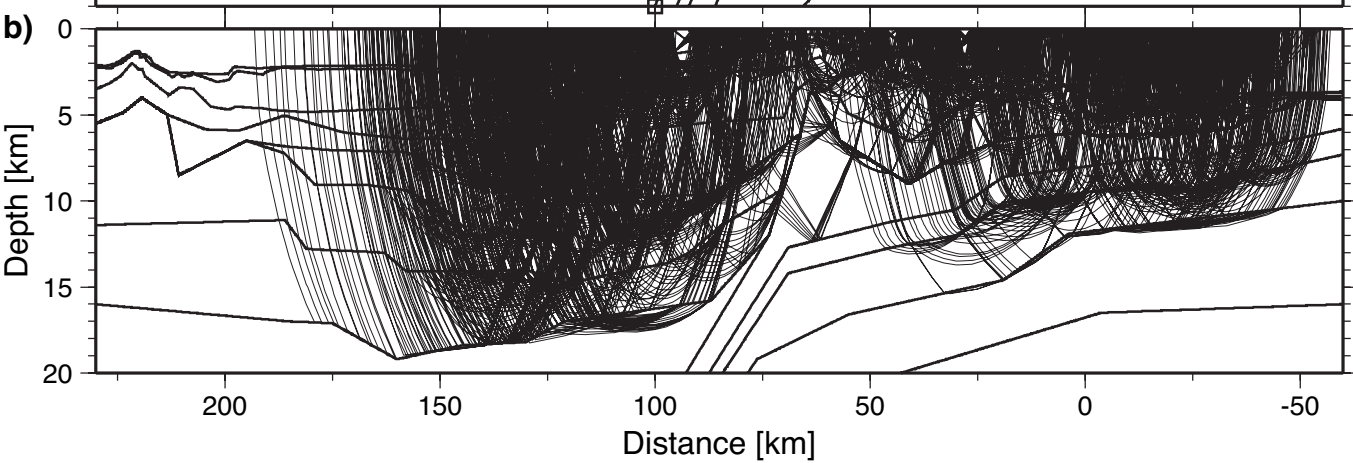
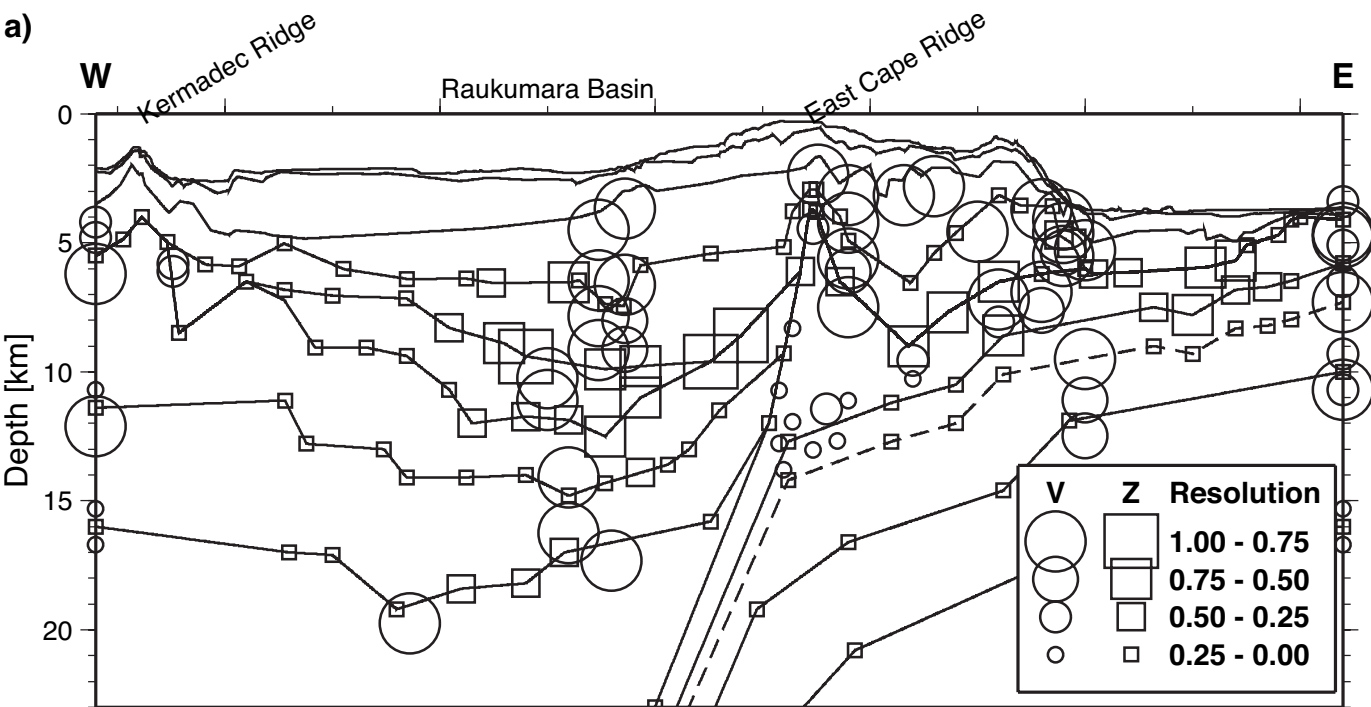


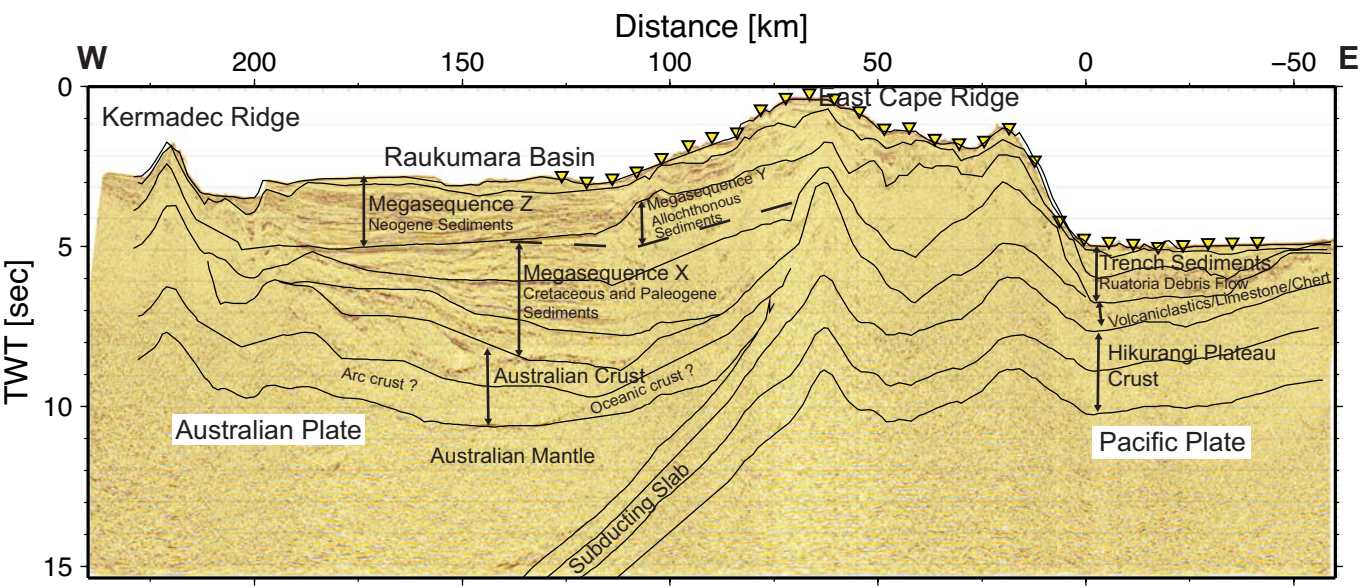


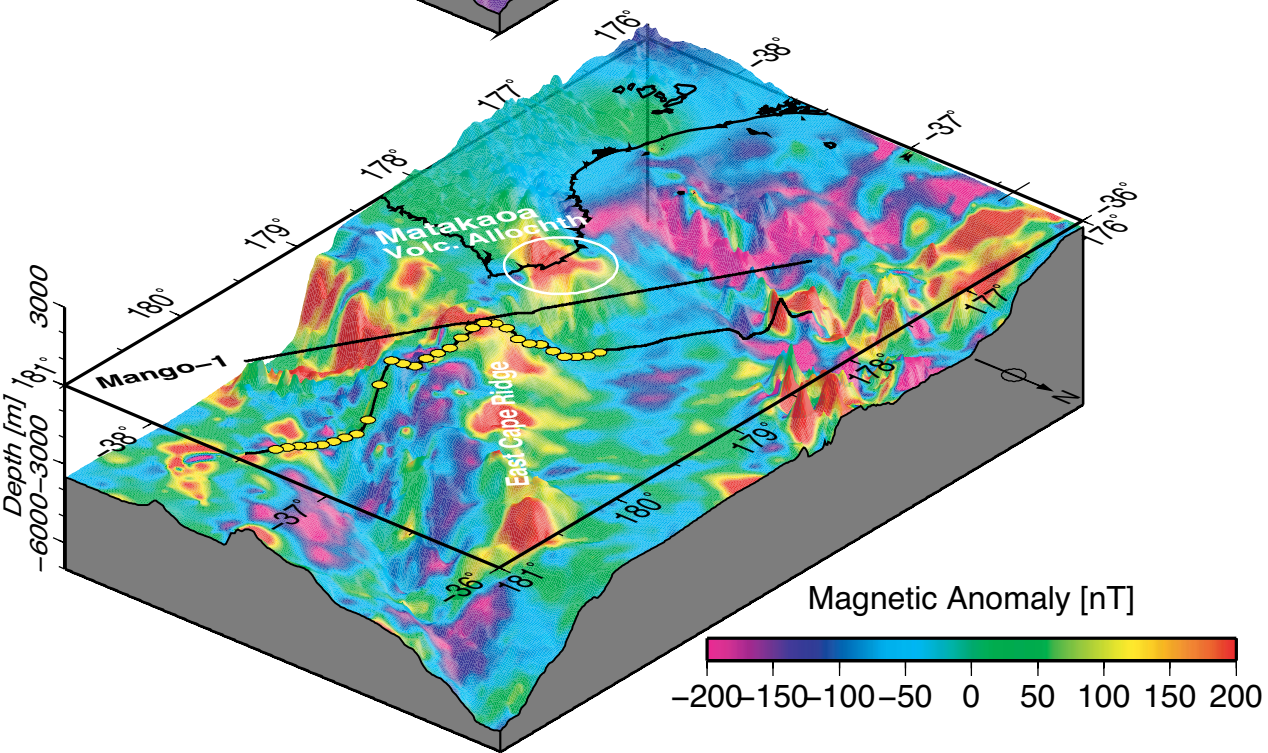
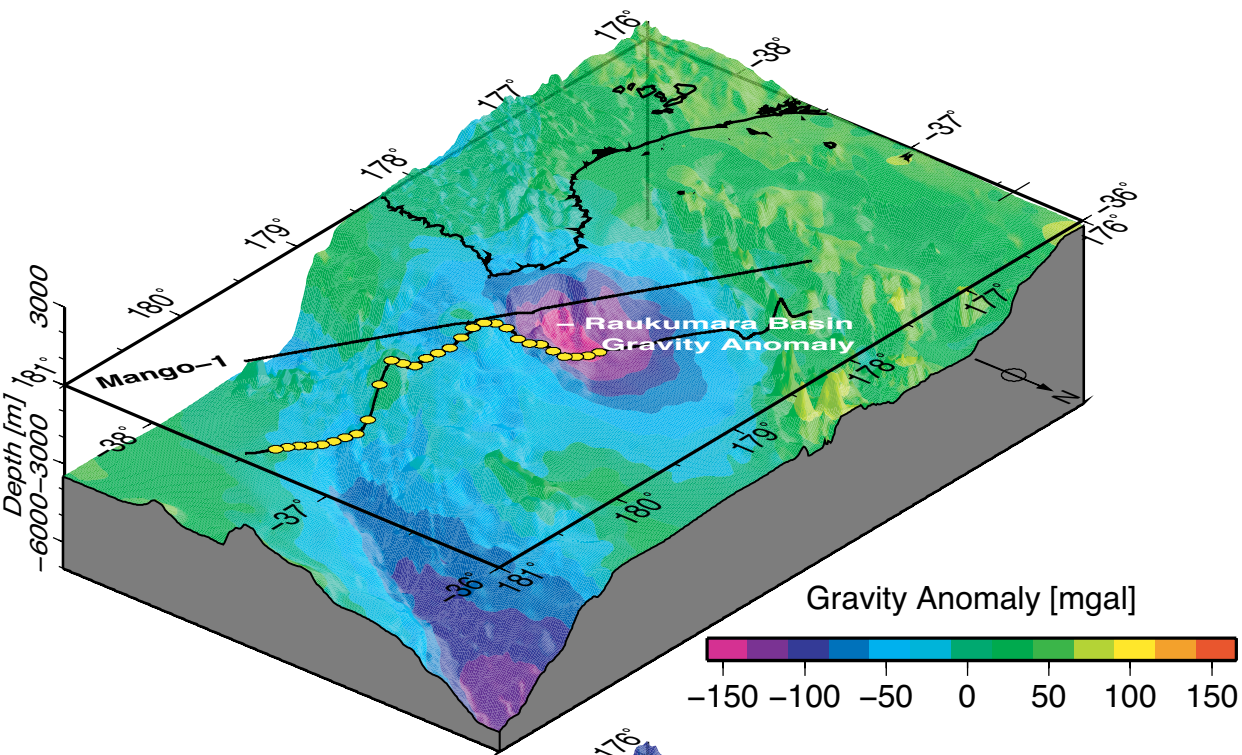


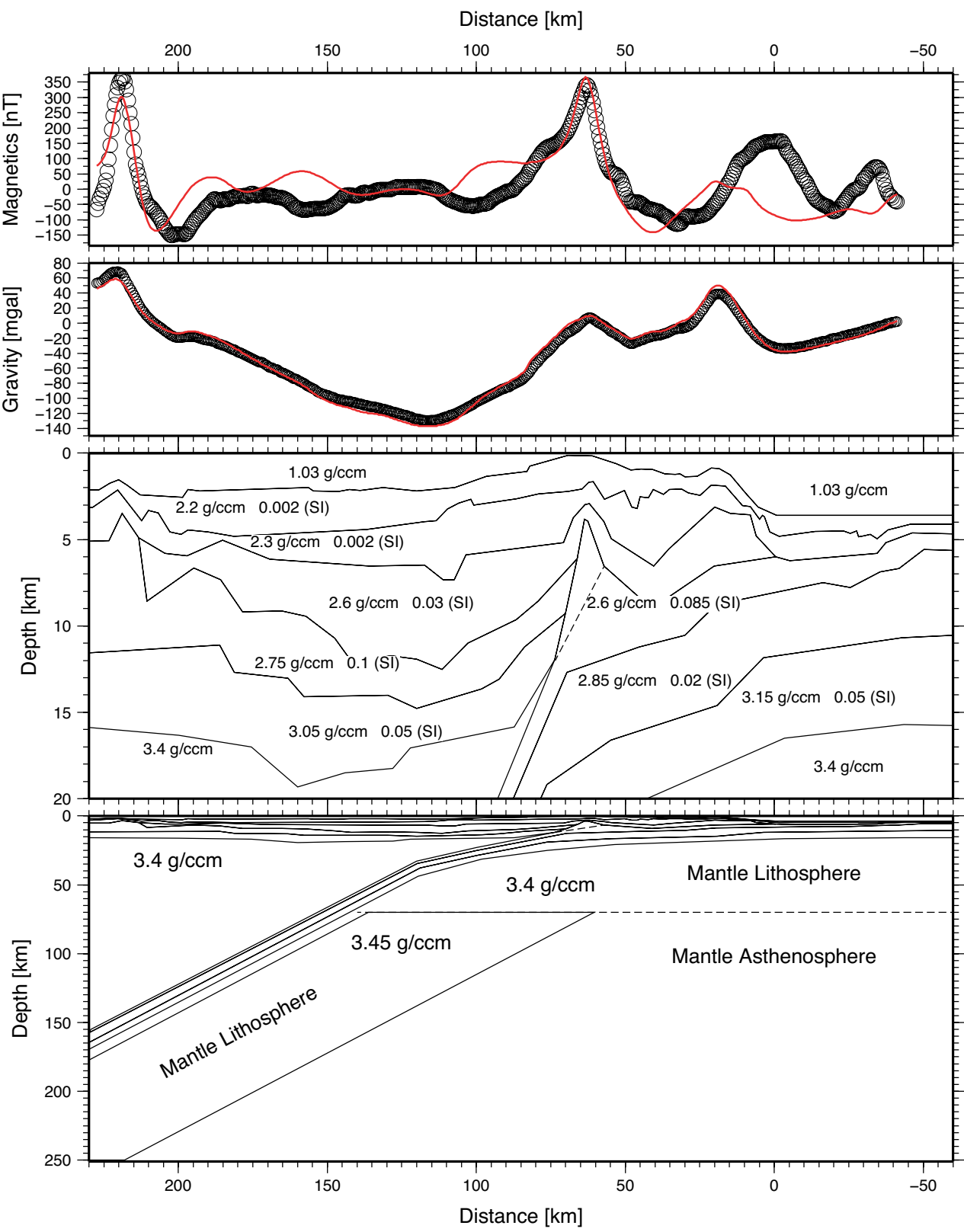


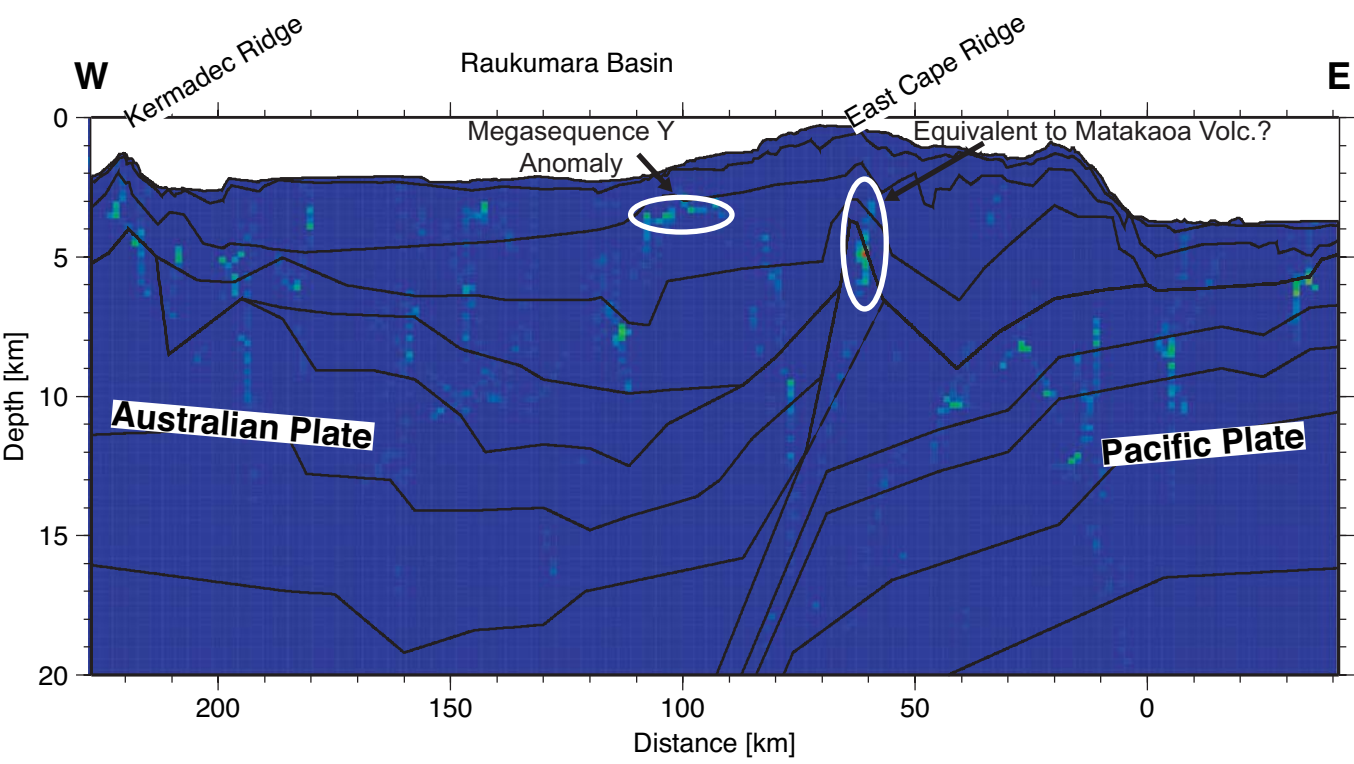


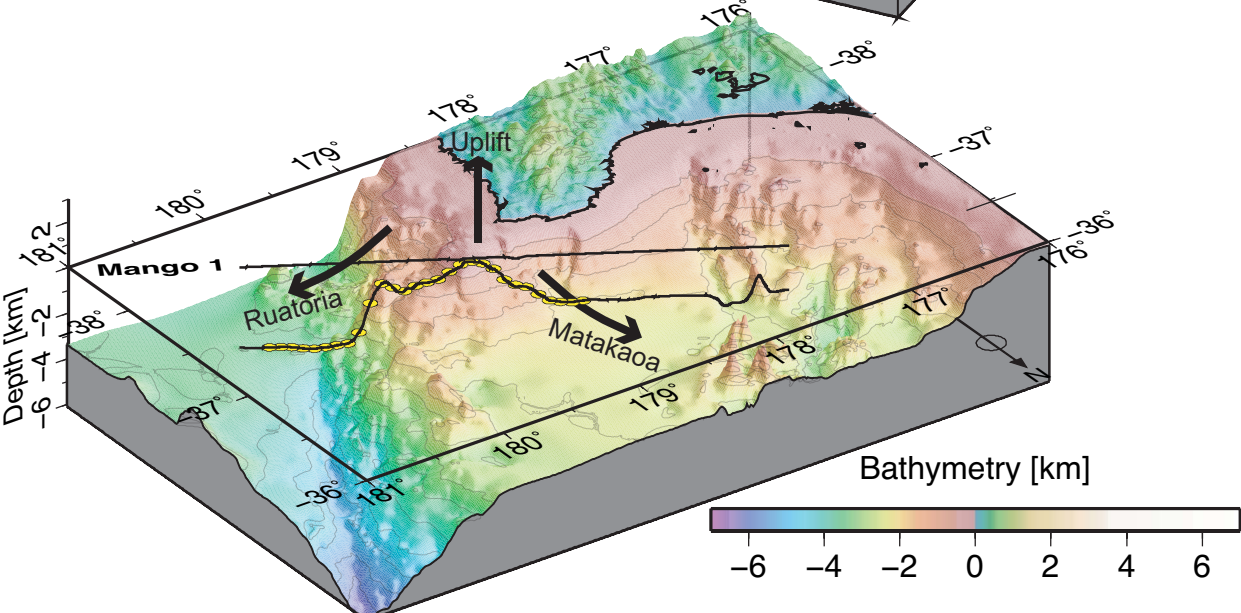
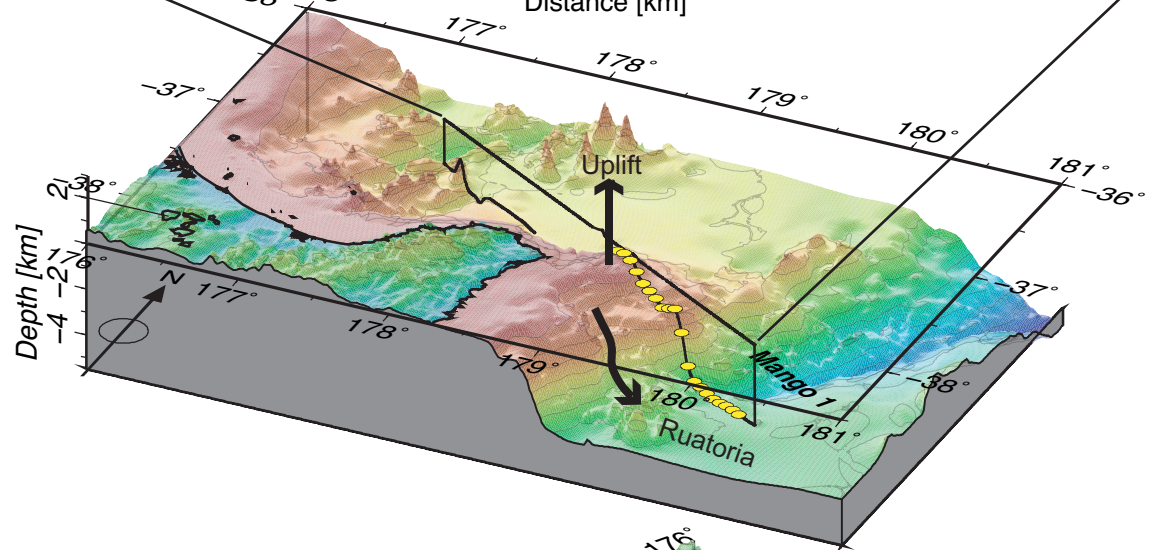
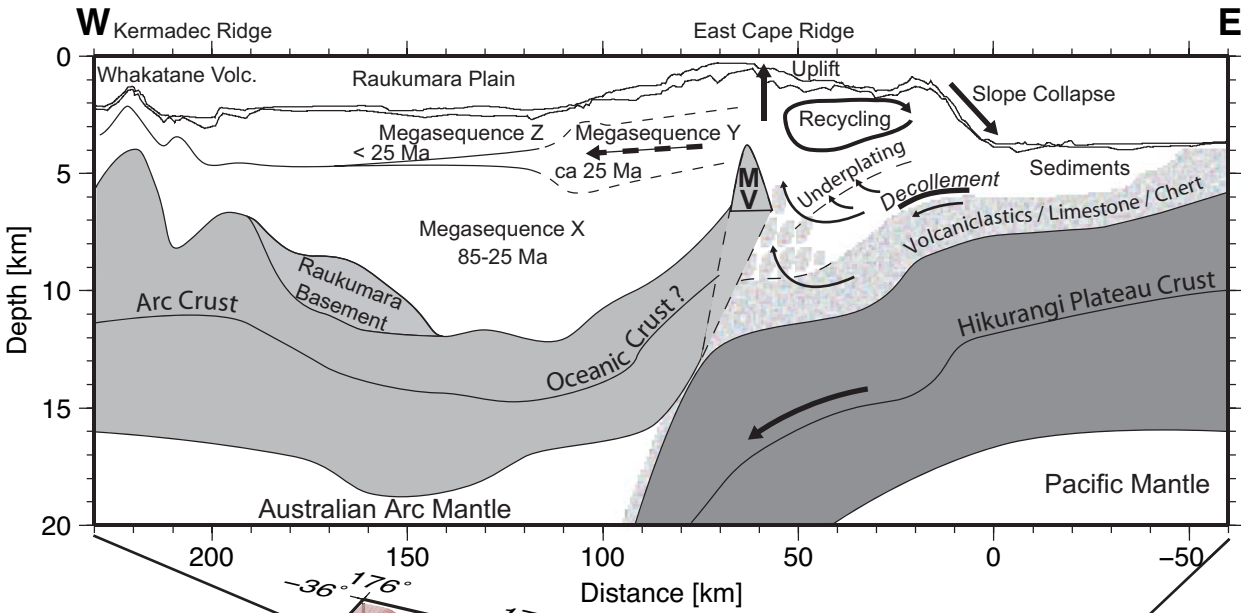














Reactivation of tectonics, crustal underplating, and uplift after 60 Myr of passive subsidence, Raukumara Basin, Hikurangi-Kermadec fore arc, New Zealand: Implications for global growth and recycling of continents

Rupert Sutherland,¹ Vaughan Stagpoole,¹ Christopher Uruski,¹ Callum Kennedy,² Daniel Bassett,³ Stuart Henrys,¹ Martin Scherwath,⁴ Heidrun Kopp,⁴ Brad Field,¹ Suzannah Toulmin,¹ Daniel Barker,¹ Stephen Bannister,¹ Fred Davey,¹ Timothy Stern,³ and Ernst R. Flueh⁴

Received 5 July 2008; revised 13 May 2009; accepted 9 July 2009; published 28 October 2009.

[1] We use seismic reflection and refraction data to determine crustal structure, to map a fore-arc basin containing 12 km of sediment, and to image the subduction thrust at 35 km depth. Seismic reflection megasequences within the basin are correlated with onshore geology: megasequence X, Late Cretaceous and Paleogene marine passive margin sediments; megasequence Y, a $\sim 10,000$ km³ submarine landslide emplaced during subduction initiation at 22 Ma; and megasequence Z, a Neogene subduction margin megasequence. The Moho lies at 17 km beneath the basin center and at 35 km at the southern margin. Beneath the western basin margin, we interpret reflective units as deformed Gondwana fore-arc sediment that was thrust in Cretaceous time over oceanic crust 7 km thick. Raukumara Basin has normal faults at its western margin and is uplifted along its eastern and southern margins. Raukumara Basin represents a rigid fore-arc block >150 km long, which contrasts with widespread faulting and large Neogene vertical axis rotations farther south. Taper of the western edge of allochthonous unit Y and westward thickening and downlap of immediately overlying strata suggest westward or northwestward paleoslope and emplacement direction rather than southwestward, as proposed for the correlative onshore allochthon. Spatial correlation between rock uplift of the eastern and southern basin margins with the intersection between Moho and subduction thrust leads us to suggest that crustal underplating is modulated by fore-arc crustal thickness. The trench

slope has many small extensional faults and lacks coherent internal reflections, suggesting collapse of indurated rock, rather than accretion of >1 km of sediment from the downgoing plate. The lack of volcanic intrusion east of the active arc, and stratigraphic evidence for the broadening of East Cape Ridge with time, suggests net fore-arc accretion since 22 Ma. We propose a cyclical fore-arc kinematic: rock moves down a subduction channel to near the base of the crust, where underplating drives rock uplift, oversteepens the trench slope, and causes collapse toward the trench and subduction channel. Cyclical rock particle paths led to persistent trench slope subsidence during net accretion. Existing global estimates of fore-arc loss are systematically too high because they assume vertical particle paths.

Citation: Sutherland, R., et al. (2009), Reactivation of tectonics, crustal underplating, and uplift after 60 Myr of passive subsidence, Raukumara Basin, Hikurangi-Kermadec fore arc, New Zealand: Implications for global growth and recycling of continents, *Tectonics*, 28, TC5017, doi:10.1029/2008TC002356.

1. Introduction

[2] The Raukumara Plain lies adjacent to northeast North Island, New Zealand, and is part of the fore-arc region of the Hikurangi-Kermadec subduction zone (Figure 1). Marine geophysical surveys carried out during the 1970s and 1980s revealed sediment cover, but it was not until a multichannel seismic reflection (MCS) line was acquired in 1990 (line OGS90) that a thick sedimentary fill reaching ~ 13 km thickness was identified in one location [Davey *et al.*, 1997; Gillies and Davey, 1986]. During the period 2005 to 2007, three new seismic reflection-refraction surveys were acquired and these data have allowed us to map out and describe what we now refer to as Raukumara Basin (Figure 1). We develop a seismic stratigraphy for the basin, discuss stratigraphic correlations between onshore and offshore, and we analyze the architecture of the basin and consider its genesis and evolution. Our detailed images and analyses of Raukumara Basin are in the context of its well understood tectonic

¹GNS Science, Lower Hutt, New Zealand.

²New Zealand Ministry of Economic Development, Wellington, New Zealand.

³Environment and Earth Sciences, School of Geography, Victoria University of Wellington, Wellington, New Zealand.

⁴Leibniz Institute of Marine Sciences at University of Kiel (IFM-GEOMAR), Kiel, Germany.

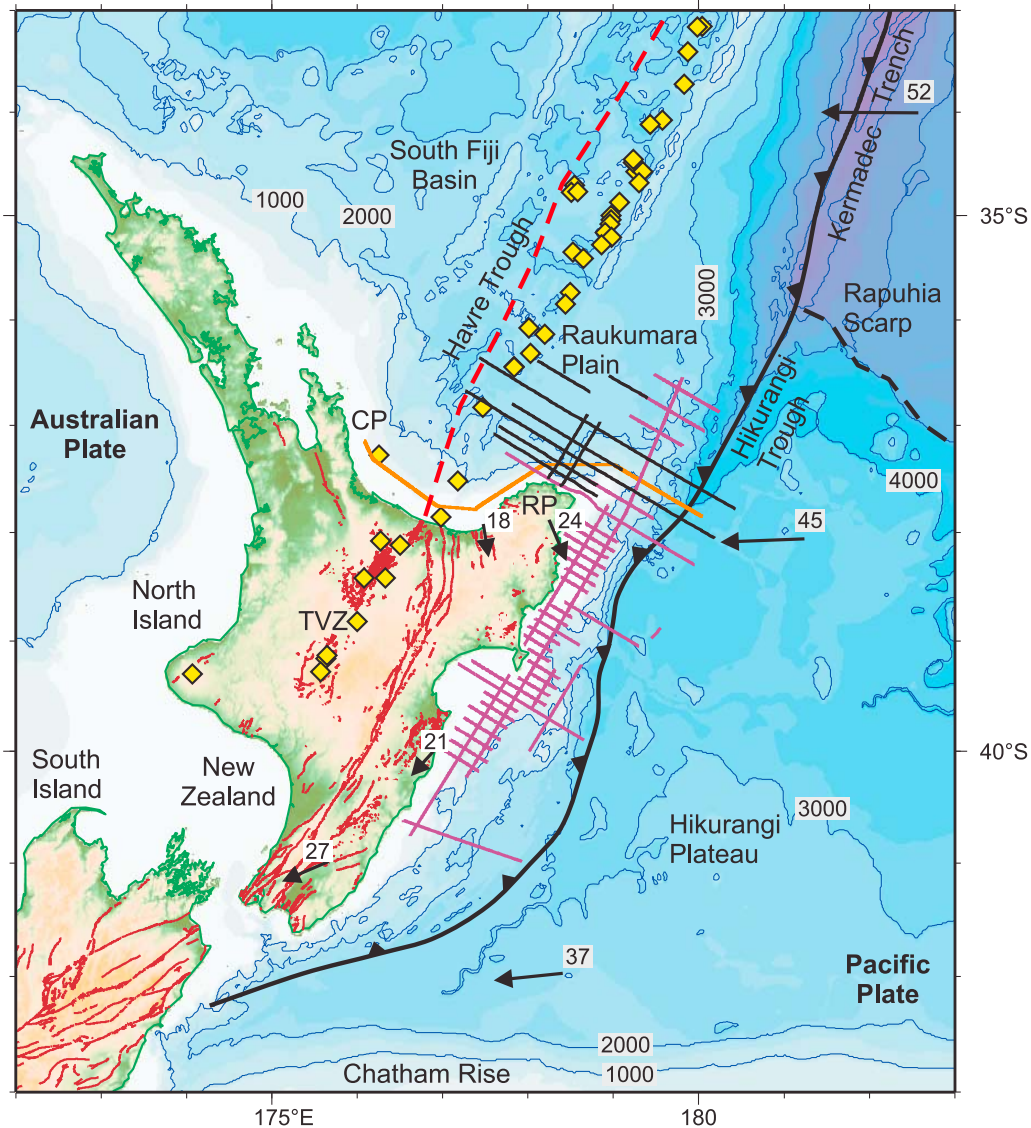


Figure 1. Location of the Raukumara Basin between the Hikurangi Trough subduction front and the Havre Trough back-arc spreading center. Also labeled are the Raukumara Peninsula (RP) and Coromandel Peninsula (CP) and Taupo Volcanic Zone (TVZ). Arrows show long-term motion of the Pacific plate [DeMets *et al.*, 1994] and short-term (GPS) motion of the fore arc [Wallace *et al.*, 2004] relative to a fixed Australian plate. Diamonds show known locations of significant Holocene volcanic centers [de Ronde *et al.*, 2001, 2007; Wright *et al.*, 1996, 2006]. Onshore active faults are shown in dark red (<http://data.gns.cri.nz/af>). Offshore seismic lines are colored OGS90 (orange); 05CM (magenta); and RAU07 (black). Bathymetric contours are at 1000 m interval. The Rapuhia Scarp is the boundary between the Hikurangi Plateau large igneous province and Mesozoic ocean crust [Davy and Collot, 2000; Wood and Davy, 1994].

setting and hence provide insights into active tectonic and basin processes, and may provide a useful analogy for other fore-arc basins.

[3] The Raukumara Basin fore arc and its along-strike transition is of particular relevance to understanding processes and rates of sediment subduction, subduction erosion, and hence the global growth of continental crust. Based upon characterization of the seabed and sedimentary

basins at many different subduction margins, it has been suggested that net removal of fore-arc crustal material into the mantle is prevalent globally, and that a significant proportion of incoming sediment may be subducted into the mantle, even at rapidly accreting margins [Clift and Vannucchi, 2004; VonHuene and Scholl, 1991]. On the basis of similar arguments, the region of Raukumara Basin has previously been inferred to be one of net crustal loss

through sediment subduction and subduction erosion [Clift and Vannucchi, 2004; Collot and Davy, 1998; VonHuene and Scholl, 1991]. On the basis of our new data and analysis, we challenge this view and suggest an alternate hypothesis that fore-arc accretion through lower crustal underplating of subducted material is significant. We are able to conclude this because we have well-mapped and dated stratigraphy in the context of known plate motions, and we have a profound change in crustal structure along strike within the fore arc that provides us with controlled experimental conditions. If we are correct that a significant volume of material is moved to the lower crust of the fore arc, rather than moved into the mantle by subduction, and our results can be generalized to other subduction margins, then the global flux of crustal materials into the mantle at subduction margins is significantly lower than previously thought and new estimates of global crustal growth fluxes are required.

[4] Our new discovery and mapping of the basin is also of substantial regional significance. Raukumara Basin preserves Cretaceous and Paleogene strata, structures, and environmental records in a region that in most other places have been highly deformed during the Cenozoic; and we tentatively identify a fragment of the Mesozoic Gondwana trench slope preserved beneath the western margin of the basin. Raukumara Basin stratigraphy and structure provide constraints on the processes of initiation of Tonga-Kermadec-Hikurangi subduction, and on subsequent fore-arc rotations. The very deep fore-arc basin and associated negative gravity anomaly, by analogy with other subduction zones [Song and Simons, 2003; Wells et al., 2003], may have mechanical significance for the nucleation and propagation of great subduction earthquakes, and is hence also of social and economic interest. Furthermore, it is possible that this newly discovered basin may host significant petroleum resources.

2. Present Tectonic Setting

[5] Relative plate motion between the Australian and Pacific plates, according to the NUVEL-1A model [DeMets et al., 1994], is 47 mm/yr near the Raukumara Plain, but back-arc extension of 13–16 mm/yr in the Taupo Volcanic Zone and Havre Trough [Lamarche et al., 2006; Wallace et al., 2004; Wright et al., 1996] causes the fore arc to move independently of the Australian plate and increases the subduction rate to ~60 mm/yr (Figure 1). Numerous volcanoes, caldera, and active hot vent sites are located near to the axis of back-arc extension [de Ronde et al., 2001, 2007; Wright et al., 2006].

[6] The subduction interface and crustal structure onshore, beneath Raukumara Peninsula (Figure 1), has previously been imaged using natural earthquake sources and a dense array of seismometers [Reyners et al., 1999]. The maximum thickness of continental crust is 30–40 km beneath western Raukumara Peninsula, as inferred from crustal V_p estimates of 5.5–6.5 km s⁻¹ [Reyners et al., 1999]. Earthquake hypocenters cluster within the upper part of the subducting plate, and in the crust between the east coast of Raukumara Peninsula and the subduction front.

Earthquake focal mechanisms indicate downdip tensional strain within the subducting plate, and NNW–SSE extensional strain within the shallow part of the upper plate [Reyners and McGinty, 1999], consistent with geological and geodetic observations [Arnadóttir et al., 1999]. The uppermost ~10 km of the mantle of the subducted slab consistently has $V_p > 8.5$ km s⁻¹, and reduces to more normal mantle velocities of approximately $V_p = 8.2$ km s⁻¹ beneath [Reyners et al., 1999].

3. Lithostratigraphy and Structure of Raukumara Peninsula

3.1. Jurassic and Cretaceous Gondwana Fore Arc

[7] The oldest rocks on Raukumara Peninsula are Jurassic and Cretaceous mudstones, sandstones, conglomerate with clasts of silicic igneous rock, and mélangé that includes blocks of chert, spilitic basalt and limestone (Figure 2). Indurated, heavily faulted, and isoclinally folded rocks of probable Late Jurassic and Early Cretaceous age contain metamorphic pumpellyite, prehnite, epidote, laumontite (common), datolite, heulandite and stilbite and are locally referred to as the Waioeka terrane of the Torlesse Supergroup (Figure 3) [Coombs et al., 1976; Mazengarb and Speden, 2000; Mortimer, 1994].

3.2. Cretaceous Syntectonic Sedimentation

[8] Mudstones, sandstones and conglomerates of the Matawai Group are mostly less indurated than Torlesse Supergroup rocks, but are otherwise similar and overlie Torlesse beds with local angular unconformity [Mazengarb and Harris, 1994; Mazengarb and Speden, 2000]. The entire sequence is interpreted to have been deposited in a tectonically active marine fore-arc shelf basin and trench slope [Crampton, 1996; Mazengarb and Harris, 1994; Mazengarb and Speden, 2000; Speden, 1975; Wellman, 1959]. There is probably no regional unconformity that separates the Torlesse and Matawai groups, and an overlap in age between the two groups is indicated by the occurrence of index fossils with ages 108.4–117.5 Ma in both groups [Crampton et al., 2004] and confirmed by SHRIMP U/Pb and fission track ages as young as circa 100 Ma from Torlesse zircons [Cawood et al., 1999; Kamp, 1999].

[9] Ruatoria Group sediments are correlative in age to the Matawai Group, but are only exposed in the eastern part of the region, where they are thought to be allochthonous (see below and Figures 2 and 3). The Matawai and Ruatoria groups (circa 118–84 Ma) show a general trend from shelf or upper slope depositional environments in the west to deeper and more distal deep-water fans (trench settings) in the east [Mazengarb and Harris, 1994; Moore, 1988b]. Eastern domains apparently do not record the older (118–100 Ma) deformation events seen farther west, where successive deformation events are associated with a progressive shallowing of inferred depositional environments from deep-water fans to upper slope facies with time [Mazengarb and Harris, 1994]. Silicic tuffs are present within the Matawai Group [Mazengarb and Speden, 2000].

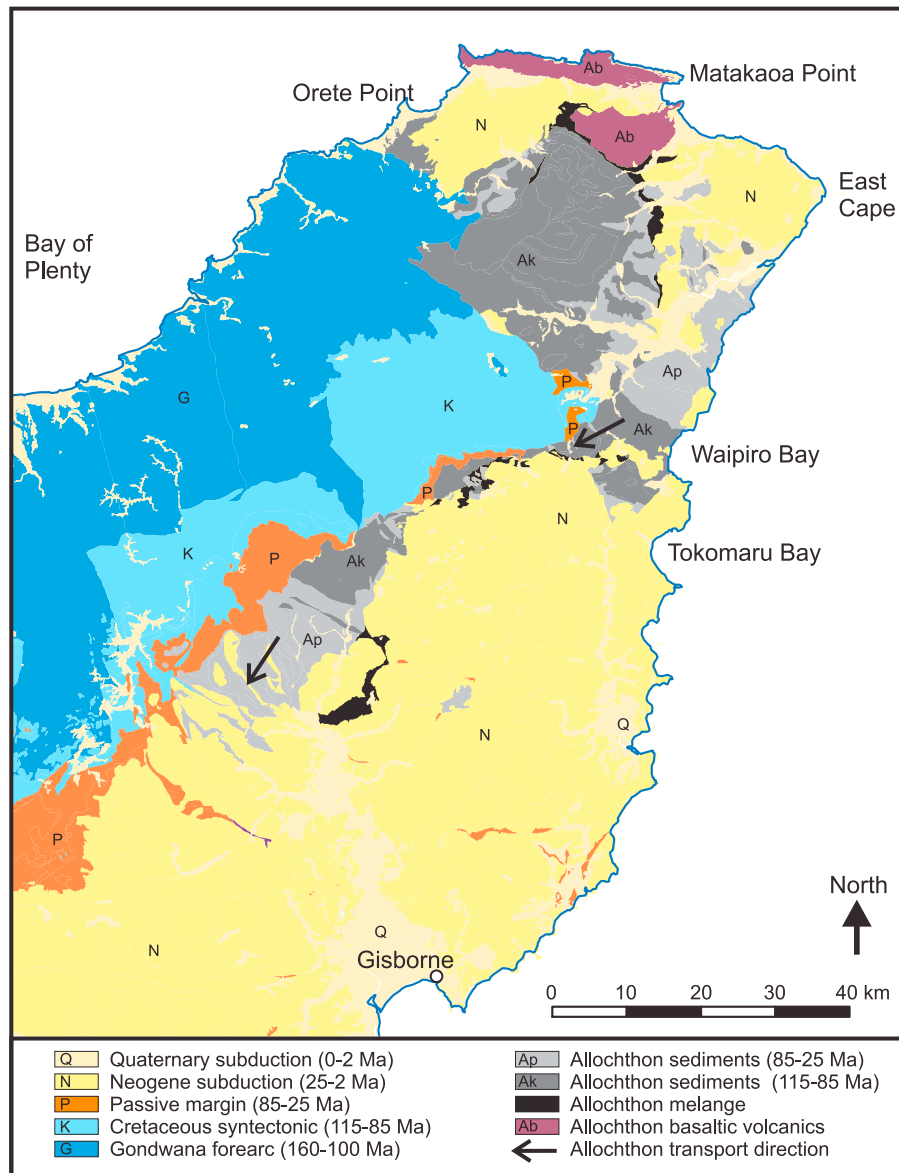


Figure 2. Geology of onshore Raukumara Peninsula [Mazengarb and Speden, 2000] showing autochthonous units: Torlesse Supergroup (Gondwana fore-arc sediments); Matawai Group (Cretaceous syntectonic megasequence); amalgamated Tinui and Mangatu Groups (passive margin megasequence); and amalgamated Tolaga and Mangaheia groups and Quaternary sediments (Neogene megasequence). The East Coast Allochthon is differentiated into Matakaoa volcanics; melange; Ruatoria Group sediments (115–85; correlatives of the Matawai Group); and amalgamated Tinui and Mangatu groups (85–25 Ma). Allochthon transport direction is shown for southern and central exposures, where detailed structural analysis has been completed [Rait *et al.*, 1991; Stoneley, 1968]. See Figure 3.

Stratigraphic relationships above and below the unconformity that defines the top of the Matawai Group demonstrate that Cretaceous folding locally continued until at least 84–86 Ma [Crampton *et al.*, 2004; Mazengarb and Harris, 1994; Mazengarb and Speden, 2000].

3.3. Late Cretaceous and Paleogene Passive Margin

[10] Marine mudstones with subordinate siltstones and sandstones were deposited in shelf and slope environments

between circa 85 Ma and circa 25 Ma and these strata are generally concordant and only gently deformed, with an inferred Neogene age of deformation, suggesting a passive margin setting for the depositional interval [Field and Uruski, 1997; Mazengarb and Speden, 2000; Moore *et al.*, 1986].

[11] The oldest sediments within this megasequence (basal Tinui Group e.g., Tahora Formation) contain fine-grained sandstone facies with a typical thickness of ~100 m, though the thickness may reach 500 m in western Raukumara

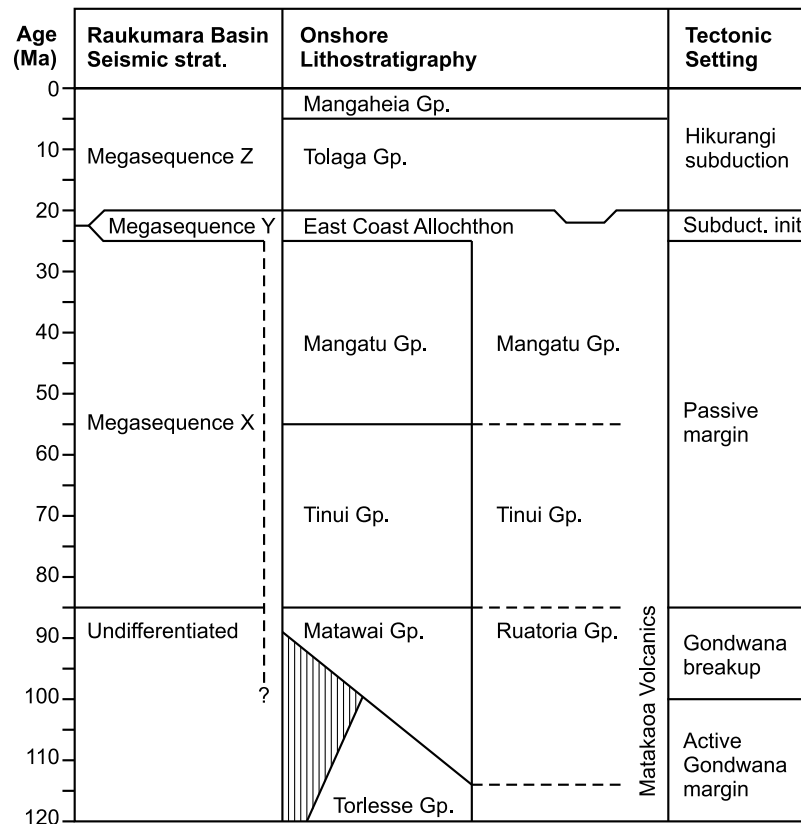


Figure 3. Correlation of seismic stratigraphy with onshore lithostratigraphy.

Peninsula (e.g., coastal and inner shelf facies of Maungataniwha Member) and is transitional with interbedded siltstones farther east (outer shelf or slope facies of Mutuera Member) [Crampton and Moore, 1990; Field and Uruski, 1997; Isaac et al., 1991]. This sandy basal unit is overlain by 300–600 m of siliceous mudstone (Whangai Formation) that is inferred to thicken and become more calcareous in the east (within the East Coast Allochthon – see below); the mudstone is mostly inferred to have been deposited in deep water (>200–400 m) and contains rare debris flows [Field and Uruski, 1997; Lillie, 1953; Moore, 1988a]. The uppermost part of the Tinui Group is a thin (~20 m) black shale (Waipawa Formation) of late Paleocene age that has high (typically 2–6%) total organic carbon [Hollis et al., 2005; Killops et al., 2000; Moore, 1989].

[12] A further 600 m thickness of mud-rich sediments (Mangatu Group) were deposited at midbathyal depths (>400 m) during Eocene and Oligocene time [Field and Uruski, 1997]. Eocene mudstones (Wanstead Formation) are commonly calcareous and glauconitic, and locally contain a relatively high proportion of smectite; glauconitic Eocene sandstones are also locally present. Oligocene sediments (Weber Formation) are calcareous, alternating, glauconitic sandstone and mudstone, and bioturbated calcareous massive mudstone [Field and Uruski, 1997; Mazengarb and Speden, 2000; Moore et al., 1986].

3.4. East Coast Allochthon

[13] Rocks older than Miocene in the north and east of Raukumara Peninsula are inferred from structural mapping to be allochthonous [Mazengarb and Speden, 2000; Rait et al., 1991; Stoneley, 1968]. Fault-bounded rock slices of what is referred to as the East Coast Allochthon are imbricated and internally deformed, and it is thought they were emplaced southwestward by tens or even hundreds of kilometers of displacement along low-angle detachment faults [Rait et al., 1991].

[14] Correlative rock types for most of the in-place (autochthonous) sedimentary units (described above) can be found within the allochthon, along with some additional rock types (Figures 2 and 3). Of particular note are the Matakaoa Volcanics, which are primarily subalkaline and tholeiitic basaltic eruptive facies that are exposed near the northern tip of Raukumara Peninsula (Figure 2). Attempts to K/Ar date Matakaoa Volcanics have so far produced ages that are younger than the ages of intercalated sediment, which is inferred from foraminifera and radiolaria to have late Early Cretaceous (Albian; 112–100 Ma), Late Cretaceous and Paleocene ages; and so it is inferred that radiometric ages were partially reset during deformation [Aita and Sporli, 1992; Brothers and Delaloye, 1982; Sporli and Aita, 1994; Strong, 1976; Strong, 1980]. It has been postulated, based upon geochemical comparisons, that the Matakaoa Vol-

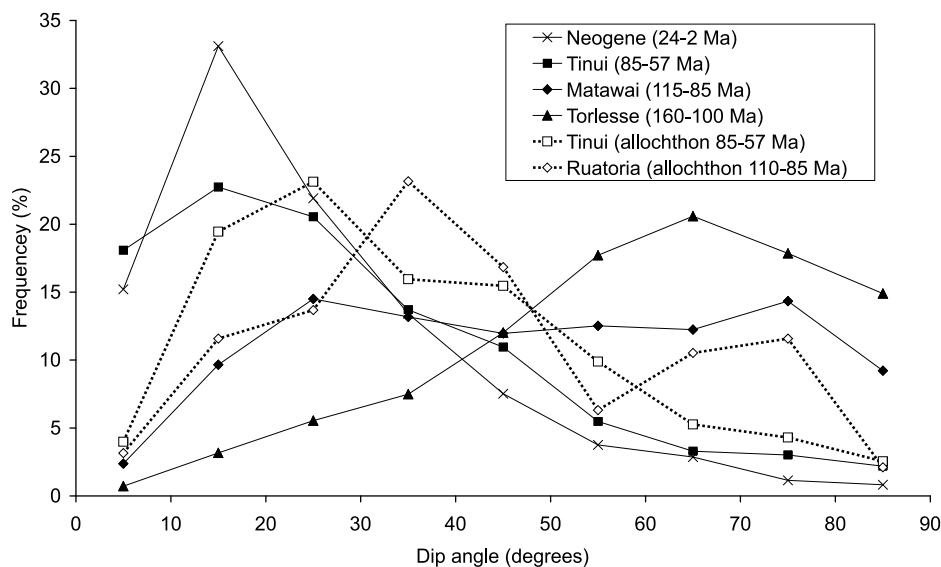


Figure 4. Histogram of sedimentary dip angles from onshore Raukumara Peninsula autochthonous (in place) Neogene ($N = 1223$), Tinui Group ($N = 365$), Matawai Group ($N = 1813$), and Torlesse Supergroup ($N = 1389$) sedimentary rocks; and allochthonous Tinui Group ($N = 627$) and Ruatoria Group ($N = 94$) sediments [Mazengarb and Speden, 2000]. Proportion of localities with overturned or transposed beds are 2%, 11%, and 10% for autochthonous Tinui, Matawai, and Torlesse groups, respectively; and 10% and 36% for allochthonous Tinui and Ruatoria groups, respectively. See Figures 2 and 3.

canics are fragments of the Hikurangi Plateau that have been accreted to the fore arc by subduction processes. The Hikurangi Plateau probably formed at circa 122 Ma, but has numerous younger seamounts erupted on to it [Mortimer and Parkinson, 1996; Wood and Davy, 1994].

[15] The timing and environment of allochthon emplacement are constrained by stratigraphic observations. The youngest preemplacement sediments (Weber Formation) are biostratigraphically dated as 25–22 Ma (Waitakian stage); the oldest sediments deposited in “piggyback” basins above the allochthon (e.g., Whakai Formation) are biostratigraphically dated as 22–16 Ma (Otaian to Altonian stages); and sediments dated at 25–19 Ma (Waitakian to Otaian stages) are tuffaceous in places and commonly contain coarse blocks of older sediment, rounded pebbles of basalt and gabbro, and hence some are inferred to be synemplacement deposits [Field and Uruski, 1997; Mazengarb and Speden, 2000].

3.5. Neogene Subduction Margin

[16] There was a profound change in depositional environment during and after emplacement of the East Coast Allochthon. Oligocene sediments that predate allochthon emplacement are predominantly clay-rich pelagic mudstone and limestone (above), whereas the Miocene (Tolaga Group) and Pliocene (Mangaheia Group) sedimentary sequence is much thicker and composed of marine sandstone, siltstone, and mudstone with minor conglomerate, limestone and reworked tuffaceous deposits [Field and Uruski, 1997; Mazengarb and Speden, 2000]. The Neogene sequence

represents a range of marine shelf and trench slope depositional environments and is characterized by abundant terrigenous clastic and minor volcanoclastic sediment input, consistent with the onset of significant Australia-Pacific plate displacement through central New Zealand and the local establishment of a subduction plate boundary with a volcanic arc [Cande and Stock, 2004; Herzer, 1995; Rait et al., 1991].

3.6. Onshore Structure

[17] Neogene sediments are gently or moderately dipping (Figure 4) and folded about NNE–SSW axes that are subparallel to the modern plate boundary [Mazengarb and Speden, 2000]. Neogene shortening of the fore arc represents only a very small proportion of the total plate shortening, which is mostly accommodated near to the subduction interface [Nicol et al., 2007; Nicol and Wallace, 2007]. Uplift of the Raukumara ranges is inferred to have been primarily driven by crustal underplating near the subduction interface or changes in the type of lithosphere being subducted, rather than through widespread faulting and crustal thickening associated with large-scale pure shear of the overriding plate [Eberhart-Phillips and Reyners, 1999; Reyners et al., 1999; Uruski et al., 2006; Walcott, 1987; Wilson et al., 2007].

[18] The Matawai Group (115–85 Ma) was deposited during a phase of Cretaceous deformation and beds were progressively tilted as further deposition occurred [Mazengarb and Harris, 1994]. This has resulted in a broad range of observed dips (Figure 4) that depend upon stratigraphic

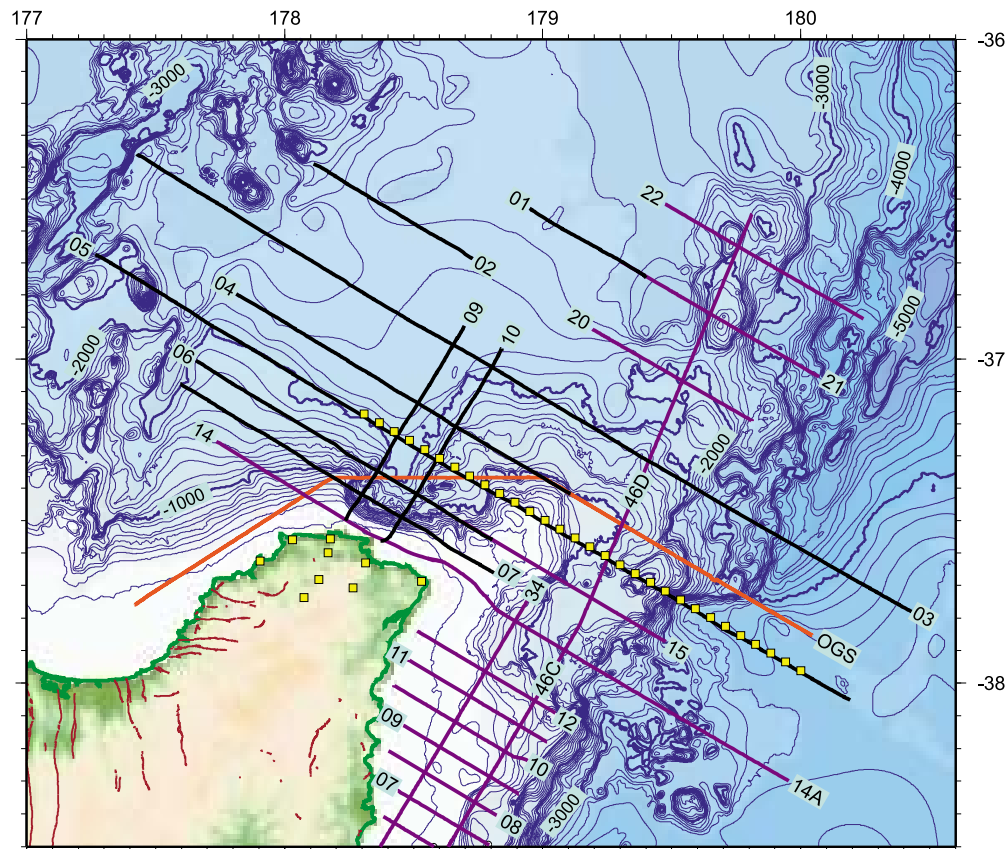


Figure 5. Location of RAU07 (black), 05CM (purple), and OGS90 (orange) surveys; labels indicate line numbers. Yellow squares show locations of onshore and ocean bottom recording stations. Bathymetric contours are at 100 m increments [CANZ, 2008].

age and location. In contrast, Torlesse Supergroup sediments (160–100 Ma) are predominantly steeply dipping (Figure 4). This may partially be the result of deformation that predates deposition of the Matawai Group, but it could also be that the distribution of Torlesse bedding orientations represents an end point for the deformation style that occurred during Matawai Group deposition, i.e., the earlier deformation was completely overprinted.

[19] Emplacement of the East Coast Allochthon in latest Oligocene and earliest Miocene times (25–19 Ma) was associated with large displacements of weakly lithified sediments along low-angle faults and internal shortening of nappes along thrust faults and folds [Mazengarb and Speden, 2000; Rait *et al.*, 1991; Stoneley, 1968]. Despite large inferred displacements, most beds within the allochthon have gentle or moderate dips (typically 15–45°; Figure 4). The deformation event caused an increase in average dip of the previously undeformed Tinui Group, and a reduction in average dip of Ruatoria Group beds (correlative to the Matawai Group), which were also deformed during Cretaceous time. The event also produced overturned nappes and isoclinal folds: 10% of Tinui Group and 36% of Ruatoria Group localities have overturned bedding.

[20] The allochthon is inferred to have been emplaced toward the southwest in the southern and central areas,

where its structure has been studied in detail (Figure 2) [Kenny, 1984; Rait *et al.*, 1991; Stoneley, 1968]. Melange was formed during emplacement of the East Coast Allochthon and appears best developed near the top of the allochthon (Figure 2). Local structural mapping demonstrates that allochthonous material, particularly melange and Wanstead Formation mudstone, is weak and associated with Neogene diapiric deformation and Quaternary slope failure [Mazengarb and Speden, 2000].

4. Seismic Reflection Data

[21] We have used results from three MCS surveys (Figure 5), supplemented by older data, to map and understand Raukumara Basin. The RAU07 survey was acquired in 2007 using a 86.5 l (5280 cu in) source and 7.3 km streamer, with 37.5 m shotpoint spacing and 13.3 s record length for all lines except RAU07-05, which had 50 m shotpoint spacing and 15.3 s record length. Details of data processing are given elsewhere (Fugro Seismic Imaging, Raukumara Basin 2D Seismic Survey—RAU07, New Zealand unpublished open file petroleum report 3743, 2007). The 05CM data set was acquired in 2005 using a 67.8 l (4140 cu in) source and streamer that varied between 12 km and 4 km (due to shark attacks), with 37.5 m

shotpoint spacing and 8 s or 12 s record length (G. Maslen, Fast track seismic processing of selected data from the 05CM Survey offshore east coast New Zealand, unpublished open file petroleum report 3182, 2005; Multiwave, 05CM 2D seismic survey, offshore east coast–North Island, New Zealand, unpublished open file petroleum report, 3136, 2005). The OGS90 line was acquired in 1990 using a 45.2 l (2756 cu in) source and 3 km streamer, with 50 m shotpoint spacing and 16 s record length [Davey *et al.*, 1997], and was reprocessed with the RAU07 data (Fugro Seismic Imaging, unpublished report, 2007).

5. Seismic Reflection Stratigraphy

5.1. Megasequence Z

[22] The upper surface of megasequence Z is the seabed; and the lower surface is defined in central parts of the basin as being the lowermost reflector within a unit of continuous or semicontinuous reflectors that becomes thicker toward the northwest; elsewhere the base is correlated geometrically to where it is defined in central or eastern parts of the basin (Figure 6). Reflectors near to the base of the unit are mostly continuous and northwest dipping, have high amplitude, and have a geometry that fans and thickens toward the center of the basin. Onlap and downlap relationships within the unit are interpreted as slope and basin floor fans. Toward the top of the megasequence there are several units characterized by discontinuous reflectors or that have no coherent internal acoustic structure, and in some places have a reverse polarity reflection at the base; we interpret these as internally chaotic mass transport deposits. The uppermost units of this type in central and southern parts of the basin are interpreted to be associated with the Matakaoa Submarine Instability Complex, which was active from circa 600 ka to 40 ka and has left notable erosional scarps and stranded blocks of debris at the seabed [Lamarche *et al.*, 2008].

[23] The eastern limb of the basin underlies East Cape Ridge, which is adjacent to the Hikurangi trench slope and active plate boundary (Figure 7). Strata of the eastern basin limb dip WNW toward the center of the basin, as does the submarine topographic slope, where several modern and ancient submarine slope failures and associated deposits are identified. A complex and faulted stratigraphy of angular unconformities is identified within megasequence Z on East Cape Ridge. The trench slope is highly faulted and poorly imaged, and we agree with previous workers that normal faulting is widespread on the upper part of the slope and across some parts of East Cape Ridge [Collot and Davy, 1998; Collot *et al.*, 1996]. On the basis of improved seismic reflection coverage and a detailed bathymetric grid [CANZ, 2008], we have not been able to confirm the presence of major linear strike-slip faults on the upper part of East Cape Ridge, as have been previously postulated [Collot and Davy, 1998; Davey *et al.*, 1997], though significant faults (with curved geometry) are imaged near the crest of the ridge and we have not made a detailed study of the trench slope.

[24] Reflectors in the upper half of megasequence Z have higher amplitude and frequency content at the western basin

margin than is typical for the central basin, and are semi-continuous and variable in character. Sequences thin and downlap toward the basin center, and we interpret these sequences as being associated with arc volcanoclastic input. Megasequence Z becomes indistinct at some places along the northwestern edge of the basin, where there is topographic and geothermal-geochemical evidence for active volcanism [de Ronde *et al.*, 2001, 2007; Wright *et al.*, 2006]. We interpret the loss of coherent reflectors within megasequence Z at the northwestern edge of the basin to be locally associated with volcanic and hydrothermally altered rocks adjacent to active volcanic centers.

[25] At the southern margin of the basin, megasequence Z has been uplifted and strata dip northward toward the basin center (Figure 8). Repeated slope failures associated with this uplift are responsible for the Matakaoa Erosional Complex, which is the source of debris avalanche deposits that are mapped in central parts of the basin [Lamarche *et al.*, 2008].

[26] The thickness of megasequence Z increases toward the north from ~1 s two-way traveltime (twt) near the shelf edge to >2.5 s twt (2–3 km thickness) in northern parts of the basin (Figure 9). The southern margin has reduced thickness due to both a smaller accommodation space and erosion because of late Neogene uplift. The base of megasequence Z rises gently to the south and to the east, and is offset by normal faults at its western margin in the Havre Trough (Figures 7 and 10). The Tokata Anticline [Lamarche *et al.*, 2008] deforms megasequence Z and is mapped along the base of the western edge of East Cape Ridge (Figure 10), where it is locally faulted (Figure 7). An array of minor tensional faults are mapped in the northeastern part of the basin, and several significant normal faults are mapped near to the crest of East Cape Ridge (Figure 10).

5.2. Megasequence Y

[27] Megasequence Y is only present between East Cape Ridge and the center of the basin. It is defined as a unit of chaotic and variably dipping discontinuous reflections (Figure 6) with a typical thickness of ~1 s twt, and pinching out toward the center of the basin (Figures 6, 7, and 9). Coherent blocks of dipping reflectors within the unit are interpreted as large blocks of sedimentary material. Numerous small faults are interpreted that bound these blocks and in other places the unit appears acoustically chaotic or transparent, which we interpret to be highly deformed sedimentary or volcanic material. The top of the unit has numerous small “piggyback” basins with continuous high-amplitude reflections that typically dip toward the center of each depression. We interpret megasequence Y as a single very large submarine slope failure with depressions on its top being filled with synemplacement reworked sediment.

[28] Megasequence Y dips northwestward beneath the flank of East Cape Ridge (Figure 10) and is subparallel to the seabed, dropping ~2 km beneath the ridge and central basin. Numerous small faults within megasequence Z, mostly normal faults, appear to root into megasequence Y. We also speculate that the Tokata Anticline, visible at the

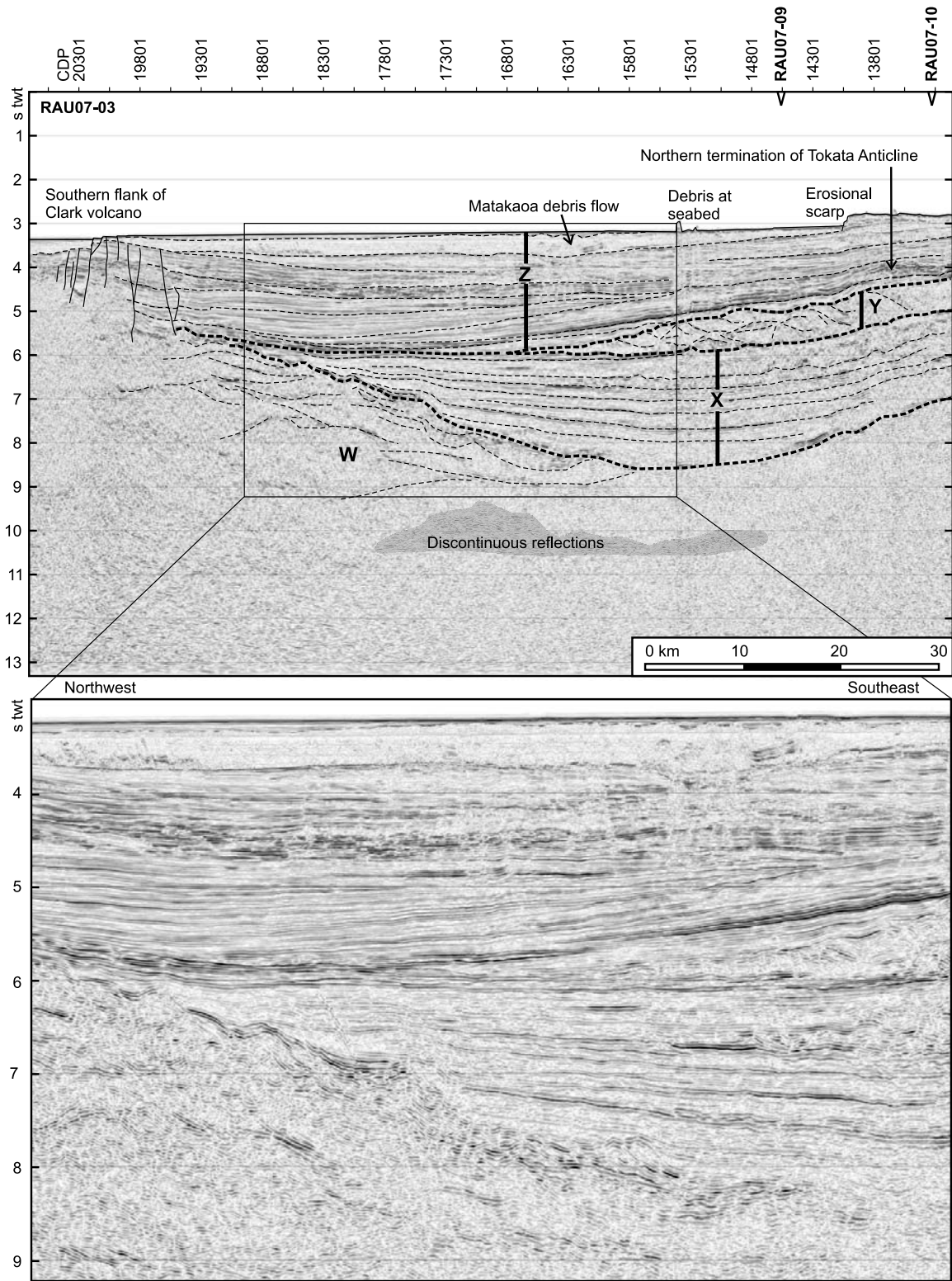


Figure 6. Seismic stratigraphy (megasequences X, Y, Z labeled) illustrated on seismic reflection section RAU07-03. The area labeled W is the wedge-shaped unit of coherent but semicontinuous reflections inferred to be the Cretaceous Gondwana fore-arc trench slope (see main text).

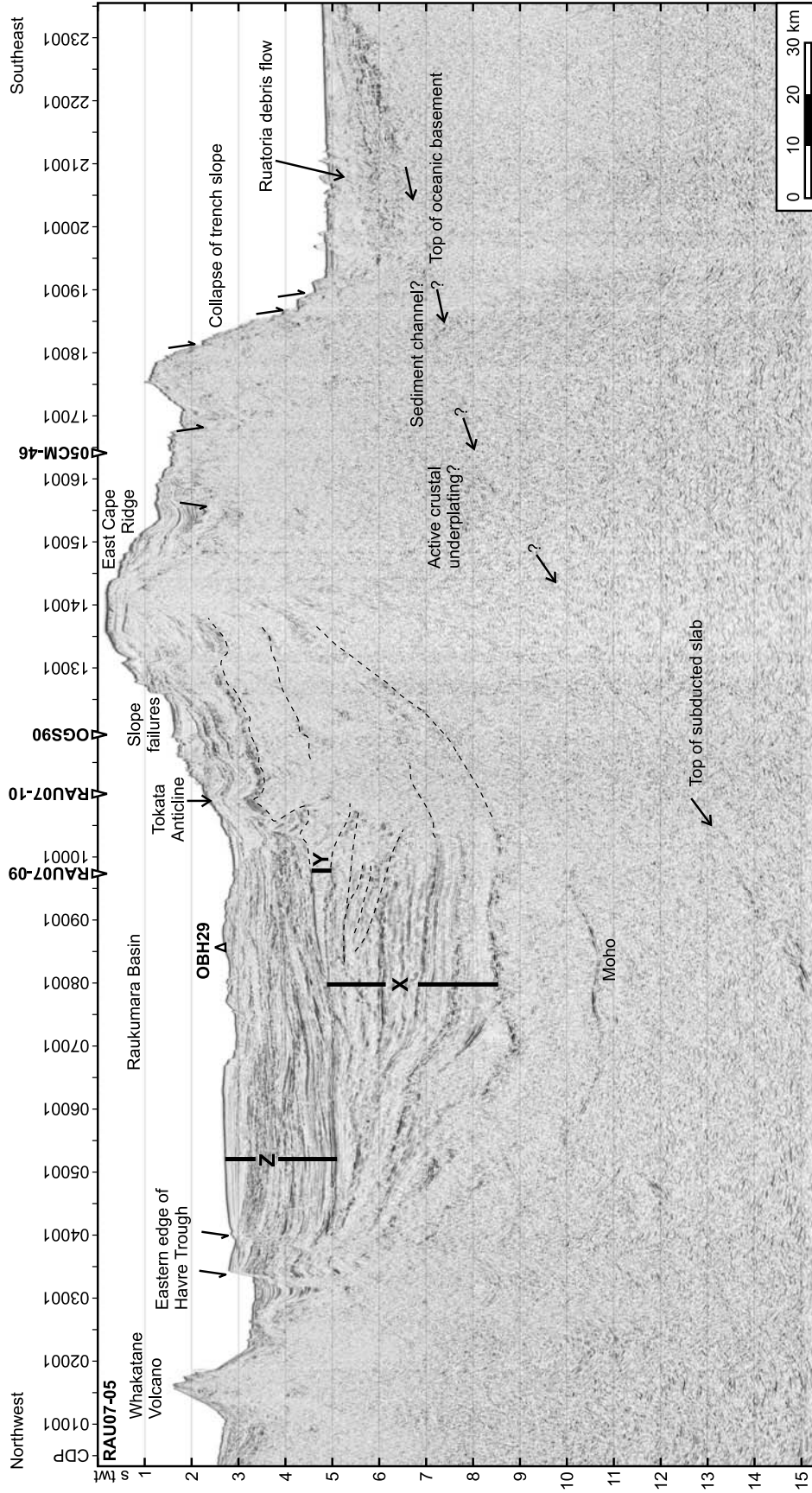


Figure 7. Seismic reflection line RAU07-05 illustrating downdip structure of Raukumara Basin. Location of OBH29 is shown (Figure 11).

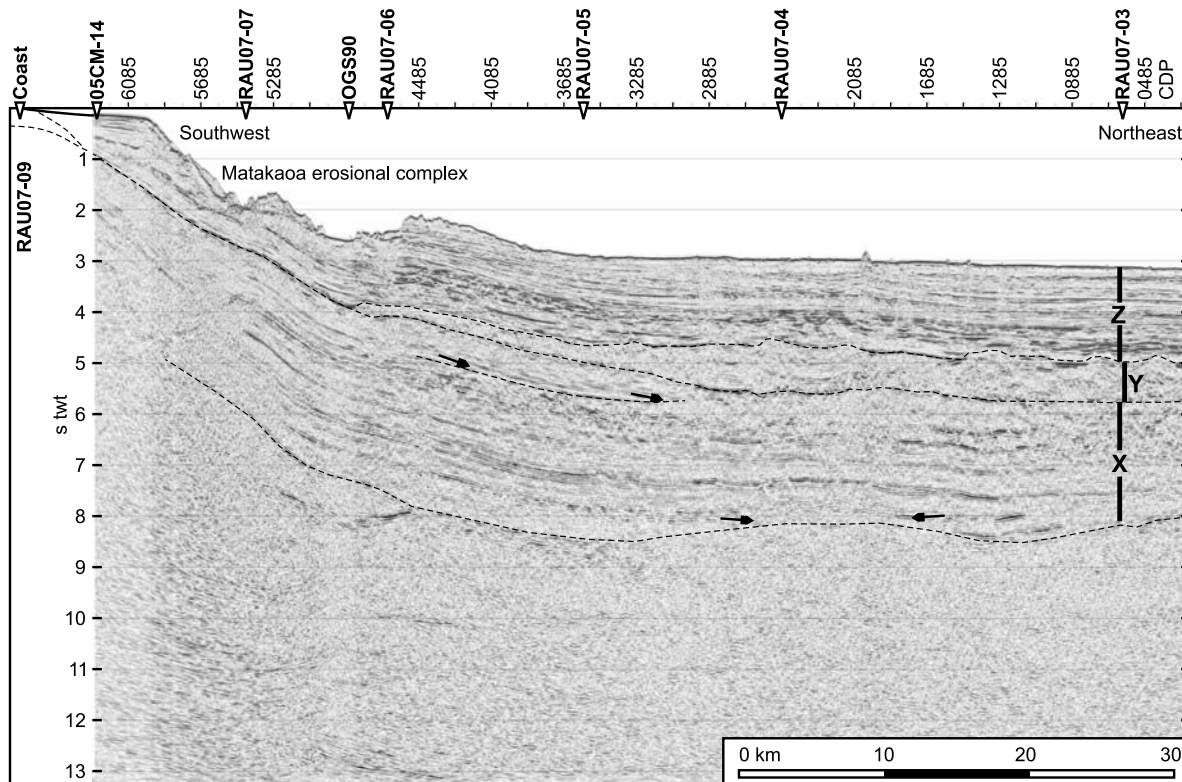


Figure 8. Seismic reflection line RAU07-09 showing along-strike structure of Raukumara Basin. Small arrows show downlap relationships discussed in text. Matakaoa Volcanics are exposed on the coast and are considered allochthonous, but it is not known if the allochthon offshore is precisely the same stratigraphic age. An alternate correlation with the base of the Matakaoa Volcanics is the marked sequence boundary with northward downlapping relationships above it.

base of the slope (Figures 6, 7, and 10), and the faulted anticline on line RAU07-05 may be part of a large Quaternary slope failure detaching through megasequence Y and driven by the topography of East Cape Ridge.

[29] Megasequence Y also dips northward away from the coast, but thins and is not present offshore near to the coast. However, there is a significant downlapping sequence boundary within the upper part of megasequence X directly beneath (Figure 8). This is discussed further when offshore-onshore correlations are considered.

5.3. Megasequence X

[30] The top of megasequence X is defined as the first continuous or semicontinuous reflector below megasequence Y, or by the equivalent stratigraphic level at which megasequence Y was emplaced (Figure 6). This corresponds in the center of the basin to the deepest in a packet of high-amplitude reflections at the base of megasequence Z; a packet that we interpret as being the sedimentary unit that was deposited at the time megasequence Y was emplaced.

[31] Megasequence X is characterized in central and western parts of the basin by continuous or semicontinuous reflectors that dip and fan toward the east, causing the unit to increase in thickness from <1 s twt near the margin of the

Harve Trough to 3–4 s twt (~5–8 km) in the center of the basin (Figure 9). There are at least five sequences within megasequence X that can be distinguished on the basis of reflection amplitude, onlap, and sequence geometry. The base of megasequence X is defined by the deepest continuous or semicontinuous reflector with the unit.

[32] Megasequence X is less well imaged beneath East Cape Ridge, on the east flank of the basin, where west dipping high-amplitude discontinuous reflectors are probably continuous with megasequence X in the central basin and suggest the unit has a similar or slightly lower thickness (Figure 9). The lower part of megasequence X has been deformed into northeast trending open folds along the western basin margin, suggesting minor convergent deformation before emplacement of megasequence Y.

5.4. Acoustic Basement

[33] Acoustic basement is defined as everything below megasequences X-Z (Figure 6). In eastern parts of the basin there are continuous high-amplitude reflectors and packets of coherent reflectors that we interpret as faults and tilted or fault-bounded sediment packages. In the central basin, most units show several high-amplitude semicontinuous reflections at 8–9 s twt that we infer to be a significant acoustic impedance contrast at the base of the sedimentary section

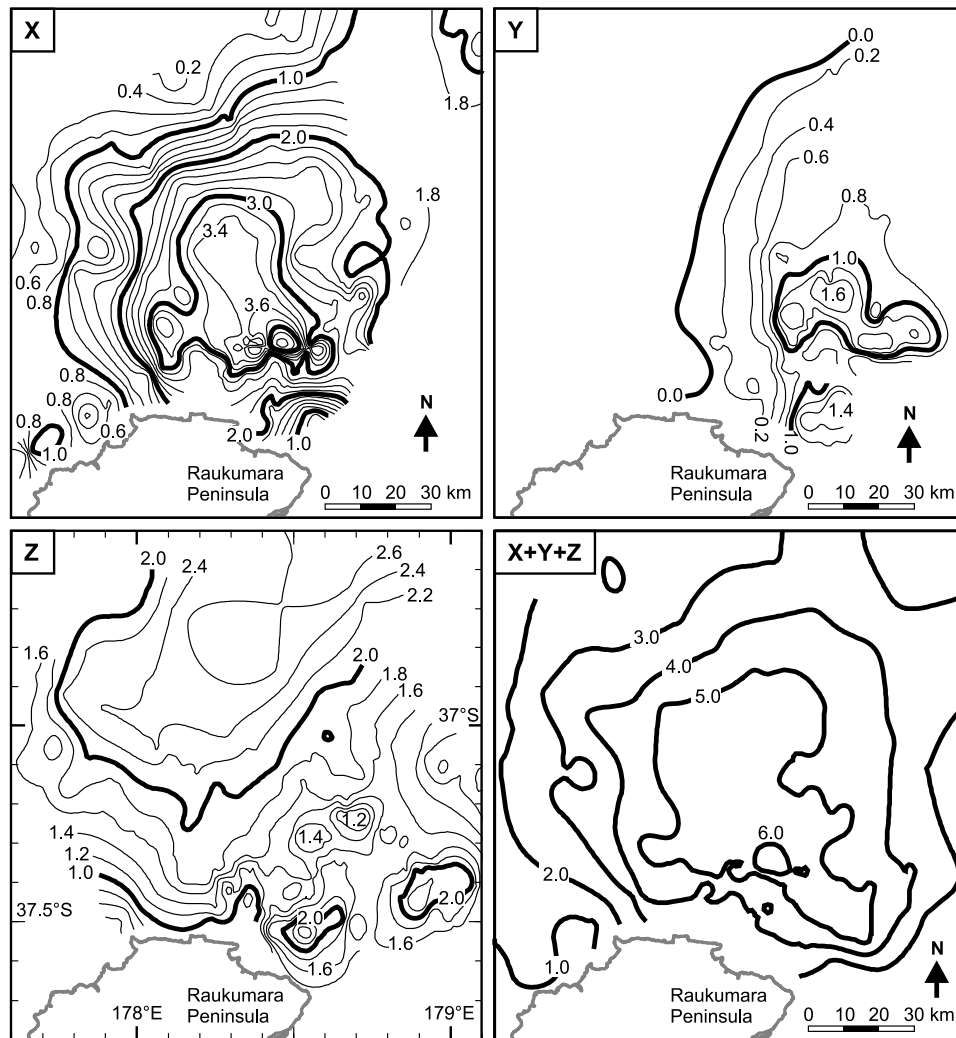


Figure 9. Isopach maps of megasequences X, Y, Z and total sediment thickness (X + Y + Z) in s twt.

(acoustic basement). We identify individual high-amplitude semicontinuous reflections or packets of discontinuous reflections at 10–11 s twt beneath the center of the basin (e.g., Figure 6), that we associate with the Moho; and we show this with refraction data (below). West dipping reflections between 13 and 15 s twt are identified beneath the central basin on line RAU07-05 (Figure 7), which appear geometrically continuous and aligned with zones of enhanced reflectivity (coherent reflections) beneath East Cape Ridge, that are in turn aligned with the top of the subducted slab where it is imaged at the Hikurangi Trough. Hence, we interpret the reflections at 13–15 s twt as the top of the subducted slab.

6. Active Source Seismic Refraction Constraints on Crustal Structure

[34] In a survey by R/V *Sonne* in 2007 (MANGO; cruise SO192) shots from a 64 l (3905 cu in) air gun source were recorded using ocean bottom seismometers (OBS) and ocean

bottom hydrophones (OBH). The shots were fired along a line coincident with RAU07-05, but ocean bottom instrumentation was restricted to central and eastern parts of the line (Figure 5). We present here a preliminary interpretation from the most western instrument, OBH29 (Figures 5 and 11).

[35] A velocity forward model was constructed for OBH29 (Figure 11) on the basis that significant boundaries (reflections) and units of distinct seismic reflection character are identified from MCS data (above), and units with a similar geometry have previously been suggested from a combined interpretation of gravity data and line OGS90 [Davey *et al.*, 1997]. Our results show that our hypotheses for the geometry of the base of the basin and crust inferred from normal incidence reflections on line RAU07-05, combined with fairly typical velocities for sediment, lower crust, and mantle are consistent with observed refracted arrivals. We identify lower crust and mantle refracted arrivals; and obtain crustal velocities of 6.5–7.5 km/s and an uppermost mantle velocity of 8.0–8.2 km/s. The model Moho depth is 17 km beneath sea level and the subducted slab is located at 30–40 km (Figure 11).

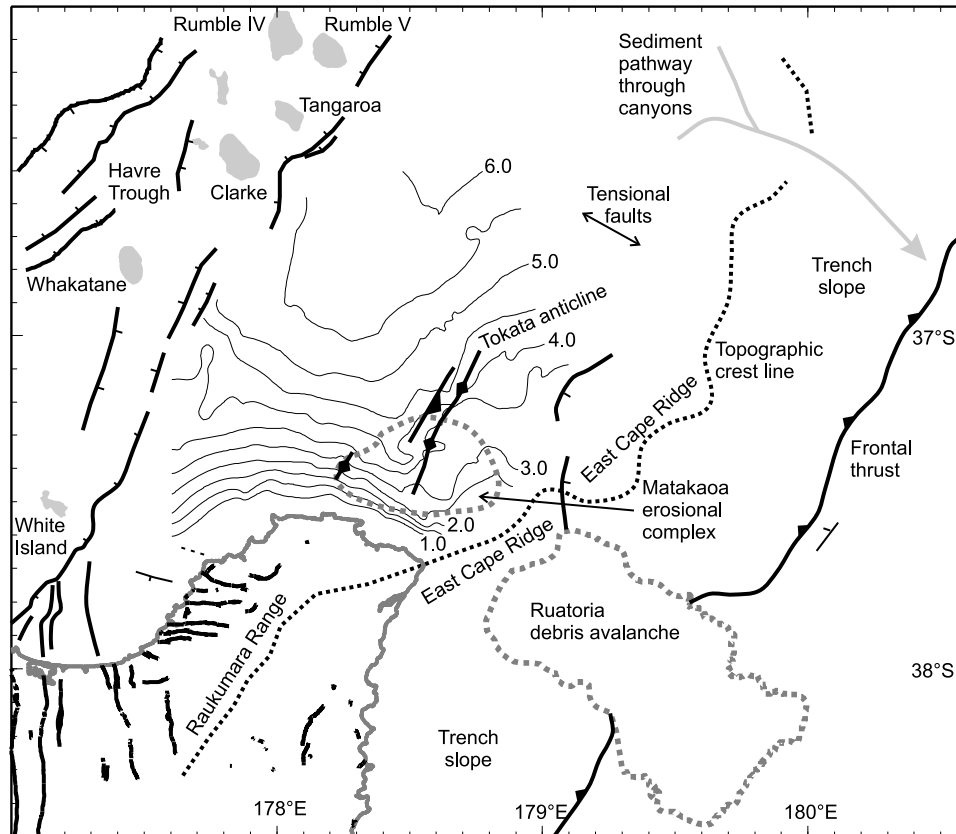


Figure 10. Map of basin structure showing: contours in s twt on the base of megasequence X; thrust faults (teeth show dip direction); major normal faults (ticks show dip direction); anticlines; and locations of Quaternary volcanoes (gray fill).

[36] In addition, shots from survey RAU07 were recorded at 7 onshore locations (Figure 5) and we present a preliminary interpretation in this paper of data from two inland stations along the projection of line RAU07-09 (Figure 12). We construct a velocity forward model for these data on the basis that: 1, the velocity of the crust beneath the stations is known from earthquake 3-D V_p tomography [Reyners *et al.*, 1999]; and 2, our models should be consistent at the intersection between lines RAU07-09 and RAU07-05 (Figure 11). Using these assumptions it is possible to successfully model the refracted onshore arrivals from shots of line RAU07-09 (Figure 12).

[37] The results imply changes in crustal structure north-eastward along the line: water and sediment thickness increases by ~ 10 km; crustal (basement rock) thickness decreases by ~ 20 km; and there is an incoming mantle wedge beneath line RAU07-09 that reaches a thickness ~ 10 km above the subducted slab at the intersection with line RAU07-05.

7. Offshore-Onshore Lithostratigraphic Correlation

[38] Megasequence Y is interpreted as a large allochthonous sheet within the basin and is hence a key unit when

considering offshore-onshore correlations. This is because a large allochthonous and internally disrupted sheet of similar thickness and scale, the East Coast Allochthon, has been described and studied in detail onshore and is an obvious correlative. In addition, we can interpolate directly between the mapped position of megasequence Y and the mapped onshore allochthon using lines RAU07-09 and RAU07-10. From this we infer that megasequence Y was emplaced at about the same time as the East Coast Allochthon in latest Oligocene or/and earliest Miocene time (25–19 Ma), and we infer that megasequence Y has similar composition and internal structural style to the East Coast Allochthon.

[39] While it is not our preferred interpretation, we cannot rule out the possibility that onshore and offshore allochthons were emplaced as separate entities at slightly different times. If this were the case, then we speculate that the onshore allochthon was emplaced slightly earlier. This is based upon the identification of reflectors downlapping northward onto a sequence boundary directly beneath megasequence Y (Figure 8) that could be interpreted as a synemplacement deposit associated with allochthonous rocks exposed onshore at Matakaoa Point. Such a correlation would make it geometrically easier to explain the extensive area of allochthonous material (Matakaoa Volcanics) exposed near the coast, because the base of the rock unit would be deeper

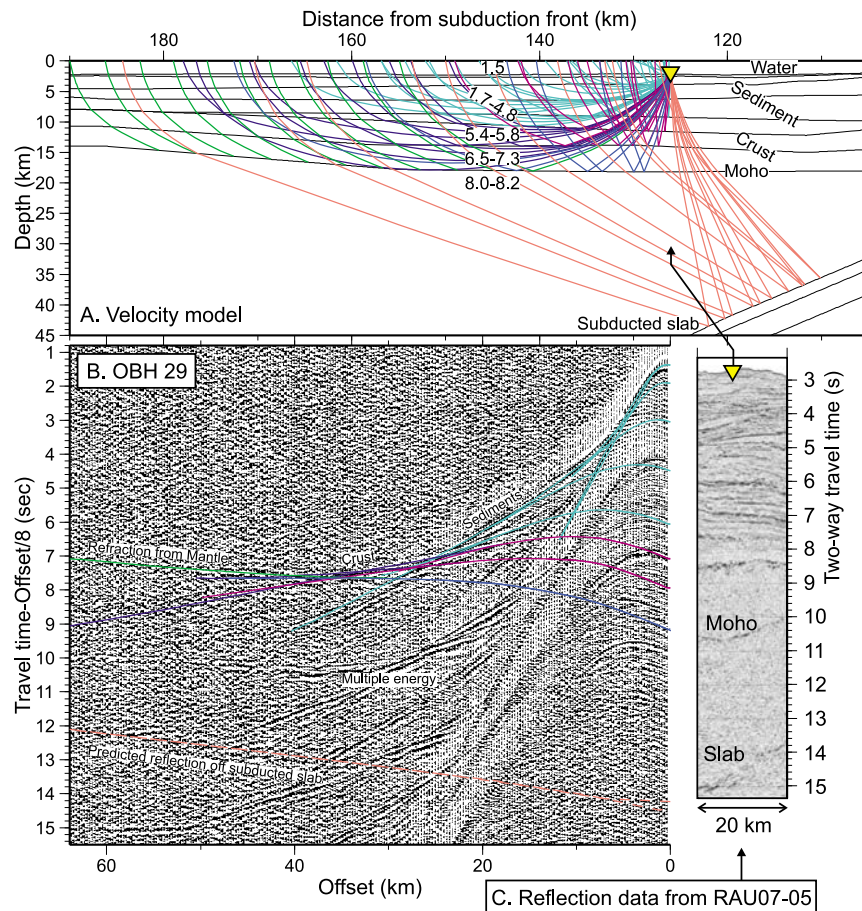


Figure 11. (a) Seismic p wave velocity (km s^{-1}) model for line RAU07-05, based on (b) receiver gather for OBH 29, which was the most western instrument deployed on voyage SO192 (see Figures 5 and 7) and has modeled arrivals indicated by colored lines. (c) Also shown is a section of the normal incidence CDP-stacked reflection record of line RAU07-05.

within the dipping stratigraphic sequence if it were emplaced earlier.

[40] It follows from our correlation of megasequence Y with the East Coast Allochthon that megasequence Z is correlative with Neogene fore-arc marine sandstones, siltstones, and mudstones (Tolaga and Mangaheia groups). It similarly follows that the upper part of megasequence X correlates with clay-rich and calcareous Paleogene mudstones (Mangatu Group). We infer a thicker Neogene sequence than a previous interpretation of line OGS90 [Davey *et al.*, 1997]; we reinterpret strata overlying a prominent angular unconformity on East Cape Ridge on line OGS90 as being within the Neogene sequence.

[41] We suggest that the angular unconformity mapped onshore that separates Cretaceous syntectonic fore arc and trench slope sediments (Matawai Group) from passive margin fine-grained sandstones and organic-rich mudstones (Tinui Group) correlates with the base of megasequence X. Our analysis of sedimentary dips measured onshore (Figure 4) supports the proposal that Matawai Group sediments are only likely to be discontinuously imaged, whereas Tinui Group sediments have a similar degree of deformation to

Neogene sediments and should, therefore, be comparably imaged. We cannot rule out a possibility that the unconformity that separates these two groups onshore may be significantly diachronous and that the base of megasequence X may be significantly older or younger than 85 Ma.

8. Gravity Model

[42] We have mapped the offshore distribution of significant sedimentary units and propose that there is a dramatic change in crustal structure within the overlying plate of the Hikurangi subduction zone north of Raukumara Peninsula. We present a 2-D gravity model along line RAU07-05 (Figure 13), to demonstrate that this independent observation is consistent with: observed topography; sedimentary architecture and the depth to the base of the crust that we have determined; the structure of the subducting Hikurangi Plateau [Davy and Wood, 1994]; and reasonable assumptions of densities for different rock types. While we acknowledge that this is a simplified consideration of the gravity field and ignores 3-D effects or complexity associated with the subducted slab, the size of modeled anomalies

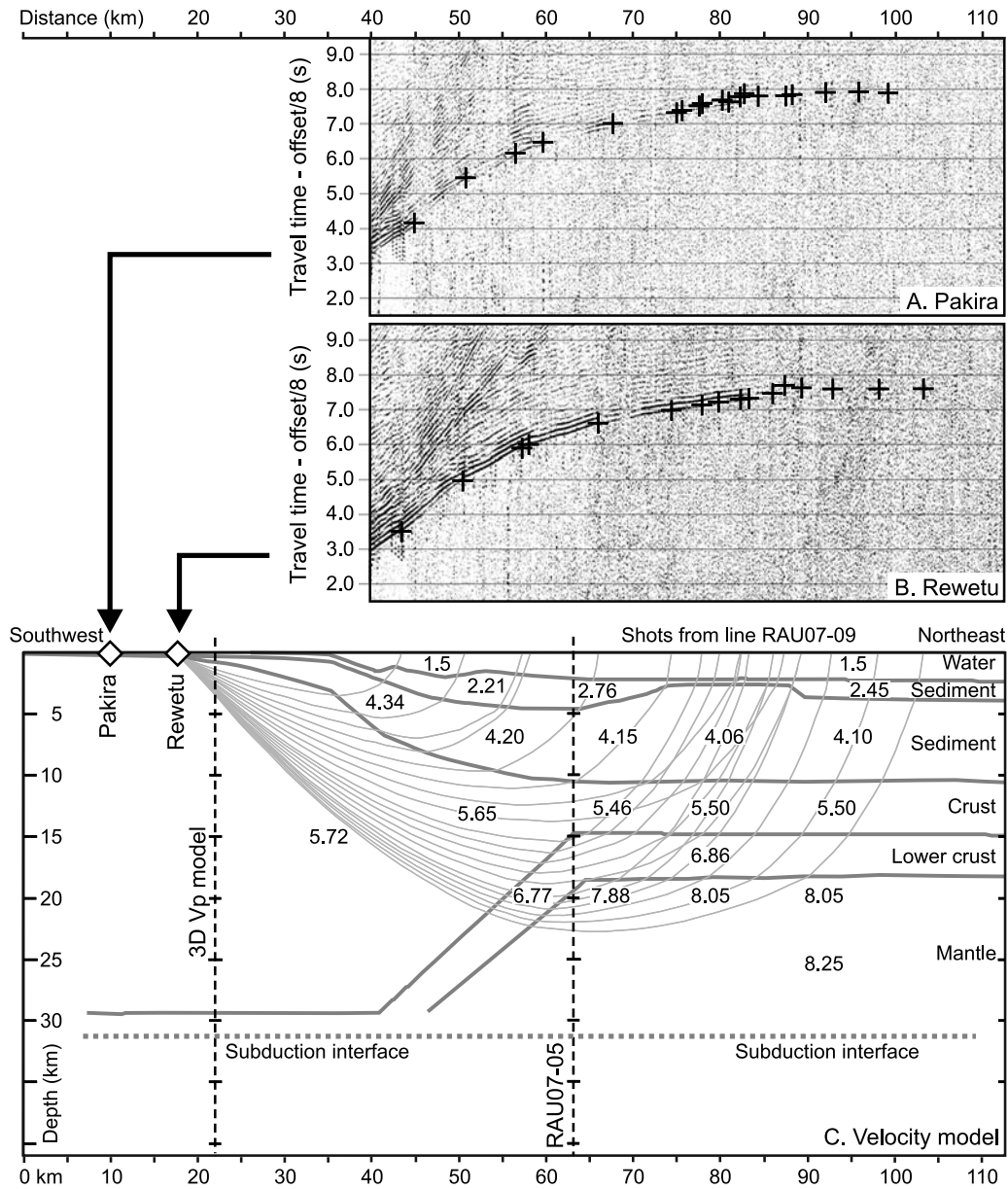


Figure 12. Onshore record of shots from line RAU07-09 and crustal structure model showing seismic velocities (km s^{-1}) and raypaths.

associated with seafloor topography, sediment thickness, and Moho topography in Raukumara Basin are large (>100 mGal), and yet it is clear from Figure 13 that it is straightforward to construct a realistic density model from our crustal model that is consistent with gravity observations. Therefore, we conclude that our crustal model is consistent with the observed gravity field.

9. Origin and Evolution of Raukumara Basin

9.1. Cretaceous Gondwana Convergent Margin (160–85 Ma)

[43] On the basis of seismic character, we identify fault-bounded sedimentary units along the western margin of

Raukumara Basin beneath megasequence X; and we correlate these with Cretaceous Matawai and Ruatoria Group marine clastic sediments that are mapped onshore [Mazengarb and Harris, 1994; Mazengarb and Speden, 2000]. In central and eastern parts of the basin, high-amplitude reflections at the top of acoustic basement are inferred as a boundary with crystalline basement rock, and in central parts of the basin, we constrain the underlying crust to have a thickness of just 6–8 km. Hence, we agree with a previous suggestion that crust in the central part of the basin has oceanic or large igneous province character and is possibly correlative to the Hikurangi Plateau [Davey *et al.*, 1997]. We, therefore, interpret the observed geometry as an east verging thrust wedge in the western basin that was emplaced above

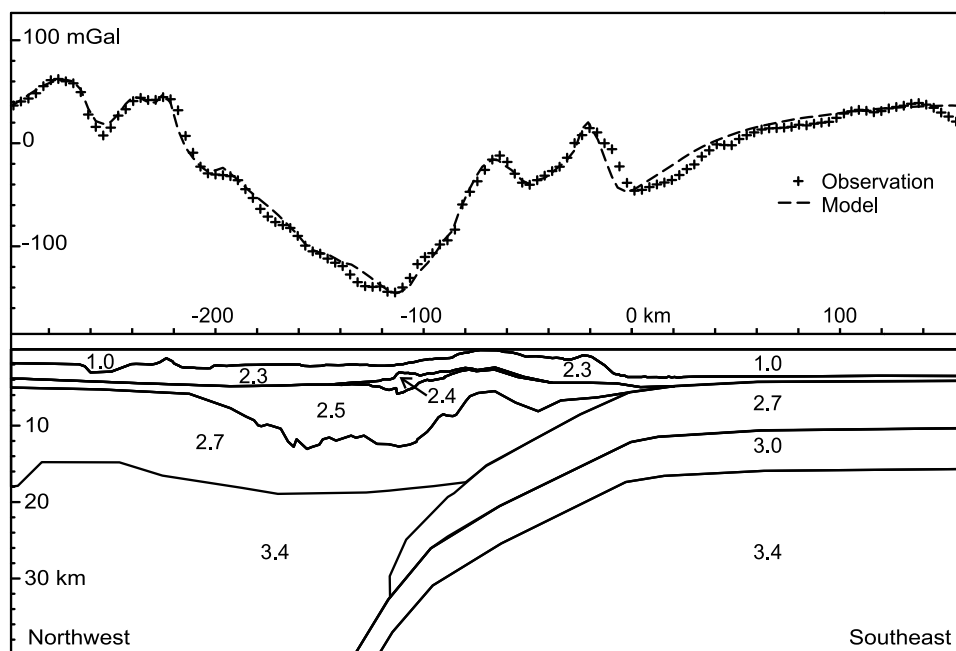


Figure 13. A 2-D gravity model along line RAU07-05 (for location, see Figure 5). Densities are shown in g cm^{-3} .

subducting oceanic crust in the central and eastern basin. The timing of cessation of Cretaceous deformation has been determined onshore to be at circa 85 Ma [Mazengarb and Harris, 1994].

[44] The tectonic history inferred by us and others [Mazengarb and Harris, 1994; Mazengarb and Speden, 2000] for Raukumara Basin and Peninsula is in marked contrast to that inferred for elsewhere in the New Zealand, eastern Australia, and Antarctic regions. The cessation of Gondwana arc-related volcanism in the New Zealand sector of Gondwana was complete by circa 105 Ma and during the interval 105–85 Ma there was widespread rift basin development (e.g., Taranaki, Great South, and Gippsland basins; Figure 14) [Cook *et al.*, 1999; King and Thrasher, 1996; Laird, 1993; Mortimer *et al.*, 1999; Waight *et al.*, 1998]. By 83–79 Ma, rifts along the southern margin of New Zealand had progressed to seafloor spreading and an isolated continent was created [Gaina *et al.*, 1998; Sutherland, 1999]. We suggest that eastern parts of Raukumara Basin preserve the Cretaceous Gondwana trench slope (Figure 14), and that this geological setting was unlike the adjacent rifted continent and was a proximal cause for the basin's atypical Cretaceous tectonic history and lack of normal-faulted basins.

9.2. Cretaceous and Paleogene Passive Margin (85–25 Ma)

[45] After cessation of Cretaceous tectonics and separation from Gondwana, most of New Zealand subsided passively, while restricted areas still underwent minor extensional faulting [Cook *et al.*, 1999; King and Thrasher, 1996; Laird, 1993]. It is likely that the regional physiography of

New Zealand during this interval was primarily inherited from the previous Cretaceous tectonic phase, with broad subsidence leading to progressive flooding of the land area. Raukumara Basin lay on the northern marine margin of New Zealand throughout this interval of northward drift (Figure 14).

[46] We correlate megasequence X with this phase of passive margin deposition. It is clear from the isopach map (Figure 9) that Raukumara Basin was a significant depocenter during this interval, and this was probably a consequence of its anomalous Cretaceous tectonic history. The total sediment thickness for this interval (~ 5 – 8 km) is one of the greatest known from the New Zealand region. This observation is significant for interpretations of past environment and sedimentary facies: it may be that there was an indentation in the margin and inherited structural control of onshore sediment pathways toward the depocenter.

[47] Although megasequence X was continuously deposited in a passive setting until circa 25 Ma, activity at the Australia-Pacific boundary started north and south of New Zealand at circa 45 Ma [Sutherland, 1995]. Rift basins of southern New Zealand were the manifestation of an extensional plate boundary that increased in extension rate farther south, where seafloor spreading was developed [Lamarche *et al.*, 1997; Sutherland, 1995; Wood *et al.*, 1996]. The occurrence of smectite-rich clays in Eocene-Oligocene sediments of Raukumara Peninsula may reflect the distal onset of arc volcanism and subduction to the north. It may be that open folding of the lower part of megasequence X along the western basin margin is related to reactivation of Cretaceous thrust faults during the Eocene onset of subduction north of New Zealand.

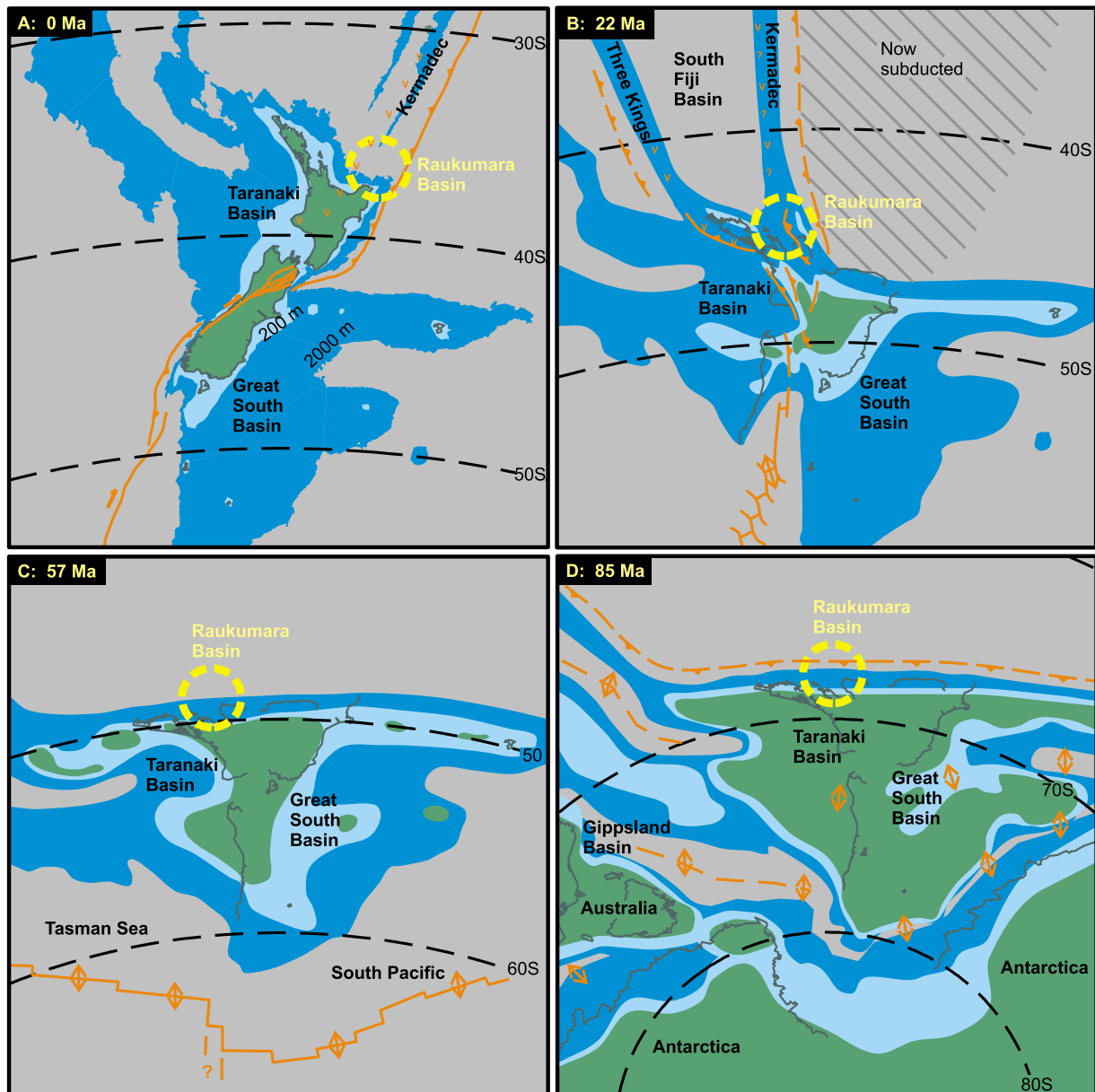


Figure 14. Tectonic evolution of Raukumara Basin. (a) Present tectonic setting with plate boundary shown in orange and the active volcanic chain marked (v). (b) Immediately after emplacement of allochthonous material into Raukumara Basin (megasequence Y) and the establishment of the modern Kermadec subduction system. (c) Passive margin deposition corresponding to megasequence X. (d) The end of Gondwana margin tectonics and establishment of the architecture of western Raukumara Basin.

9.3. Subduction Initiation and Allochthon Emplacement (25–19 Ma)

[48] There was a significant change in Australia-Pacific plate motions during the interval 30–20 Ma [Cande and Stock, 2004] that led to the onset of subduction beneath northern New Zealand. The oldest arc-related calc-alkaline volcanoes are dated at circa 24–22 Ma [Herzer, 1995], and the onset of subduction was accompanied by emplacement of large-scale allochthonous sheets [Brothers and Deloyle,

1982; Field and Uruski, 1997; Isaac et al., 1994; Mazengarb and Speden, 2000; Rait et al., 1991; Stoneley, 1968]. We identify and map an allochthonous unit within Raukumara Basin (megasequence Y) that correlates in character, stratigraphic position, and is approximately geometrically continuous with the East Coast Allochthon.

[49] We interpret the wedge-shaped unit within acoustic basement beneath the western limb of the basin (labeled W in Figure 6) to be the Cretaceous Gondwana fore arc, but we see no evidence for Cenozoic reactivation of the Cretaceous

subduction thrust. We suggest that this is a key observation and implies that Cenozoic subduction thrust evolution and linkage did not require reactivation of the structure. This resulted in the unique preservation of Raukumara Basin, but it is not possible to more fully understand the reasons for basin preservation without a regional consideration of Tonga-Kermadec-Hikurangi subduction zone evolution, which is outside the scope of this paper.

9.4. Neogene Fore Arc Basin (22–0 Ma)

[50] Megasequence Z represents the fore-arc basin fill associated with Neogene development of the modern Hikurangi-Kermadec subduction system. Multiple sequence boundaries can be recognized within the basin and it is outside the scope of this work to describe those in more detail, but we speculate briefly below on some of the processes and regional events that may ultimately be the cause of significant sequence boundaries within the basin.

[51] Regional changes in subduction geometry may reflect evolution of slab and back-arc geometries at scales >100 km. It has been suggested that at circa 12 Ma the current Kermadec trend of arc volcanoes propagated southward into central North Island [Herzer, 1995]. In Coromandel Peninsula, andesitic volcanism of similar chemistry was erupted from circa 18–9 Ma, with a bimodal rhyolite-basalt suite being developed during 9–7 Ma [Adams *et al.*, 1994]. During circa 6–4 Ma, there was a transition to basaltic eruptions at Coromandel Peninsula and then abandonment of those volcanic centers [Adams *et al.*, 1994]; this transition coincides with when it is thought that spreading initiated in the southern Havre Trough, though the spreading center may have progressively stepped eastward to maintain some optimal position with respect to the subduction zone [Wright *et al.*, 1996]. It is likely that key sequence boundaries within the basin may relate to these tectonic and volcanic changes, convolved with regional sea level and oceanographic change.

[52] The most obvious manifestations of subduction-related deformation are restricted to the eastern margin of Raukumara Basin, near East Cape Ridge (Figures 7 and 10). The width of the zone of uplift, faulting and slope failures is 50–100 km. Therefore, given that subduction rates during Neogene time in this region have been 40–60 km/Myr, it is expected that responses within the overriding plate will be significant at timescales of ~1–2 Myr, as the nature and geometry of the slab is replaced. We observe a complex stratigraphy of unknown age along the eastern margin of the basin and infer that subduction zone processes are responsible.

10. Cenozoic Plate Boundary Kinematics

[53] The seismic reflection data set indicates that Raukumara Basin has suffered little internal deformation, except at its eastern and western edges, and has no major deep-seated faults that offset latest Cretaceous and Paleogene strata. Therefore, the basin represents a relatively rigid block within an active plate boundary system that otherwise contains extensive distributed deformation [Beavan and Haines, 2001; Walcott, 1986].

[54] Onshore, paleomagnetic declination anomalies indicate that northern Raukumara Peninsula has rotated, relative to mean magnetic north (and hence the spin axis of Earth), at a rate similar to that predicted by Australian plate motion [Mumme *et al.*, 1989; Rowan and Roberts, 2005, 2008]. At the southern margin of Raukumara Basin, strata are gently tilted upward toward the land but are not offset by major faults (Figure 8). Therefore, we suggest that Raukumara Basin is part of the northern Raukumara fore-arc block that has moved with the Australian plate, and has been translated away from it by extension in the Havre Trough; but this block has not undergone any significant relative rotation about a local rotation pole since 22–19 Ma, as is observed farther south in eastern North Island [Mumme *et al.*, 1989; Roberts, 1992; Rowan and Roberts, 2005, 2008; Thornley, 1997; Walcott *et al.*, 1981].

11. Allochthon Emplacement Direction

[55] It was previously proposed, on the basis of observations in southern and central onshore regions of the East Coast Allochthon [Kenny, 1984; Rait *et al.*, 1991; Stoneley, 1968], that emplacement direction was toward the southwest. However, we have mapped the thinned frontal edge and tip line of the offshore allochthon (megasequence Y) and find that it trends northeast-southwest over a distance of 100–150 km (Figure 9). Sediments at the base of the overlying megasequence Z downlap and thicken toward the west or northwest. Therefore, we conclude that, although the local emplacement direction near the southern edge of the East Coast Allochthon may have been toward the southwest, the regional direction of allochthon emplacement was toward the west or northwest.

12. Local Tectonic Erosion and Underplating of the Crust

[56] The geometry of reflectors within Raukumara Basin constrains mass balance at the fore arc over the past 22 Myr of subduction. If there had been net tectonic erosion at the subduction interface that had moved and mixed fore-arc crust into the mantle then ancient arc volcanoes should be preserved in the western part of Raukumara Basin, because the entire fore arc would be advected trenchward if the volcano-trench distance remained approximately constant. We have no reason to believe that the type of crust being subducted or the angle of subduction has changed significantly during Neogene time, and hence no reason to believe that the trench-arc distance has changed. We observe no fossil volcanoes east of the active arc but are able to image strata of Cretaceous-Paleogene age. Our observations are not consistent with a previous suggestion of trench retreat rate of 1.5 km Myr⁻¹ (33 km since 22 Ma), which was used as input to compute global subduction fluxes [Clift and Vannucchi, 2004]. We conclude that large-scale removal of fore-arc material into the mantle by tectonic erosion has not occurred at any time since 22 Ma adjacent to Raukumara Basin.

[57] Alternatively, if there had been net addition to the fore arc, possibly through crustal accretion of sediment from the downgoing plate, then the volume of the trench slope wedge has increased with time. This would result in progressive broadening of the zone of uplift at the eastern basin margin throughout Neogene time. We see Neogene stratal relationships that are consistent with this hypothesis at both the eastern and southern basin margins, and hence we conclude that this is a possibility. We reconcile the observation that the trench slope consists of highly faulted and indurated rock [Collot and Davy, 1998], rather than accreted sediment, by suggesting that accretion of the >1 km thickness of incoming sediment and crustal debris is occurring by underplating of the middle and lower crust after transport downward via a subduction channel.

[58] It has previously been suggested that the relatively high topography of Raukumara Peninsula is the result of Neogene crustal underplating caused by subduction processes [Walcott, 1987]. This view is supported by earthquake tomographic studies that image a deep (~40 km) crustal root beneath Raukumara Peninsula that is associated with low Q_p and high V_p/V_s [Eberhart-Phillips and Chadwick, 2002; Reyners et al., 1999]. The plate interface beneath Raukumara Peninsula is shown from converted seismic waves to be characterized by a 1–2 km thick layer with anomalously low V_p of 5.0–5.4 km s⁻¹ and high V_p/V_s of 2.0; this weak layer is inferred to be a channel of actively subducting or underplating sediment [Eberhart-Phillips and Reyners, 1999]. The continuing long-wavelength uplift of Raukumara Peninsula, combined with other observations, is shown by numerical models to be consistent with the underplating hypothesis, rather than crustal thickening by shortening across faults [Litchfield et al., 2007; Upton et al., 2003].

[59] Our study allows us to compare Raukumara Peninsula with the region farther north, where fore-arc crustal thickness is much less. We infer a long-lived depocenter in Raukumara Basin from the geometry of megasequence X and hence the crustal thickness beneath Raukumara Basin has been less than that of Raukumara Peninsula since Late Cretaceous time. This is consistent with the oceanic crust type inferred from seismic reflection character, thickness and p wave refraction velocities. The character of the trench slope and fill is similar in both regions, so it is reasonable to infer that similar processes are occurring on the shallow subduction interface and that the trench slope materials and processes are similar. We determine a depth to the Moho beneath Raukumara Basin of ~17 km and observe that the subduction interface has a depth of ~10–15 km beneath East Cape Ridge. In contrast, the crustal thickness of Raukumara Peninsula is ~35–40 km and the subduction interface has a depth of ~30–40 km beneath the Raukumara Range. The intersection between the Moho and the subduction thrust correlates spatially with where crustal underplating occurs (Figure 15). Therefore, it appears that existing crustal thickness plays a key role in determining the depth to which crustal material can be transported down a subduction channel.

[60] Based upon the observed crustal character and geometry (above), we suggest a cyclical process of: sediment and crust are faulted into a “subduction channel” at the subduction thrust; material within the subduction channel is transported arcward and downward; this material is then underplated near the base of the crust where it is thermally weakened and of much lower density than the deeper mantle wedge; crustal underplating drives local rock uplift; which causes steepening of the trench slope above its critical angle of stability and results in collapse of material back toward the subduction front (Figure 15).

[61] If the underplating rate was the same beneath East Cape Ridge and Raukumara Peninsula, then more rapid collapse of the trench slope adjacent to East Cape Ridge would be expected, because East Cape Ridge is closer to the subduction front than Raukumara Peninsula so the slope angle would be increased more rapidly by the same uplift rate. This is consistent with general observations of the intensity of faulting of the trench slope adjacent to East Cape Ridge, but we have insufficient data to quantify along-strike variation in rock uplift rate and geometry.

13. Implications for Growth and Recycling of Continental Crust

[62] Subduction margins play a key role in generating new continental crust through igneous activity at arcs, recycling crust by accretion of continent-derived sediment, and they are the most obvious locations where continental crust could be mixed back into the mantle. It is, therefore, important but extremely difficult to directly quantify these fluxes through the direct measurement of observable products: arcs, accretionary wedges, and trench slope subsidence histories.

[63] A highly cited study of seismic profiles through arcs of known (estimated) Phanerozoic activity led to a global arc growth rate estimate of 1.65 km³ yr⁻¹ [Reymer and Schubert, 1984]. Uncertainties in this study are unquantified: material may have escaped measurement because it was not identified (e.g., it was eroded or erupted to form sediment); or may have been incorrectly included in the calculation even though it was older than the time period being explicitly considered. The study is significant for our discussion because geochemical and freeboard arguments require that the rate of crustal growth and remixing of crustal material back into the mantle have been approximately similar during Phanerozoic time, with a slight net growth of continents implied [Clift and Vannucchi, 2004; Dewey and Windley, 1981; Reymer and Schubert, 1984; VonHuene and Scholl, 1991].

[64] Estimates of the flux of subducted sediment and continental material have increased as additional data have become available from 0.6 to 1.0 km³ yr⁻¹ [Dewey and Windley, 1981], to 1.3–1.8 km³ yr⁻¹ [VonHuene and Scholl, 1991], to 3.9 km³ yr⁻¹ [Clift and Vannucchi, 2004]. The primary reason for the progressive increase in this estimate arises from the recognition of trench slope regions that are not composed of young accreted sediment and that have subsided rapidly during subduction activity. Trench slope

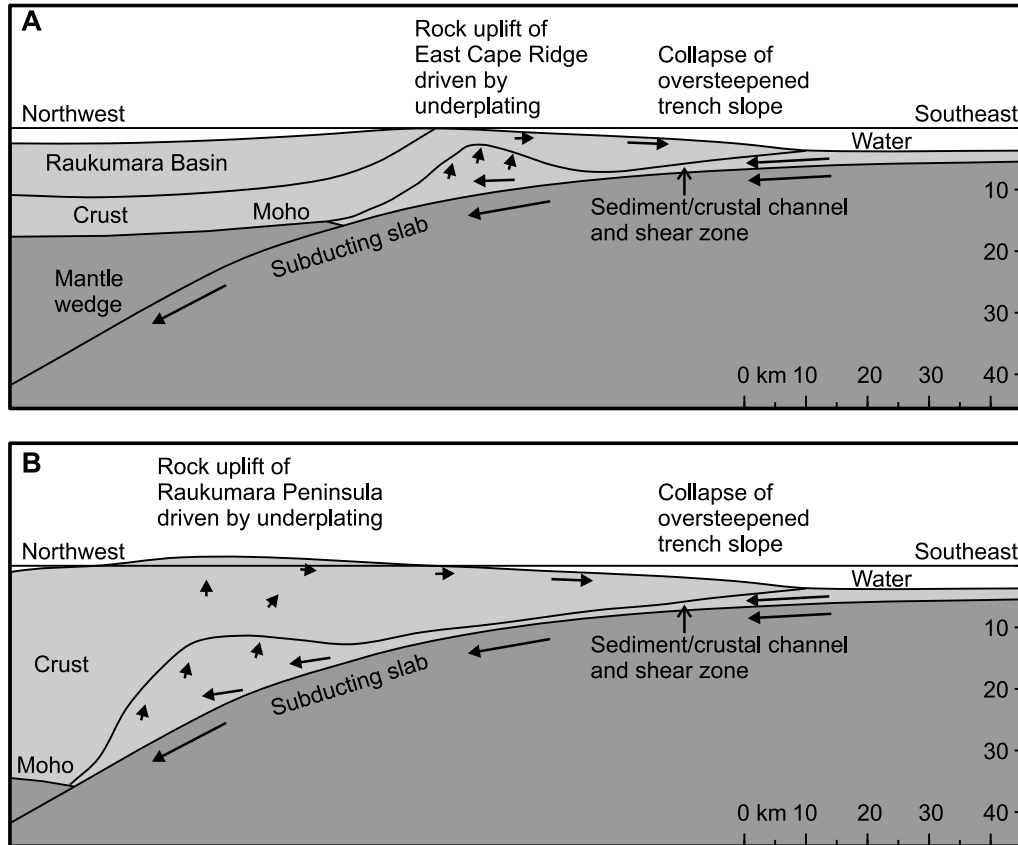


Figure 15. Cartoon showing rock uplift causing oversteepening and collapse of the trench slope; then collapsed material and incoming sediment is translated down a “subduction channel” and underplated to the lower crust, causing further uplift. The locus of uplift is closer to the subduction front (a) in Raukumara Basin than (b) at Raukumara Peninsula, where the crust is thicker; leading us to suggest that the Moho is a fundamental control on underplating processes.

subsidence values are typically converted to tectonic erosion values assuming constant average wedge taper through time and vertical rock trajectories as the base of the wedge is removed by subduction erosion [Clift and Vannucchi, 2004].

[65] Previous global subduction budgets have included our study region as one of net subduction erosion [Clift and Vannucchi, 2004; VonHuene and Scholl, 1991], based upon evidence for frontal tectonic erosion, subsidence and collapse of the trench slope. We agree with the observations that were used, but propose an alternative interpretation that involves no net loss in volume of the fore arc.

[66] To satisfy all of our observations, we propose a cyclical crustal kinematic within the fore arc: material is tectonically eroded at the toe of the trench slope; it is moved down a subduction channel to near the base of the crust; underplating near the Moho causes rock uplift and steepening of the trench slope; which in turn causes extension, subsidence, and collapse of the slope toward the trench; and material falls back into the subduction channel and completes the cycle. Material may be added from the incoming plate or lost into the mantle, but it is also possible for the fore arc to establish a geometrical dynamic equilibrium

where there is no net change in volume or shape of the fore arc, but the cyclical rock particle paths lead to persistent collapse and subsidence of the trench slope. Hence, estimates of fore-arc loss based upon trench slope subsidence may systematically overestimate the rate that crustal material is mixed into the mantle.

[67] Our hypothesis is supported by numerical and analog models. Previous theoretical considerations of subduction erosion have shown that it is straightforward to reproduce a subduction channel moving with the subducted plate within the crust [Lallemand *et al.*, 1994], but density contrasts between crust and mantle can result in underplating at the base of the crust [Ellis *et al.*, 1999], or a return flow of crustal material from greater depths within the subduction system back upward to the crust [Gerya *et al.*, 2002]. Our hypothesis is also supported by geochemical data. For example, the flux of young subducted sediment into Tongan lavas [George *et al.*, 2005] is much less than predicted by simple models of trench slope subsidence [Clift and MacLeod, 1999].

[68] Our conclusion that subsidence rates measured on trench slopes systematically overestimate the rate of removal of crustal material into the mantle implies that aggregate

global estimates are too high. We submit that the true uncertainties involved in making estimates of crustal growth and loss based upon direct measurement of arc and fore-arc volumes through time remain sufficiently large that it is still difficult to use these data to draw robust conclusions about the net growth and recycling rate of continental crust during Phanerozoic time.

14. Conclusions

[69] New seismic reflection and refraction data allow us to identify and map Raukumara Basin (Figures 1, 4, and 9) and determine the crustal architecture of part of the Hikurangi fore-arc region. Raukumara Basin has a maximum of ~ 12 km sediment thickness and we recognize three seismic reflection megasequences (Figures 6, 7, and 8) that we correlate with onshore lithostratigraphic units (Figures 2 and 3): X, a Late Cretaceous and Paleogene marine passive margin megasequence; Y, a sheet of allochthonous material that we interpret as a large submarine landslide emplaced during the onset of subduction beneath East Cape Ridge at circa 21 Ma; and Z, a Neogene subduction margin marine megasequence (Figure 14).

[70] The base of the crust is shown to lie at ~ 17 km beneath the center of the basin, but the crust thickens southward and the base of the crust lies at ~ 35 km beneath Raukumara Peninsula (Figures 11, 12, and 13). Beneath the western basin margin, we recognize reflective units that we interpret to be deformed sediment of the Gondwana fore arc that was thrust in Cretaceous time over oceanic crust with a thickness of ~ 7 km. West dipping reflection events at 13–15 s twt are interpreted as the active subduction thrust lying at ~ 35 km beneath the basin center (Figures 7 and 11).

[71] Raukumara Basin has normal faults at its western margin and is broadly uplifted along its eastern and southern margin, but is only weakly deformed over most of its area (Figure 10). Hence, we infer that Raukumara Peninsula and Basin have behaved as a large (>150 km long) and relatively rigid fore-arc block that has been translated from the Australian plate by spreading in the Havre Trough; this conclusion is in contrast to large Neogene vertical axis rotations that have been inferred on the basis of paleomagnetic data from the Hikurangi fore arc farther south [Mumme *et al.*, 1989; Roberts, 1992; Rowan and Roberts, 2005, 2008; Thornley, 1997; Walcott *et al.*, 1981].

[72] We infer that initial uplift of East Cape Ridge was associated with subduction initiation in latest Oligocene or early Miocene time and resulted in the emplacement of a large ($\sim 10,000$ km³) submarine landslide westward or northwestward into the basin (megasequence Y). Kinematic

indicators from correlative onshore allochthonous rocks indicate southwestward movement [Kenny, 1984; Rait *et al.*, 1991; Stoneley, 1968], but we suggest that this conclusion cannot be generalized to the entire >200 km strike length of allochthonous rocks, because the general westward taper of the western edge of the allochthonous sheet and the westward downlap of immediately overlying strata in Raukumara Basin suggests a westward or northwestward paleoslope and emplacement direction (Figures 6, 8, and 9).

[73] The lack of fossil arc volcanoes in the western basin and broadening of the zone of uplift in the eastern basin lead us to conclude that net crustal accretion to the fore arc has occurred during Neogene time. However, the many small faults that are evident on swath bathymetry and seismic reflection data from the trench slope and the lack of coherent internal reflections beneath the trench slope indicate collapse of indurated rock, rather than accretion of sediment from the downgoing plate. We infer fore-arc accretion by crustal underplating, which drives rock uplift beneath East Cape Ridge. We conclude that the underplating process is modulated by crustal thickness, because we observe the locus of uplift to be spatially correlated with the intersection between the Moho and subduction thrust: uplift of Raukumara Peninsula is ~ 110 km from the subduction front where the Moho is at ~ 35 km depth; and uplift of East Cape Ridge is ~ 60 km from the subduction front where the Moho is at ~ 17 km depth (Figure 15).

[74] We propose a cyclical fore-arc kinematic: rock moves down a subduction channel to near the base of the crust, where underplating drives rock uplift and oversteepens the trench slope, causing collapse back toward the trench and subduction channel. The cyclical rock particle paths lead to persistent collapse and subsidence of the trench slope, and hence existing estimates of fore-arc loss based upon trench slope subsidence [Clift and Vannucchi, 2004; VonHuene and Scholl, 1991] systematically overestimate the rate that crustal material is mixed into the mantle. We submit that the true uncertainties in direct measurement of arc and fore-arc volumes through time remain sufficiently large that it remains a substantial challenge to draw robust conclusions about the net global growth rate of continental crust during Phanerozoic time.

[75] **Acknowledgments.** We thank Kip Hodges; Margi Rusmore, and two anonymous reviewers. Primary funding for this work was from the New Zealand Ministry of Economic Development and the Foundation for Research Science and Technology. Refraction data were collected by R/V *Somme* and analysis by German coauthors was funded by BMBF grant 03G0192C. The RAU07 data set was acquired by CGG *Veritas Marine* using vessel CGG *Duke* and processed by Fugro Seismic Imaging. The 05CM data set was acquired by Multiwave using the vessel *Pacific Titan* and was processed by GNS Science and Fugro Seismic Imaging.

References

- Adams, C. J., I. J. Graham, D. Seward, and D. N. B. Skinner (1994), Geochronological and geochemical evolution of late Cenozoic volcanism in the Coromandel Peninsula, New Zealand, *N. Z. J. Geol. Geophys.*, *37*, 359–379.
- Aita, Y., and K. B. Sporli (1992), Tectonic and paleobiogeographic significance of radiolarian microfossils in the Permian to Mesozoic basement rocks of the North Island, New Zealand, *Palaeogeogr. Palaeoclimatol. Palaeoecol.*, *96*, 103–125, doi:10.1016/0031-0182(92)90062-A.
- Árnadóttir, T., S. Thornley, F. F. Pollitz, and D. J. Darby (1999), Spatial and temporal strain rate variations at the northern Hikurangi margin, New Zealand, *J. Geophys. Res.*, *104*, 4931–4944, doi:10.1029/1998JB900109.
- Beavan, J., and J. Haines (2001), Contemporary horizontal velocity and strain rate fields of the Pacific-Australian plate boundary zone through New Zealand, *J. Geophys. Res.*, *106*, 741–770, doi:10.1029/2000JB900302.

- Brothers, R. N., and M. Delaloye (1982), Obducted ophiolites of North Island, New Zealand: Origin, age, emplacement and tectonic implications for Tertiary and Quaternary volcanicity, *N. Z. J. Geol. Geophys.*, **25**, 257–274.
- Cande, S. C., and J. M. Stock (2004), Pacific-Antarctic-Australia motion and the formation of the Macquarie Plate, *Geophys. J. Int.*, **157**, 399–414, doi:10.1111/j.1365-246X.2004.02224.x.
- CANZ (2008), New Zealand region bathymetry, 1:4,000,000, 2nd ed., chart, *Misc. Ser.* 73, Natl. Inst. of Water and Atmos. Res., Lower Hutt.
- Cawood, P. A., A. A. Nemchin, A. Leverenz, A. Aseed, and P. F. Balance (1999), U/Pb dating of detrital zircons; implications for the provenance record of Gondwana margin terranes, *Geol. Soc. Am. Bull.*, **111**, 1107–1119, doi:10.1130/0016-7606(1999)111<1107:UPDODZ>2.3.CO;2.
- Clift, P. D., and C. J. MacLeod (1999), Slow rates of subduction erosion estimated from subsidence and tilting of the Tonga forearc, *Geology*, **27**(5), 411–414, doi:10.1130/0091-7613(1999)027<0411:SROSEE>2.3.CO;2.
- Clift, P., and P. Vannucchi (2004), Controls on tectonic accretion versus erosion in subduction zones: Implications for the origin and recycling of the continental crust, *Rev. Geophys.*, **42**, RG2001, doi:10.1029/2003RG000127.
- Collot, J. Y., and B. W. Davy (1998), Forearc structures and tectonic regimes at the oblique subduction zone between the Hikurangi Plateau and the southern Kermadec margin, *J. Geophys. Res.*, **103**, 623–650, doi:10.1029/97JB02474.
- Collot, J. Y., et al. (1996), From oblique subduction to intra-continental transpression: Structures of the southern Kermadec-Hikurangi margin from multi-beam bathymetry, side-scan sonar and seismic reflection, *Mar. Geophys. Res.*, **18**(2–4), 357–381, doi:10.1007/BF00286085.
- Cook, R. A., R. Sutherland, and H. Zhu (1999), *Cretaceous-Cenozoic Geology and Petroleum Systems of the Great South Basin, New Zealand*, *Inst. Geol. Nucl. Sci. Monogr.*, vol. 20, 188 pp., Inst. of Geol. and Nucl. Sci. Ltd., Lower Hutt, New Zealand.
- Coombs, D. S., C. A. Landis, R. J. Norris, J. M. Sinton, D. J. Boms, and D. Craw (1976), The Dun Mountain Ophiolite Belt, New Zealand, its tectonic setting, constitution, and origin, with special reference to the southern portion, *Am. J. Sci.*, **276**, 561–603.
- Crampton, J. S. (1996), *Inoceramid Bivalves From the Late Cretaceous of New Zealand*, *Inst. Geol. Nucl. Sci. Monogr.*, vol. 14, Inst. of Geol. and Nucl. Sci. Ltd., Lower Hutt, New Zealand.
- Crampton, J. S., and P. R. Moore (1990), Environment of deposition of the Maungataniwha Sandstone (Late Cretaceous), Te Hoe River area, western Hawke's Bay, New Zealand, *N. Z. J. Geol. Geophys.*, **33**, 333–348.
- Crampton, J. S., C. J. Hollis, J. I. Raine, L. Roncaglia, P. Shchioler, C. P. Strong, and G. J. Wilson (2004), Cretaceous, in *The New Zealand Geological Time-scale*, *Inst. Geol. Nucl. Sci. Monogr.*, vol. 22, edited by R. A. Cooper, pp. 103–124, Inst. of Geol. and Nucl. Sci., Lower Hutt, New Zealand.
- Davey, F. J., S. Henrys, and E. Lodolo (1997), A seismic crustal section across the East Cape convergent margin, New Zealand, *Tectonophysics*, **269**, 199–215, doi:10.1016/S0040-1951(96)00165-5.
- Davy, B. W., and J.-Y. Collot (2000), The Rapuhia Scarp (northern Hikurangi Plateau): Its nature and subduction effects on the Kermadec Trench, *Tectonophysics*, **328**, 269–295, doi:10.1016/S0040-1951(00)00211-0.
- Davy, B., and R. Wood (1994), Gravity and magnetic modelling of the Hikurangi Plateau, *Mar. Geol.*, **118**, 139–151, doi:10.1016/0025-3227(94)90117-1.
- DeMets, C., R. G. Gordon, D. F. Argus, and S. Stein (1994), Effect of recent revisions to the geomagnetic time scale on estimates of current plate motions, *Geophys. Res. Lett.*, **21**, 2191–2194, doi:10.1029/94GL02118.
- de Ronde, C., E. Baker, G. Massoth, J. Lupton, I. Wright, R. Feely, and R. Greene (2001), Intra-oceanic subduction-related hydrothermal venting, Kermadec volcanic arc, New Zealand, *Earth Planet. Sci. Lett.*, **193**, 359–369, doi:10.1016/S0012-821X(01)00534-9.
- de Ronde, C., et al. (2007), Submarine hydrothermal activity along the mid-Kermadec Arc, New Zealand: Large-scale effects on venting, *Geochem. Geophys. Geosyst.*, **8**, Q07007, doi:10.1029/2006GC001495.
- Dewey, J. F., and B. F. Windley (1981), Growth and differentiation of the continental-crust, *Philos. Trans. R. Soc. London, Ser. A*, **301**, 189–206, doi:10.1098/rsta.1981.0105.
- Eberhart-Phillips, D., and M. Chadwick (2002), Three-dimensional attenuation model of the shallow Hikurangi subduction zone in the Raukumara Peninsula, New Zealand, *J. Geophys. Res.*, **107**(B2), 2033, doi:10.1029/2000JB000046.
- Eberhart-Phillips, D., and M. Reyners (1999), Plate interface properties in the northeast Hikurangi subduction zone, New Zealand, from converted seismic waves, *Geophys. J. Int.*, **26**, 2565–2568.
- Ellis, S., C. Beaumont, and O. A. Pfiffner (1999), Geodynamic models of crustal-scale episodic tectonic accretion and underplating in subduction zones, *J. Geophys. Res.*, **104**, 15,169–15,190, doi:10.1029/1999JB900071.
- Field, B. D., and C. I. Uruski (1997), *Cretaceous-Cenozoic Geology and Petroleum Systems of the East Coast Region*, *Inst. Geol. Nucl. Sci. Monogr.*, vol. 19, 301 pp., Inst. of Geol. and Nucl. Sci. Ltd., Lower Hutt, New Zealand.
- Gaina, C., D. R. Mueller, J.-Y. Royer, J. Stock, J. L. Hardebeck, and P. Symonds (1998), The tectonic history of the Tasman Sea: A puzzle with 13 pieces, *J. Geophys. Res.*, **103**, 12,413–12,433, doi:10.1029/98JB00386.
- George, R., S. Turner, J. Morris, T. Plank, C. Hawkesworth, and J. Ryan (2005), Pressure-temperature-time paths of sediment recycling beneath the Tonga-Kermadec arc, *Earth Planet. Sci. Lett.*, **233**(1–2), 195–211, doi:10.1016/j.epsl.2005.01.020.
- Gerya, T. V., B. Stöckhert, and A. L. Perchuk (2002), Exhumation of high-pressure metamorphic rocks in a subduction channel: A numerical simulation, *Tectonics*, **21**(6), 1056, doi:10.1029/2002TC001406.
- Gillies, P. N., and F. J. Davey (1986), Seismic reflection and refraction studies of the Raukumara forearc basin, New Zealand, *N. Z. J. Geol. Geophys.*, **29**, 391–403.
- Herzer, R. H. (1995), Seismic stratigraphy of a buried volcanic arc, Northland, New Zealand and implications for Neogene subduction, *Mar. Pet. Geol.*, **12**(5), 511–531, doi:10.1016/0264-8172(95)91506-K.
- Hollis, C. J., G. R. Dickens, B. D. Field, C. M. Jones, and C. P. Strong (2005), The Paleocene-Eocene transition at Mead Stream, New Zealand; a southern Pacific record of early Cenozoic global change, *Palaeogeogr. Palaeoclimatol. Palaeoecol.*, **215**, 313–343, doi:10.1016/j.palaeo.2004.09.011.
- Isaac, M. J., P. R. Moore, and Y. J. Joass (1991), Tahora Formation: The basal facies of a Late Cretaceous transgressive sequence, northeastern New Zealand, *N. Z. J. Geol. Geophys.*, **34**, 227–236.
- Isaac, M. J., R. H. Herzer, F. J. Brook, and B. W. Hayward (1994), *Cretaceous and Cenozoic Sedimentary Basins of Northland, New Zealand*, *Inst. Geol. Nucl. Sci. Monogr.*, vol. 8, 230 pp., Inst. of Geol. and Nucl. Sci. Ltd., Lower Hutt, New Zealand.
- Kamp, P. J. J. (1999), Tracking crustal processes by FT thermochronology in a forearc high (Hikurangi margin, New Zealand) involving Cretaceous subduction termination and mid-Cenozoic subduction initiation, *Tectonophysics*, **307**, 313–343, doi:10.1016/S0040-1951(99)00102-X.
- Kenny, J. A. (1984), Stratigraphy, sedimentology and structure of the Ihungia decollement, Raukumara Peninsula, North Island, New Zealand, *N. Z. J. Geol. Geophys.*, **27**, 1–19.
- Killops, S. D., C. J. Hollis, H. E. G. Morgans, R. Sutherland, B. D. Field, and D. A. Leckie (2000), Paleoclimatographic significance of late Paleocene dysaerobia at the shelf/slope break around New Zealand, *Palaeogeogr. Palaeoclimatol. Palaeoecol.*, **156**, 51–70, doi:10.1016/S0031-0182(99)00131-5.
- King, P. R., and G. P. Thrasher (1996), *Cretaceous-Cenozoic Geology and Petroleum Systems of the Taranaki Basin, New Zealand*, *Inst. Geol. Nucl. Sci. Monogr.*, vol. 13, 243 pp., Inst. of Geol. and Nucl. Sci. Ltd., Lower Hutt, New Zealand.
- Laird, M. G. (1993), Cretaceous continental rifts: New Zealand region, in *Sedimentary Basins of the World*, vol. 2, *South Pacific Sedimentary Basins*, edited by P. F. Balance, pp. 37–49, Elsevier, Amsterdam.
- Lallemand, S. E., P. Schnurle, and J. Malavieille (1994), Coulomb theory applied to accretionary and nonaccretionary wedges: Possible causes for tectonic erosion and or frontal accretion, *J. Geophys. Res.*, **99**, 12,033–12,055, doi:10.1029/94JB00124.
- Lamarche, G., J. Y. Collot, R. A. Wood, M. Sosson, R. Sutherland, and J. Deltail (1997), The Oligo-Miocene Pacific-Australia plate boundary, south of New Zealand: Evolution from oceanic spreading to strike-slip faulting, *Earth Planet. Sci. Lett.*, **148**, 129–139, doi:10.1016/S0012-821X(97)0026-5.
- Lamarche, G., P. M. Barnes, and J. M. Bull (2006), Faulting and extension rate over the last 20,000 years in the offshore Whakatane Graben, New Zealand continental shelf, *Tectonics*, **25**, TC4005, doi:10.1029/2005TC001886.
- Lamarche, G., C. Joanne, and J.-Y. Collot (2008), Successive, large mass-transport deposits in the south Kermadec fore-arc basin, New Zealand: The Matakaoa Submarine Instability Complex, *Geochem. Geophys. Geosyst.*, **9**, Q04001, doi:10.1029/2007GC001843.
- Lillie, A. R. (1953), The geology of the Dannevirke subdivision, *N. Z. Geol. Surv. Bull.*, **46**, 1–156.
- Litchfield, N., S. Ellis, K. Berryman, and A. Nicol (2007), Insights into subduction-related uplift along the Hikurangi Margin, New Zealand, using numerical modeling, *J. Geophys. Res.*, **112**, F02021, doi:10.1029/2006JF000535.
- Mazengarb, C., and D. H. M. Harris (1994), Cretaceous stratigraphic and structural relationships of Raukumara Peninsula, New Zealand; stratigraphic patterns associated with the migration of a thrust system, *Ann. Tectonicae*, **8**(2), 100–118.
- Mazengarb, C., and I. G. Speden (2000), Geology of the Raukumara area, *1:250,000 Geol. Map 6*, 60 pp., Inst. of Geol. and Nucl. Sci. Ltd., Lower Hutt, New Zealand.
- Moore, P. R. (1988a), Stratigraphy, composition, and environment of deposition of the Whangai Formation and associated Late Cretaceous–Paleocene rocks, eastern North Island, New Zealand, *N. Z. Geol. Surv. Bull.*, **100**, 1–82.
- Moore, P. R. (1988b), Structural subdivisions of eastern North Island, *N. Z. Geol. Surv. Rec.*, **30**, 1–24.
- Moore, P. R. (1989), Stratigraphy of the Wipawa black shale (Paleocene), eastern North Island, New Zealand, *N. Z. Geol. Surv. Rep.*, **38**, 1–19.
- Moore, P. R., A. G. Adams, M. J. Isaac, C. Mazengarb, H. E. G. Morgans, and C. J. Phillips (1986), A revised Cretaceous-early Tertiary stratigraphic nomenclature for eastern North Island, *N. Z. Geol. Surv. Rep.*, **G104**.
- Mortimer, N. (1994), Origin of the Torlesse Terrane and coeval rocks, North Island, New Zealand, *Int. Geol. Rev.*, **36**, 891–910, doi:10.1080/00206819409465494.
- Mortimer, N., and D. Parkinson (1996), Hikurangi Plateau: A Cretaceous large igneous province in the southwest Pacific Ocean, *J. Geophys. Res.*, **101**, 687–696, doi:10.1029/95JB03037.
- Mortimer, N., A. J. Tulloch, R. N. Spark, N. W. Walker, E. Ladley, A. Allibone, and D. L. Kimbrough (1999), Overview of the Median Batholith, New Zealand: A new interpretation of the geology of the Median Tectonic Zone and adjacent rocks, *J.*

- Afr. Earth Sci.*, 29(1), 257–268, doi:10.1016/S0899-5362(99)00095-0.
- Mumme, T. C., S. H. Lamb, and R. I. Walcott (1989), The Raukumara paleomagnetic domain: Constraints on the tectonic rotation of the east coast, North Island, New Zealand, from paleomagnetic data, *N. Z. J. Geol. Geophys.*, 32, 317–326.
- Nicol, A., and L. M. Wallace (2007), Temporal stability of deformation rates: Comparison of geological and geodetic observations, Hikurangi subduction margin, New Zealand, *Earth Planet. Sci. Lett.*, 258(3–4), 397–413, doi:10.1016/j.epsl.2007.03.039.
- Nicol, A., C. Mazengarb, F. Chanier, G. Rait, C. I. Uruski, and L. M. Wallace (2007), Tectonic evolution of the active Hikurangi subduction margin, New Zealand, since the Oligocene, *Tectonics*, 26, TC4002, doi:10.1029/2006TC002090.
- Rait, G., F. Chanier, and D. W. Waters (1991), Landward and seaward-directed thrusting accompanying the onset of subduction beneath New Zealand, *Geology*, 19(3), 230–233, doi:10.1130/0091-7613(1991)019<0230:LASDTA>2.3.CO;2.
- Reymer, A., and G. Schubert (1984), Phanerozoic addition rates to the continental-crust and crustal growth, *Tectonics*, 3, 63–77, doi:10.1029/TC003i001p00063.
- Reyners, M., and P. McGinty (1999), Shallow subduction tectonics in the Raukumara Peninsula, New Zealand, as illuminated by earthquake focal mechanisms, *J. Geophys. Res.*, 104, 3025–3034, doi:10.1029/1998JB900081.
- Reyners, M., D. Eberhart-Phillips, and G. Stuart (1999), A three-dimensional image of shallow subduction: Crustal structure of the Raukumara Peninsula, New Zealand, *Geophys. J. Int.*, 137, 873–890, doi:10.1046/j.1365-246x.1999.00842.x.
- Roberts, A. P. (1992), Paleomagnetic constraints on the tectonic rotation of the southern Hikurangi margin, New Zealand, *N. Z. J. Geol. Geophys.*, 35, 311–323.
- Rowan, C. J., and A. P. Roberts (2005), Relocation of the tectonic boundary between the Raukumara and Wairoa Domains (East Coast, North Island, New Zealand): Implications for the rotation history of the Hikurangi margin, *N. Z. J. Geol. Geophys.*, 48, 185–196.
- Rowan, C. J., and A. P. Roberts (2008), Widespread remagnetizations and a new view of Neogene tectonic rotations within the Australia-Pacific plate boundary zone, New Zealand, *J. Geophys. Res.*, 113, B03103, doi:10.1029/2006JB004594.
- Song, T. R. A., and M. Simons (2003), Large trench-parallel gravity variations predict seismogenic behavior in subduction zones, *Science*, 301, 630–633, doi:10.1126/science.1085557.
- Speden, I. G. (1975), Cretaceous stratigraphy of Raukumara Peninsula, part 1: Cretaceous stratigraphy of Koranga (parts N87 and N88; part 2: Geology of the Lower Waimana and Waitohi valleys (part N78), *N. Z. Geol. Surv. Bull.*, 91, 1–69.
- Sporli, K. B., and Y. Aita (1994), Tectonic significance of Late Cretaceous radiolaria from the obducted Matakaoa Volcanics, East Cape, North Island, New Zealand, *Geosci. Rep.*, 20, pp. 115–133, Shizuoka Univ., Shizuoka, Japan.
- Stoneley, R. (1968), A lower Tertiary decollement on the East Coast, North Island, New Zealand, *N. Z. J. Geol. Geophys.*, 11, 128–156.
- Strong, C. P. (1976), Cretaceous foraminifera from the Matakaoa Volcanic Group, *N. Z. J. Geol. Geophys.*, 19, 140–143.
- Strong, C. P. (1980), Early Paleogene foraminifera from Matakaoa Volcanic Group, *N. Z. J. Geol. Geophys.*, 23, 267–272.
- Sutherland, R. (1995), The Australia-Pacific boundary and Cenozoic plate motions in the SW Pacific; some constraints from Geosat data, *Tectonics*, 14, 819–831, doi:10.1029/95TC00930.
- Sutherland, R. (1999), Basement geology and tectonic development of the greater New Zealand region; an interpretation from regional magnetic data, *Tectonophysics*, 308(3), 341–362, doi:10.1016/S0040-1951(99)00108-0.
- Thornley, S. (1997), Neogene tectonics of Raukumara Peninsula, northern Hikurangi margin, New Zealand, Ph.D. thesis, Victoria Univ. of Wellington, Wellington, New Zealand.
- Upton, P., P. O. Koons, and D. Eberhart-Phillips (2003), Extension and partitioning in an oblique subduction zone, New Zealand: Constraints from three-dimensional numerical modeling, *Tectonics*, 22(6), 1068, doi:10.1029/2002TC001431.
- Uruski, C. I., B. D. Field, R. H. Funnell, C. J. Hollis, A. Nicol, and G. Maslen (2006), Developments in the central and northeastern East Coast Basin, North Island, New Zealand, *APPEA J.*, 46, 215–235.
- VonHuene, R., and D. W. Scholl (1991), Observations at convergent margins concerning sediment subduction, subduction erosion, and the growth of continental crust, *Rev. Geophys.*, 29(3), 279–316, doi:10.1029/91RG00969.
- Waight, T. E., S. D. Weaver, and R. J. Muir (1998), Mid-Cretaceous granitic magmatism during the transition from subduction to extension in southern New Zealand; a chemical and tectonic synthesis, *Lithos*, 45(1–4), 469–482, doi:10.1016/S0024-4937(98)00045-0.
- Walcott, R. I. (1986), The kinematics of the plate boundary zone through New Zealand: A comparison of short- and long-term deformations, *Geophys. J. R. Astron. Soc.*, 79, 613–633.
- Walcott, R. I. (1987), Geodetic strain and the deformational history of the North Island of New Zealand during the late Cainozoic, *Philos. Trans. R. Soc. London, Ser. A*, 321, 163–181, doi:10.1098/rsta.1987.0009.
- Walcott, R. I., T. C. Mumme, and D. A. Christoffel (1981), Bending within the axial tectonic belt of New Zealand in the last 9 Myr from paleomagnetic data, *Earth Planet. Sci. Lett.*, 52(2), 427–434, doi:10.1016/0012-821X(81)90195-3.
- Wallace, L. M., J. Beavan, R. McCaffrey, and D. Darby (2004), Subduction zone coupling and tectonic block rotations in the North Island, New Zealand, *J. Geophys. Res.*, 109, B12406, doi:10.1029/2004JB003241.
- Wellman, H. W. (1959), Divisions of the New Zealand Cretaceous, *Trans. R. Soc. N. Z.*, 87, 99–163.
- Wells, R. E., R. J. Blakely, Y. Sugiyama, D. W. Scholl, and P. A. Dinterman (2003), Basin-centered asperities in great subduction zone earthquakes: A link between slip, subsidence, and subduction erosion?, *J. Geophys. Res.*, 108(B10), 2507, doi:10.1029/2002JB002072.
- Wilson, K., K. Berryman, U. Cochran, and T. Little (2007), Holocene coastal evolution and uplift mechanisms of the northeastern Raukumara Peninsula, North Island, New Zealand, *Quat. Sci. Rev.*, 26, 1106–1128, doi:10.1016/j.quascirev.2007.01.005.
- Wood, R., and B. Davy (1994), The Hikurangi Plateau, *Mar. Geol.*, 118, 153–173, doi:10.1016/0025-3227(94)90118-X.
- Wood, R. A., G. Lamarche, R. H. Herzer, J. Delleil, and B. Davy (1996), Paleogene seafloor spreading in the southeast Tasman Sea, *Tectonics*, 15, 966–975, doi:10.1029/96TC00129.
- Wright, I. C., L. M. Parson, and J. A. Gamble (1996), Evolution and interaction of migrating cross-arc volcanism and backarc rifting; an example from the southern Havre Trough (35°20′–37°S), *J. Geophys. Res.*, 101, 22,071–22,086, doi:10.1029/96JB01761.
- Wright, I. C., T. J. Worthington, and J. A. Gamble (2006), New multibeam mapping and geochemistry of the 30°–35°S sector, and overview, of southern Kermadec arc volcanism, *J. Volcanol. Geotherm. Res.*, 149, 263–296, doi:10.1016/j.jvolgeores.2005.03.021.
- S. Bannister, D. Barker, F. Davey, B. Field, S. Henrys, V. Stagpoole, R. Sutherland, S. Toulmin, and C. Uruski, GNS Science, P.O. Box 30-368, Lower Hutt, New Zealand. (r.sutherland@gns.cri.nz)
- D. Bassett and T. Stern, Environment and Earth Sciences, School of Geography, Victoria University of Wellington, P.O. Box 600, Wellington 6005, New Zealand.
- E. R. Flueh, H. Kopp, and M. Scherwath, Leibniz Institute of Marine Sciences at University of Kiel (IFM-GEOMAR), Wischhofstrasse 1-3, D-24148 Kiel, Germany.
- C. Kennedy, New Zealand Ministry of Economic Development, P.O. Box 1473, Wellington, New Zealand.

Central Tonga-Kermadec subduction zone structures - evidence for strong upper mantle anomalies from seismic wide-angle data

Scherwath, M., Kopp, H., Flueh, E.R.

Leibniz Institute of Marine Sciences, IFM-GEOMAR, Wischhofstr. 1-3, 24148 Kiel, Germany

Henrys, S.A.

GNS Science, PO Box 30-368, Lower Hutt, New Zealand

to be submitted to EPSL?

Abstract

Seismic wide-angle data from the central Tonga-Kermadec subduction zone determine the structures of the incoming Pacific plate and the overriding Australian arc near the active arc volcano Raoul Island at 29 degrees South. The subducting Pacific plate is around 5-6 km thick with seismic P-wave velocities (V_p) of 5.2-6.9 km/s, with isolated pockets of lowered V_p and covered with up to 100 m thick patches of sediments. The underlying Pacific mantle has a V_p of 7.4 km/s. These relatively low seismic velocities in crust and mantle indicate a considerable alteration of the rough and broken incoming plate which is likely to transport a significant amount of access water into the subduction zone. The arc crust is about 12 km thick with a V_p of 4.2-7.0 km/s and a 40 km wide low velocity region directly above the contact area with the subducting crust. The sediments on the arc crust are on average about 1 km thick and form an up to 3 km thick and 90 km wide forearc basin. The mantle wedge has a V_p of 7.5-7.7 km/s which is lower than typical arc mantle. We interpret these low V_p to be a result of serpentinisation caused by the large amount incoming water released directly at the frontal mantle wedge. Our results demonstrate the possibility that even in regions without significant amounts of subducting sediment relatively large amounts of free water can enter subduction zones.

Introduction

Migration of water through subduction zones plays an important role in subduction zone processes as water influences directly the arc volcanism, seismicity, and also causes the alteration of incoming and overriding structures and rock units (e.g. Peacock, 1990, 1993). One of the fundamental questions in this context is on the input and output of water, from the incoming plate to the overriding plate, and yet this has been a difficult measure to quantify. This paper illustrates one of the deeper, subsedimentary pathways of water, through the incoming crust and mantle into the shallow part of the overriding mantle wedge, as illuminated by the upper

mantle P-wave velocities of both plates involved. Seismic wide-angle data from the central Tonga-Kermadec subduction zone near Raoul Island, in the western Pacific at 29 degrees South (Fig. 1), determine the upper lithospheric structures and in addition are investigated to infer some of the connections between the input and output in subduction zones.

Generally, most of the incoming fluids in subduction zones are supplied by the incoming sediments (where present) and the shallow oceanic crust. Trench sediments are usually saturated by the ocean. The crust below can contain both remnant water from its creation from mid-oceanic ridges as well as additional water that enters cracks and fissures during plate bending prior to subduction. Overlying sediments can cap the oceanic crust and thus reduce water percolation into the crust below. However, in the case of outcropping basement, where the sediments are either sparse or perturbed by the crust, larger volumes of water can still enter the crust. The underlying oceanic mantle can also become enriched with water and hence serpentinised, as indicated by greatly reduced seismic velocities measured at incoming upper mantles. Thus, greatly reduced upper mantle velocities of the incoming plate can indicate greater volumes of water entering the subduction, even in the case of thin sediments at the trench. We show that the central Tonga-Kermadec subduction zone is an example where the incoming, sparsely sedimented lithosphere supplies a significant amount of water through subduction to the overriding lithosphere, as the overlying mantle also exhibits reduced seismic velocities indicative of a surplus of water.

This paper focuses on the central Tonga-Kermadec subduction zone which is one of the lesser studied subduction zone systems. In previous studies, the main focus in this region has been the arc volcanism (de Ronde et al., 2007), and structural information comes mainly from bathymetry and gravity studies (e.g. Collot and Davy, 1997). For the first time, deep seismic wide-angle data were collected in 2007 as part of the MANGO (Marine Geoscientific Investigations on the Input and Output of the Kermadec Subduction Zone) project (Flueh and Kopp, 2007) in this area, and the results for northern Kermadec area are shown in this paper.

Tectonically, the seismic profile is located adjacent to the highly active arc volcano Raoul Island, which is the northernmost of the Kermadec islands of the Kermadec arc (Lloyd and Nathan, 1981). Here, the Pacific plate has been continuously subducting beneath the Australian plate since 45 Ma (Sutherland, 1995), currently at a convergence rate of 55 mm/a (DeMets et al., 1994) approximately oblique to the arc (Fig. 1). The entire Tonga-Kermadec arc zone stretches for about 2500 km between the northern Tonga Ridge and the Taupo Volcanic Zone of New Zealand. The Australian backarc is characterised by the Havre-Trough where backarc rifting or spreading has been active since 4-5 Ma, separating the now inactive Colville Ridge from the active Kermadec Ridge. The incoming Pacific plate has formed at approximately 100 Ma at the now inactive Osbourne Trough that lies about 450 km to the north (Bradshaw, 1989; Downey et al., 2007).

Seismic Data and Modelling

Seismic wide-angle reflection and refraction were acquired in April 2007 along a 475 km long profile oriented NNW-SSE, perpendicular to the northern Kermadec Trench, at the latitude of Raoul Island around 29 degrees South. The profile was covered with a total of 56 ocean bottom seismometer and hydrophone (OBS/H) stations successfully deployed at a spacing of 5.5 km. The seismic source consisted of a 64 litre (4230 cu inch) G-gun array that was fired at a nominal spacing of 150 m.

Because the OBS/H could not withstand water depth greater than 6000 m while the Kermadec Trench reaches depth of up to 10 km, a station gap of about 80 km had to be left within the profile. First, 29 OBS/H were deployed along the eastern half of the profile and then the profile was covered with airgun shots up to 45 km beyond the westernmost OBS 119 (Fig. 1). This station was then left on the seafloor and the remaining 28 stations were re-deployed along the western part of the profile which was covered with airgun shots up to 20 km east of OBS119 (Fig. 1). One station was irretrievable. In general, the data quality is good, with mantle refractions measured at offsets up to 200 km.

Multibeam bathymetry and shallow seismic reflection data from 100 m streamer deployed during the seismic wide-angle data acquisition provide a-priori information for seafloor and sedimentary structures along the data profile. These data were incorporated into the starting model for the seismic wide-angle analysis.

The seismic wide-angle analysis was carried out by measuring seismic P-wave phases from sediments, crust and upper mantle. Our goal was to derive a preferred model of seismic velocity distributions that satisfies the a-priori information and the seismic wide-angle data with the least number of model nodes and thus is a "minimum-parameter/prior structure" model (Zelt, 1999).

We used the ray-tracing method from Zelt and Smith (1992) to determine subsurface structures. The velocity model consists of layers that are assigned by variably spaced depth nodes along each model interface and velocity nodes at the top and bottom of each model layer. Forward ray-tracing through this model predicts arrival times that were compared to the measured arrivals, and the model was changed to minimise the misfit between observed and calculated times. Model changes were calculated automatically during several inversion and adjusted manually in cases of unrealistic inversion results caused by sparse data coverage or limitations of the ray-tracing method.

The velocity model consists of a 2-layer subducting crust above the mantle, covered by a thin layer of sedimentary debris. The overriding plate has two, thicker sedimentary layers, as well as a 2-layer crust and an underlying mantle.

Our final, preferred model (Fig. 2) exhibits that the incoming Pacific plate is relatively rough, between 5-6

km thick with seismic P-wave velocities (V_p) between 5.2 and 6.9 km/s, covered by relatively little, in patches up to 100 m thick sediments. The seismic velocity of the mantle around 7.4 km/s is relatively slow. The roughness of the Pacific plate in addition to some isolated pockets of slower V_p in the crust and a generally low upper mantle V_p indicate that the incoming plate appear strongly affected by plate bending as discussed below.

The overriding Australian arc crust with 12 km thickness appears relatively thin, reaching depth of just over 14 km (Fig. 2). Its seismic velocities vary between 4.2 km/s in the shallow parts to up to 7.0 km/s in the lower crust. The sediments on top are, on average, about 1 km thick but form an up to 3 km deep and about 90 km wide forearc basin (Fig. 2). Sedimentary velocities lie between 1.6 and 3.8 km/s. The uppermost arc mantle V_p is 7.5-7.7 km/s, lower than typical arc mantle velocities, which normally lie around 7.8 km/s (Hyndman et al., XXX). Just at the deformation front there appears an approximately 40 km wide region of strongly reduced velocities of the forearc crust, immediately above the plate contact zone of both plates involved. The implications of these inferred structures are discussed below.

Figures 3a-e show data example and how well the model fits these data. The top panels of these figures show the data and the interpreted phases, the central panels show all predicted phases (including those not interpreted and measured) on top of the data, and the bottom panels show the corresponding ray path only to actual picked arrivals.

In order to judge, how accurate and well resolved the lithospheric structure are, Figures 4 and 5 show the data coverage and model resolution, respectively. Resolution values vary between 0.0 (small symbols) and 1.0 (large symbols) and indicate how well each model parameter is resolved with respect to the relative number of rays. Zelt and Smith (1992) found that a node with a resolution value greater 0.5 can be considered well resolved. Disregarding the data gap around the trench where the great water depth prevented the deployment of OBS/H, the model appears relatively well resolved

In addition, we have also varied manually the layer depths and velocities and compared the predicted arrivals with the data. This allows us to estimate actual model parameter uncertainties as follow: Depth to sediments: 70-150 m; depth to crust: 100-200 m, depth to mantle: 500-1000 m; velocity of sediments: 100-300 m/s; velocity of crust 80-400 m/s; velocity of mantle: +/- 150 m/s.

Discussion

Seismic anisotropy versus mantle hydration

Measuring relatively low V_p (< 8.0 km/s) in a mature (>25 Ma) upper mantle can potentially indicate either that V_p was measured along a slow orientation of aligned mantle olivine crystals due to mantle flow and

therefore be an effect of seismic anisotropy, or that the upper mantle is altered, fractured or hydrated and thus of low V_p . Interestingly for our case, V_p from both upper mantles, incoming and overriding plates, appear relatively low, and both may be explained by the same effects, mantle flow or hydration, and they appear even to be linked.

If the incoming Pacific upper mantle V_p of 7.4 km/s is due to seismic anisotropy, a perpendicular line would reveal a higher V_p . About 200 km further north, Contreras-Reyes et al. (submitted) provide such a result from across the Louisville Ridge. They measured upper mantle V_p of 8.1-8.3 km/s, where the faster velocities lie below a seamount with slightly higher uncertainty (0.15 km/s instead of 8.1 +/- 0.1 km/s) (Contreras-Reyes et al., submitted). Their result is measured perpendicular to the adjacent Osborn Trough, a former spreading centre, which would represent a reasonable mechanism to have caused the apparent seismic anisotropy (Hess, 1964). However, as we are unable to judge what the influence of the genesis of seamounts was on the upper mantle in the region where a hotspot caused the Louisville Ridge, it is difficult to analyse and prove seismic anisotropy along our profile to the south.

The alternative for the observed discrepancy between our low incoming upper mantle V_p and the faster one to the north could be the alteration of the mantle peridotite at our southern line. The bathymetry here suggests that strong, deep-seated fracturing and faulting is accompanying plate bending (Fig. 6), possibly generating large, tsunamogenic earthquakes. The opening of cracks allows water to penetrate into the mantle as suggested offshore Central America or Chile (e.g. Ranero et al., 2003; Ivandic et al., 2008), Chile (Contreras-Reyes et al., 2007; Contreras-Reyes et al., 2008a; Contreras-Reyes et al., 2008b; Scherwath et al., 2009), or Indonesia (Planert et al., submitted). According to Carlson and Miller (2003) only a few w(%) of water can significantly reduce V_p . However, without a reference value for undisturbed upper mantle V_p in this region, we are unable to estimate an actual amount of mantle hydration.

In the upper mantle of the forearc, relatively low V_p could also have the two causes. Low V_p here could be evidence for mantle flow whereby arc-parallel mantle flow causes realignment of olivine crystals, resulting in seismic anisotropy with the fast orientation in the flow direction (arc-parallel), and we actually sampled V_p along the slow orientation as suggest in central America by Hoernle et al. (2007). The second cause for low V_p would be alteration of the forearc mantle due to hydration and serpentinisation of the mantle olivine. Access water may be provided by the subducting plate, where free water would be carried past the subduction front.

If the incoming plate carries relatively little access water and the observed low V_p of the incoming mantle is due to seismic anisotropy, than the low V_p of the overriding mantle most likely represents seismic anisotropy, too. Upper mantle anisotropy in one plate would therefore likely infer upper mantle anisotropy to be present in the other plate.

There are, however, several reasons that agree more with the concept of the shallow frontal forearc mantle being hydrated and serpentinised. Serpentine has a lower density than peridotite (REF). Serpentinisation should therefore lower the mantle density which can result in uplift. The undulation of the Moho here (Fig. 2) suggests that such an uplift in this region is possible. Bostock et al. (2002) went as far as suggesting that all mantle wedges would be serpentinised. Access free water is usually provided by downgoing sediments, or in places of absent sediments, the fluids in a competent and impervious crust are restricted to a fault-fracture mesh at the crust's periphery (Reyners et al., 2007; Nature) and can enter the mantle whose storage capacity of free water is less than 0.2 wt% (Obtani, E., 2005). Bound water is carried in the oceanic basalt and serpentine as discussed above.

On the other hand, if we would outrule that mantle hydration would be the cause of the low upper mantle Vp in the forearc, and should consider seismic anisotropy to explain our measured Vp, the subduction zone setting would need to be as unusual as in Central America (Hoernle et al., 2007). As mantle corner flow is usually arc-perpendicular, caused by the drag of the down-going plate, and hence would results in a seismic anisotropy contrary to what would be inferred by our measurement (REF).

Consequences of a hydrated mantle wedge

Bostock et al. (2002) speculate that all mantle wedges would be serpentinized. Mantle hydration is typically indicated by low arc mantle velocities that lie around 7.8 km/s (Hyndman et al., 1997). Therefore, our results appear typical for mantle wedges. An example where 2-4 km of unconsolidated material, including 2 km of sediments, on the incoming plate appear not to have an alteration effect on the overriding mantle wedge is the northern Hikurangi subduction zone (Scherwath et al., submitted). The upper mantle velocity of the frontal mantle wedge is above 8.0 km/s, and Scherwath et al. (submitted) speculate that massive underplating prevents the subduction of sediments and hence free access water. Such a scenario appears unlikely to occur at the profile presented in this paper as the frontal subduction wedge is of relatively high Vp, and neither accretion nor underplating can be inferred.

A hydrated mantle wedge would inhibit subduction zone thrust earthquakes to rupture below the Moho interception (Tichelaar and Ruff, 1993), and this holds true where thrust earthquakes follow this pattern (Bostock et al., 2002). However, a recently modeled earthquake rupture in the Kermadec margin near our profile (http://earthquake.usgs.gov/eqcenter/eqinthenews/2008/us2008xna6/finite_fault.php) suggests that deeper mega-thrust events are possible, contrary to the aforementioned Moho depth limit of mega-thrust events (Bostock et al., 2002; Tichelaar and Ruff, 1993). This would have significant consequence for hazard estimates for this margin. If the reduced Vp we observe in the uppermost mantle is a consequence of hydration of this shallow mantle wedge, and we expect normal hydration at greater depth due to water-releasing eclogitisation from subducting heated basalt (Peacock, 1993), there may be room to speculate that there exists a zone of "normal" mantle between hydrated mantle where subduction thrust can earthquakes

occur. Our data, however, are not suited to resolve such deep velocity variations which could possibly be provided by high resolution earthquake tomography where deep earthquakes in sufficient abundance are observed. The acquisition of these seismological data could, in addition, also be used to detect earthquake swarms as an indicator for fluids (Reyners et al., 2007; Tilmann et al., 2008).

What is difficult to estimate is the migration of free water up the subduction shear. Deep subduction earthquakes could also indicate that only little fluid migration up the subduction shear occurs.

Conclusion

The central Tonga-Kermadec subduction zone structures are determined by seismic wide-angle data near the active arc volcano Raoul Island at 29 degrees South. The subducting Pacific plate is around 5-6 km thick with seismic P-wave velocities (V_p) of 5.2-6.9 km/s, and exhibits isolated pockets of lowered V_p . Sedimentary cover only exists in patches up to 100 m thick. The underlying Pacific mantle shows V_p of 7.4 km/s. The relatively low seismic velocities in Pacific crust and mantle indicate a considerable alteration of the rough and broken incoming plate which is thus likely to transport a significant amount of access water into the subduction zone. The Australian arc crust is about 12 km thick with a V_p of 4.2-7.0 km/s and a 40 km wide low velocity region directly above the contact area with the subducting crust. The sediments on the arc crust are on average about 1 km thick and form an up to 3 km thick and 90 km wide forearc basin. The mantle wedge as a V_p of 7.5-7.7 km/s which is lower than typical arc mantle. We interpret these low V_p to be a result of serpentinisation caused by the large amount incoming water released directly at the frontal mantle wedge. Our results demonstrate the possibility of deep pathways for free water through subduction zones.

Acknowledgments

We thank Captain Mallon and the officers and crew of R/V Sonne for a smooth and efficient acquisition of the seismic wide-angle data during cruise SO192a; the German Ministry for Education and Research (BMBF), the New Zealand Foundation for Research Science and Technology (FRST), the New Zealand Ministry for Economic Development (MED) for funding various aspects of the data acquisition and the research. Most figures were made with GMT (Wessel and Smith, 1998).

References

Bostock M. G., R. D. Hyndman, S. Rondenay, and S. M. Peacock (2002), An inverted continental Moho and serpentinization of the forearc mantle, *Nature*, 417, 536-538.

Bradshaw, J.D., 1989. Cretaceous geotectonic patterns in the New Zealand region, *Tectonics*, 8, 803-820.

Carlson R. L., and D. J. Miller, 2003, Mantle wedge water contents estimated from seismic velocities in partially serpentinized peridotites, *Geophys. Res. Lett.*, 30(5), 1250, doi:10.1029/2002GL016600.

Collot, J.-Y., and B. Davy (1998), Forearc structures and tectonic regimes at the oblique subduction zone between the Hikurangi Plateau and the southern Kermadec margin, *J. Geophys. Res.*, 103(B1), 623-650.

Contreras-Reyes, E., Grevemeyer, I., Flueh, E.R., Scherwath, M. & Heesemann, M., 2007. Alteration of oceanic subducting lithosphere at the southern central Chile trench-outer rise, *Geochem. Geophys. Geosyst.*, 8, Q07003, doi:10.1029/2007GC001632.

Contreras-Reyes, E., Grevemeyer, I., Flueh, E.R., Scherwath, M. & Bialas, J., 2008a. Effect of trench-outer rise bending-related faulting on seismic Poisson's ratio and mantle anisotropy: a case study offshore of Southern Central Chile. *Geophys. J. Int.*, 173(1): 142-156, doi:10.1111/j.1365-246X.2008.03716.x.

Contreras-Reyes, E., Grevemeyer, I., Flueh, E.R. & Reichert, C., 2008b. Upper lithospheric structure of the subduction zone offshore of southern Arauco Peninsula, Chile at ~38° S, *J. Geophys. Res.*, 113, B07303, doi: 10.1029/2007JB005569.

Contreras-Reyes et al., submitted.

de Ronde, C., E. Baker, G. Massoth, J. Lupton, I. Wright, R. Sparks, S. Bannister, M. Reyners, S. Walker, R. Greene, J. Ishibashi, K. Faure, J. Resing, and G. Lebon (2007), Submarine hydrothermal activity along the mid-Kermadec Arc, New Zealand: Large scale effects on venting, *Geochem. Geophys. Geosyst.*, 8, Q07007, doi:891 10.1029/2006GC001495.

DeMets, C., R. G. Gordon, D. F. Argus, and S. Stein (1994), Effect of recent revisions to the geomagnetic time scale on estimates of current plate motions, *Geophys. Res. Lett.*, 21, 2191-2194.

Downey N.J., Stock J.M., Clayton R.W., 2007. History of the Cretaceous Osbourn spreading center, *J. Geophys. Res.*, 112(B4), B04102, doi:10.1029/2006JB004550.

Flueh, E. R., and H. Kopp (2007), FS Sonne Fahrtbericht/Cruise Report SO192 MANGO: Marine Geoscientific Investigations on the Input and Output of the Kermadec Subduction Zone, IFM-GEOMAR Report No. 11, pp. 127.

Grevemeyer, I., Weigel, W. & Jennrich, C., 1998. Structure and ageing of oceanic crust at 14°S on the East Pacific Rise, *Geophys. J. Int.*, 135, 573-584.

Grevenmeyer, I., Kaul, N., Villinger, H. & Weigel W., 1999. Hydrothermal activity and the evolution of the seismic properties of upper oceanic crust, *J. Geophys. Res.*, 104(B3), 5069-5080.

Hess, H.H., 1964. Seismic anisotropy of the upper mantle under oceans, *Nature*, 23, 629-631.

Hyndman R.D. & Wang K., 1993. Thermal constraints on the zone of major thrust earthquake failure - the Cascadia subduction zone, *J. Geophys. Res.*, 98(B2), 2039-2060.

Ivandic, M., Grevenmeyer, I., Berhorst, A., Flueh, E.R. & McIntosh, K., 2008. Impact of bending related faulting on the seismic properties of the incoming oceanic plate offshore of Nicaragua, *J. Geophys. Res.*, 113, B05410, doi:10.1029/2007JB005291.

Lloyd, E.F. and Nathan, S., 1981. Geology and tephrochronology of Raoul Island, Kermadec Group, New Zealand, *N. Z. Geol. Survey Bull.*, 95, 115pp. Wellington, N.Z.

Obtani, E., 2005. Water in the Mantle; *Elements* 1, 25-30.

Peacock, S.M., 1990. Fluid processes in subduction zones. *Science* 248, 329-337.

Peacock, 1993. Large-scale hydration of the lithosphere above subducting slabs, *Chemical Geology*, 108, 49-59.

Ranero, C.R., Morgan, J. Phipps, McIntosh, K. & Reichert, C., 2003. Bending, faulting, and mantle serpentinization at the Middle America trench, *Nature*, 425, 367-373.

Reyners et al., 2007; *Nature*

Scherwath et al., submitted.

Sutherland, R., 1995. The Australia-Pacific boundary and Cenozoic plate motions in the SW Pacific - some constraints from Geosat data, *Tectonics*, 14(4), 819-831.

Wessel, P., and W. H. S. Smith, 1998. New version of generic mapping tools released, *Eos Trans. AGU*, 79, 579.

Zelt, C.A., 1999. Modelling strategies and model assessment for wide-angle seismic traveltime data, *Geophys. J. Int.*, 139, 183-204.

Zelt, C.A. & Smith, R.B., 1992. Seismic traveltime inversion for 2-D crustal velocity structure, *Geophys. J. Int.*, 108, 16-34.

Figures

Figure 1: Basemap (a) of the Tonga-Kermadec subduction zone, (b) the working area with its tectonic features, plate motion indicated as black arrows relative to the Australian plate (after DeMets et al., 1994), and (c) the seismic line Mango-4, the red line representing the shots and the white circles the ocean bottom receivers.

Figure 2: Final proposed velocity model derived from ray-tracing of seismic wide-angle data.. Velocity contours are in km/s.

Figure 3a-e: Data examples of five representative receiver gathers along the profile. Top panels show uninterpreted data highlighting the interpreted phases, the middle panels show all predicted P-wave arrivals drawn on top of the seismic data, and the bottom panels show only those rays for the picked arrivals used to determine the model.

Figure 4: Ray coverage of all rays from all stations determining the final model.

Figure 5: Model resolution, with depth nodes (squares) and velocity nodes (circles) drawn to scale indicating node resolution; values larger than 0.5 are considered well resolved.

Figure 6: Sketch of interpretation, indicating deep hydration pathways through the incoming plate into the arc crust and frontal shallow mantle wedge.

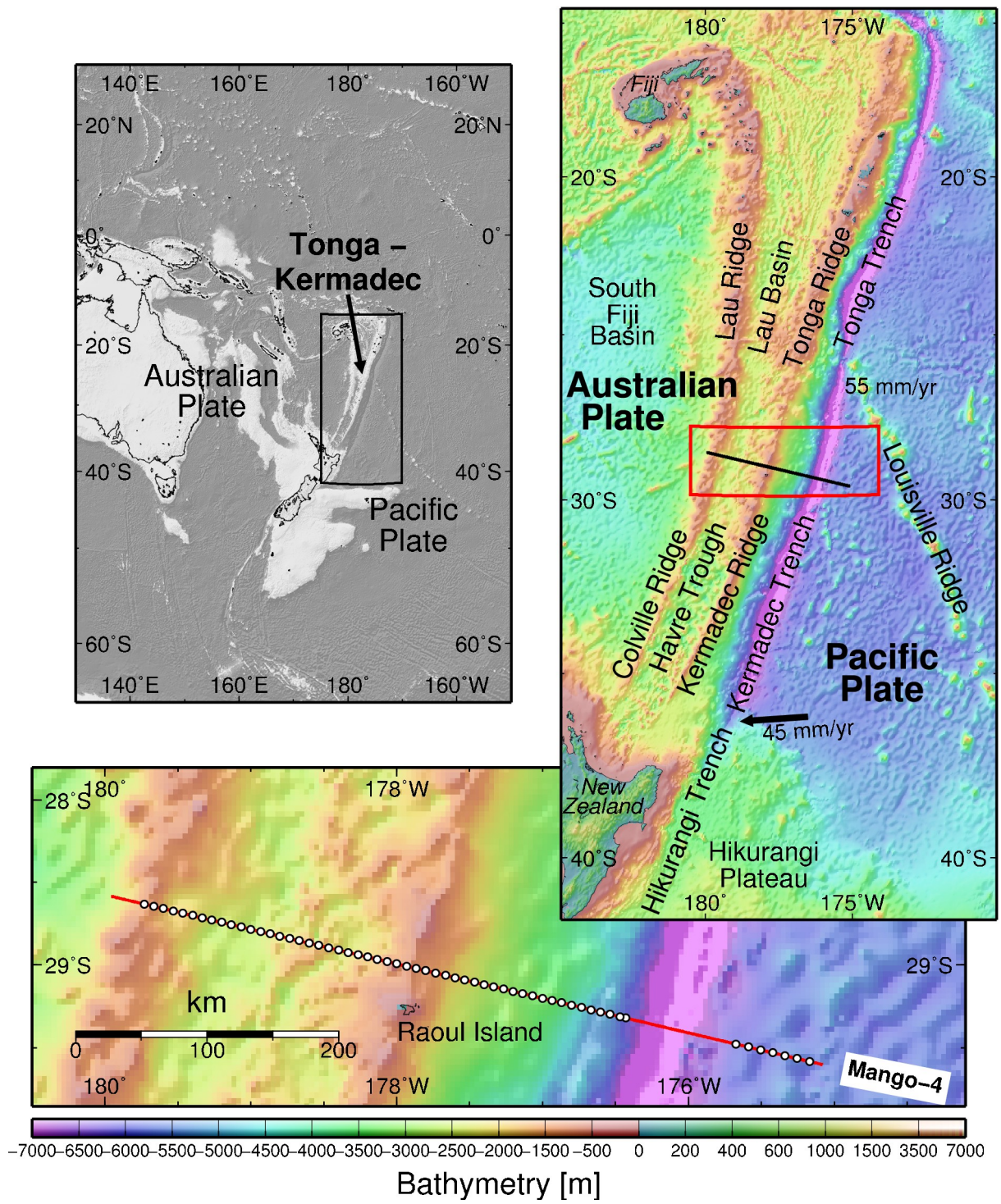


Figure 1.

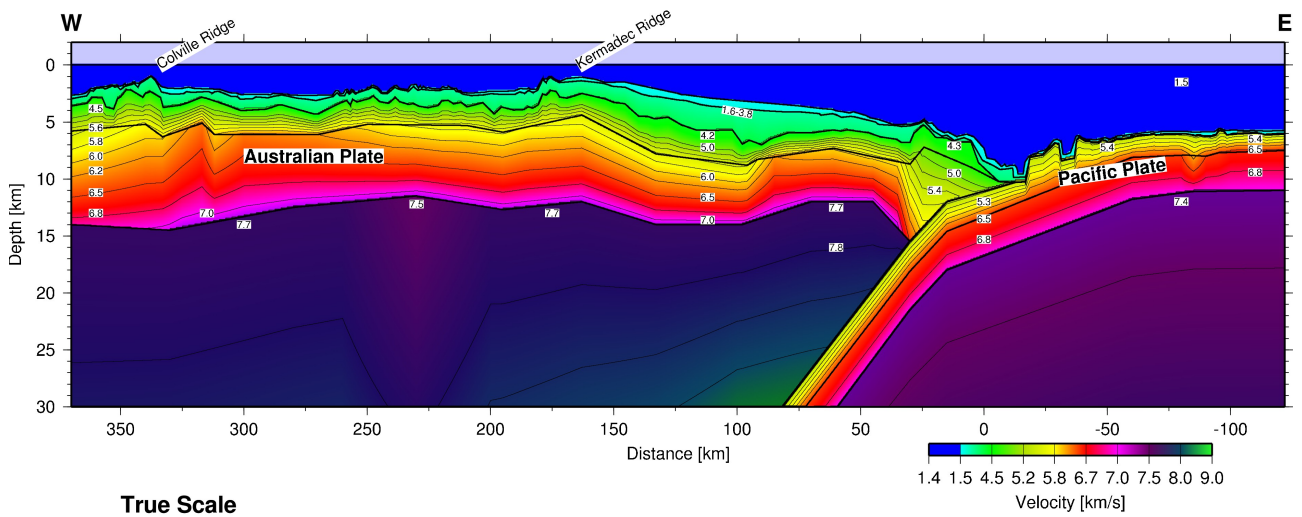


Figure 2.

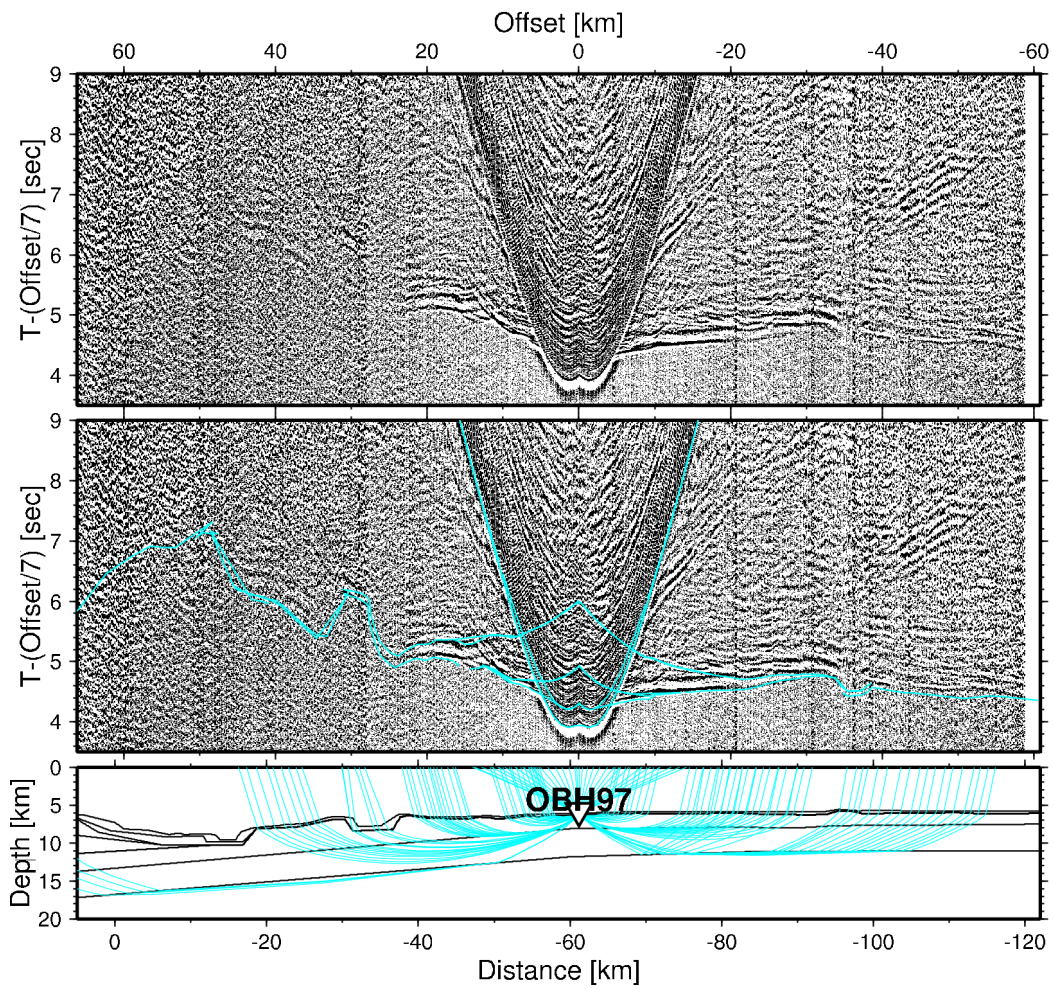


Figure 3a.

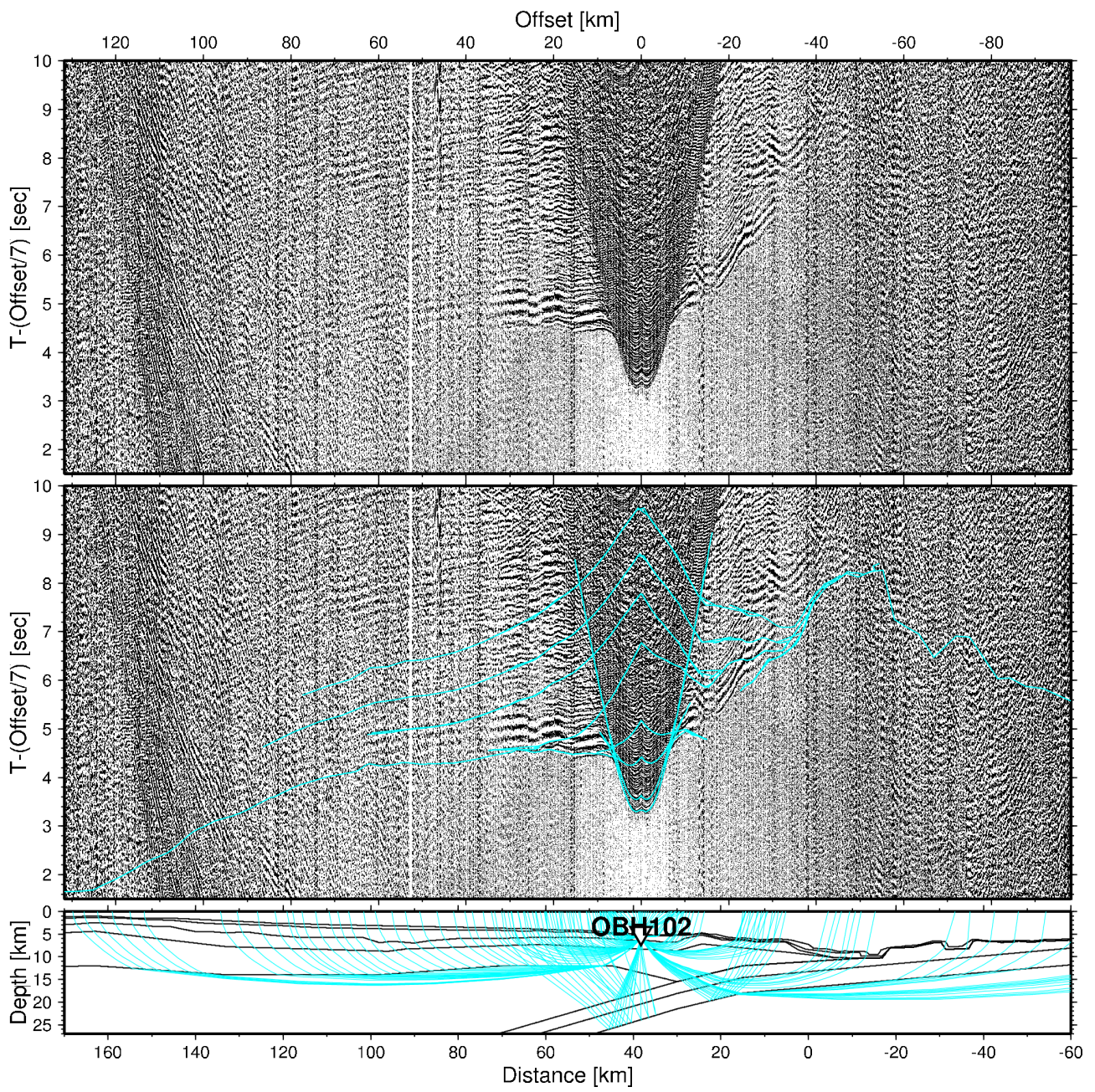


Figure 3b.

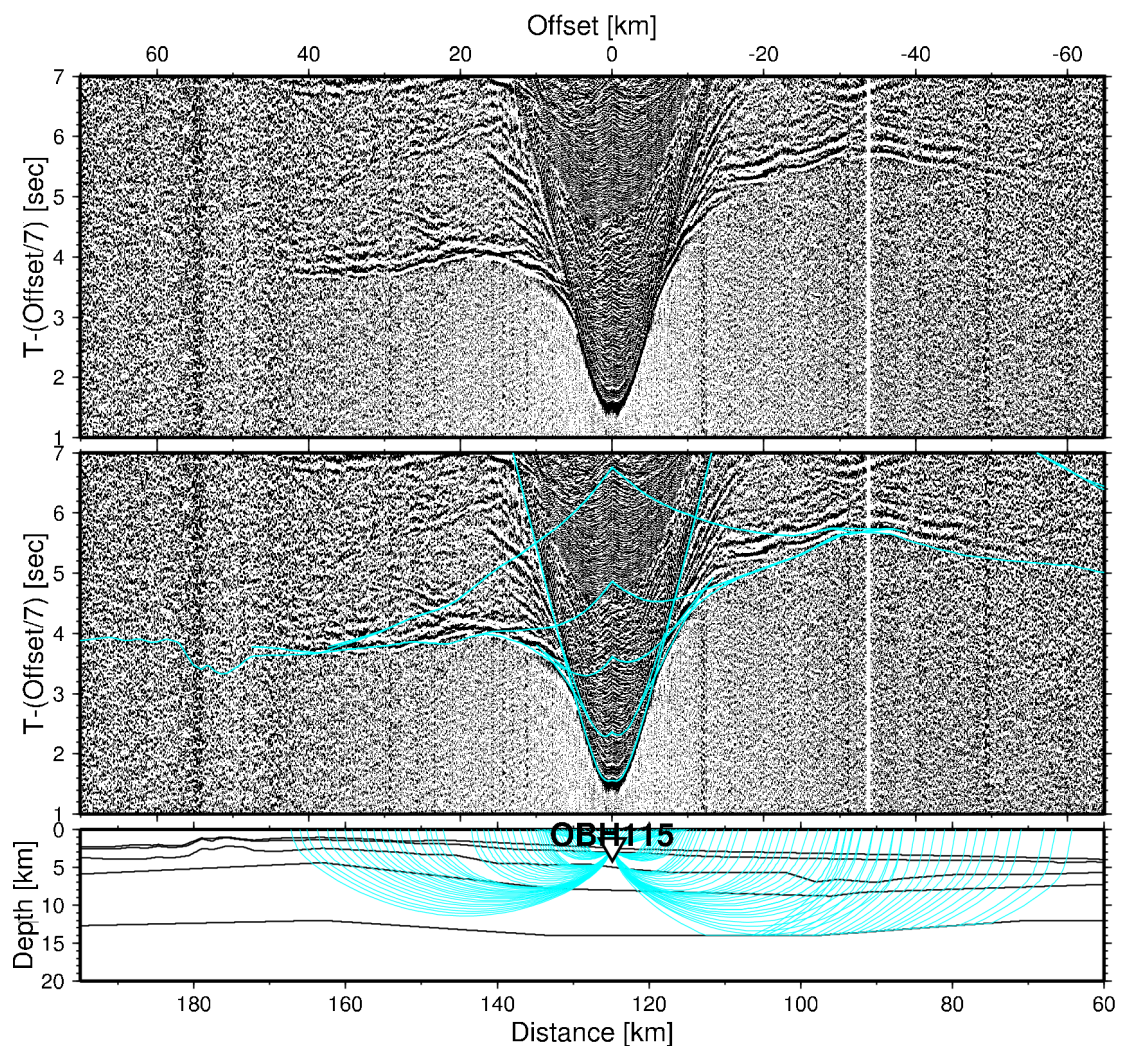


Figure 3c.

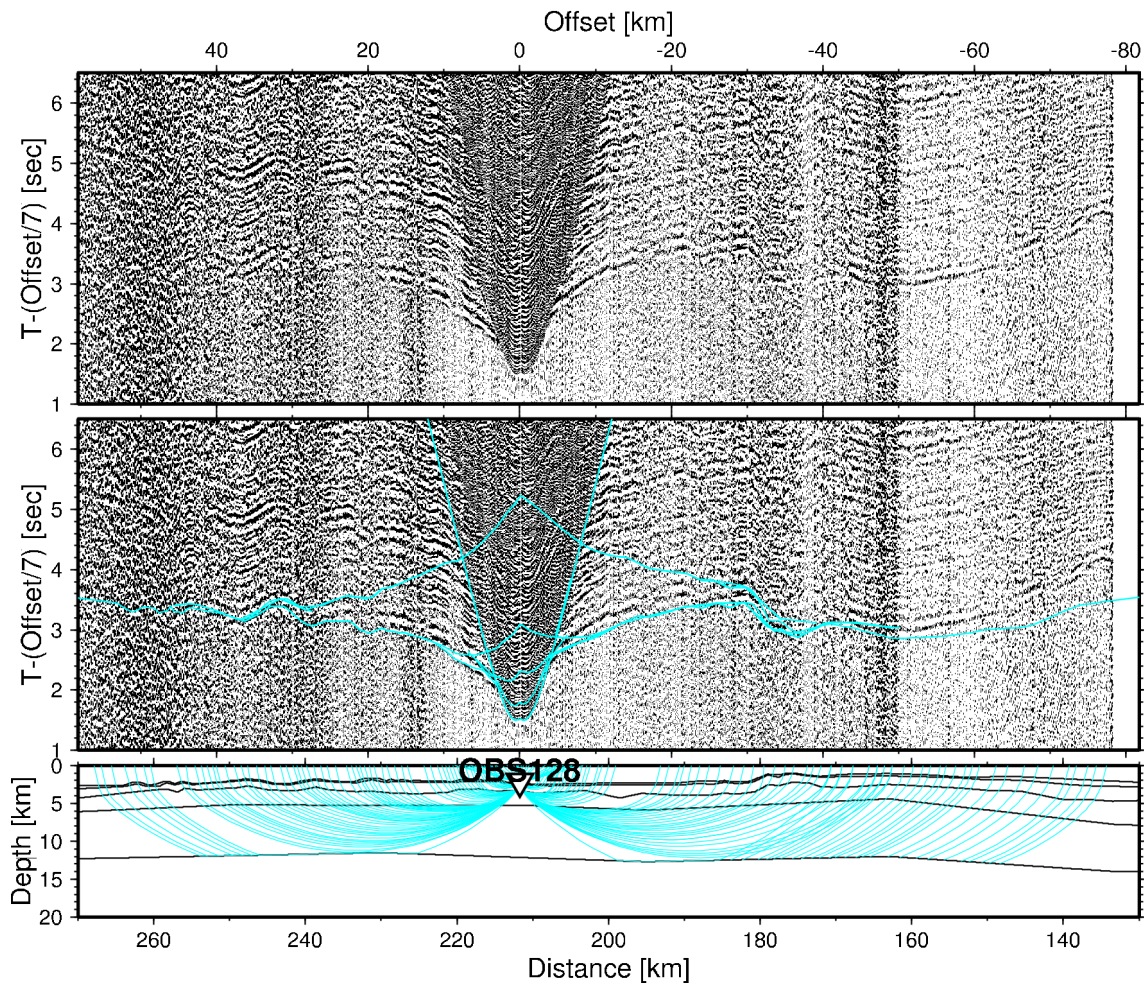


Figure 3d.

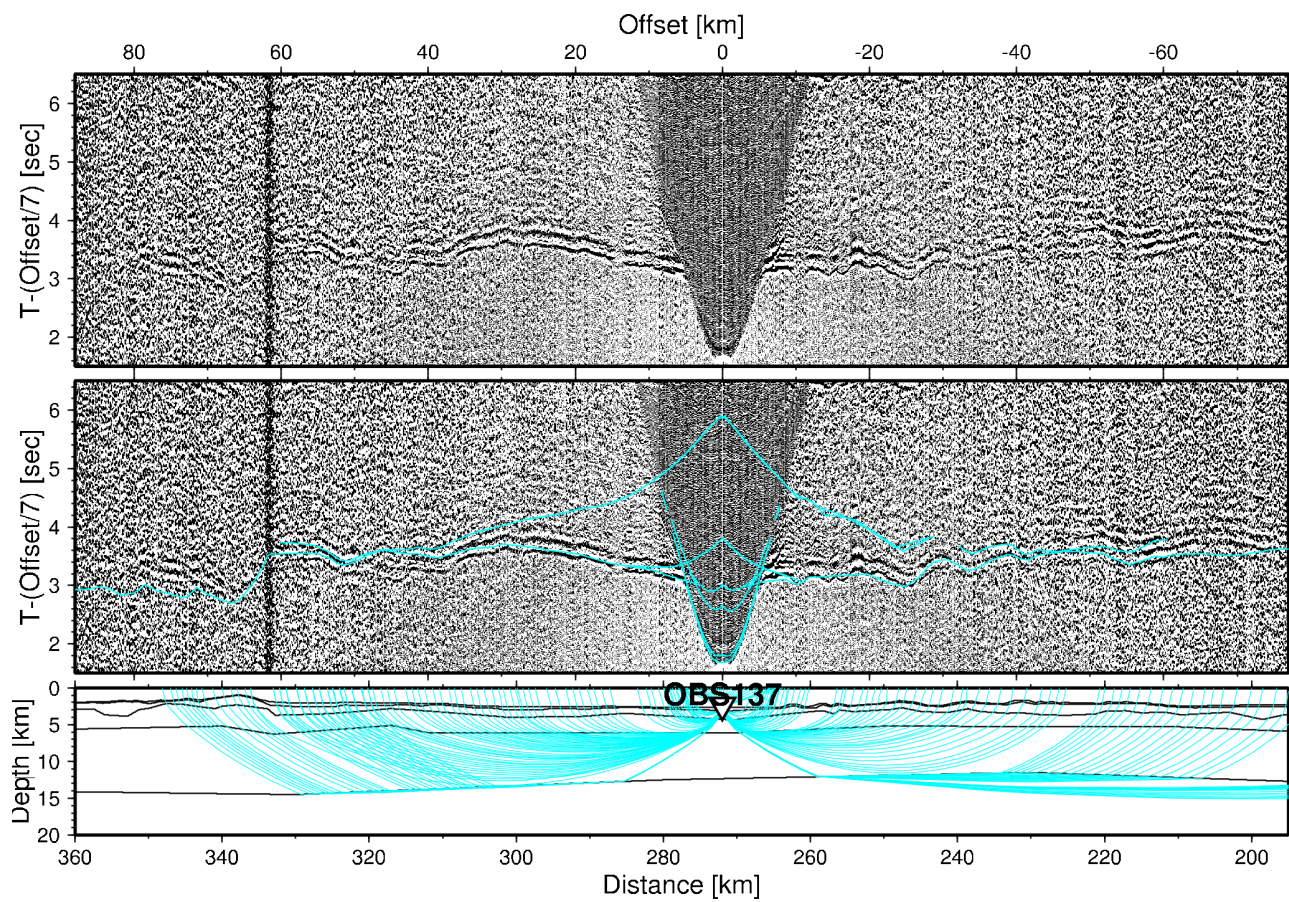


Figure 3e.

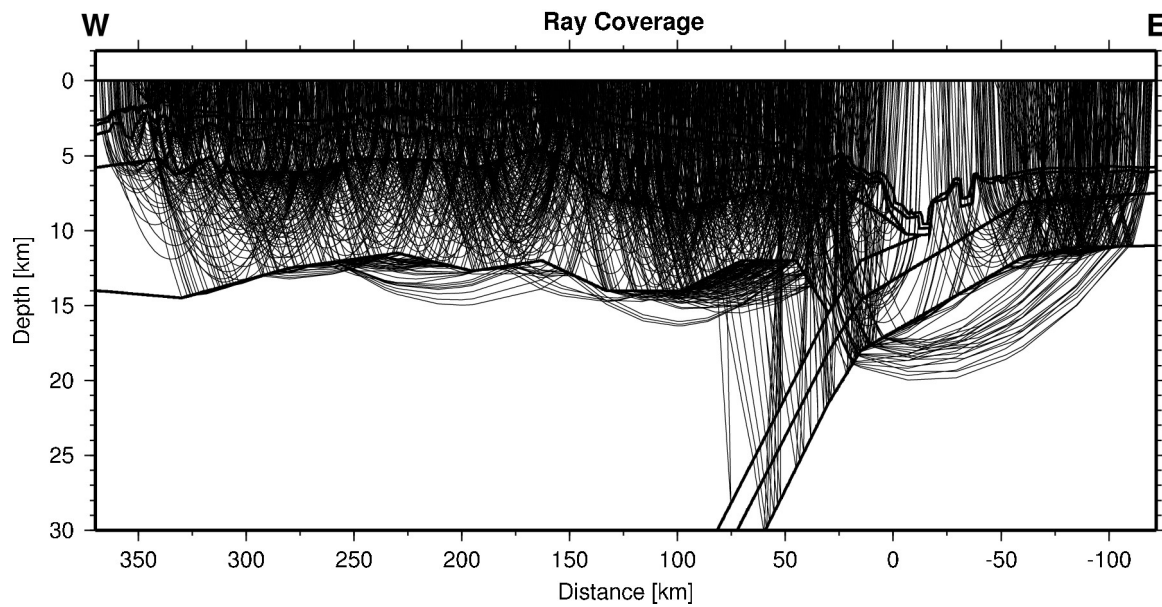


Figure 4.

Model Resolution in Crust and Mantle

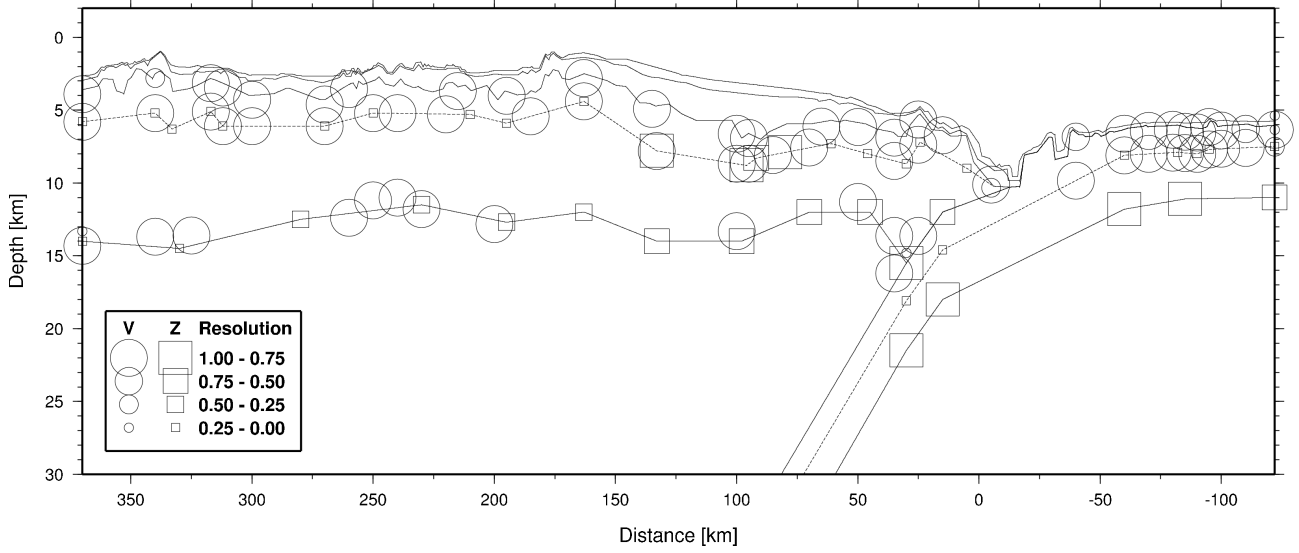


Figure 5.

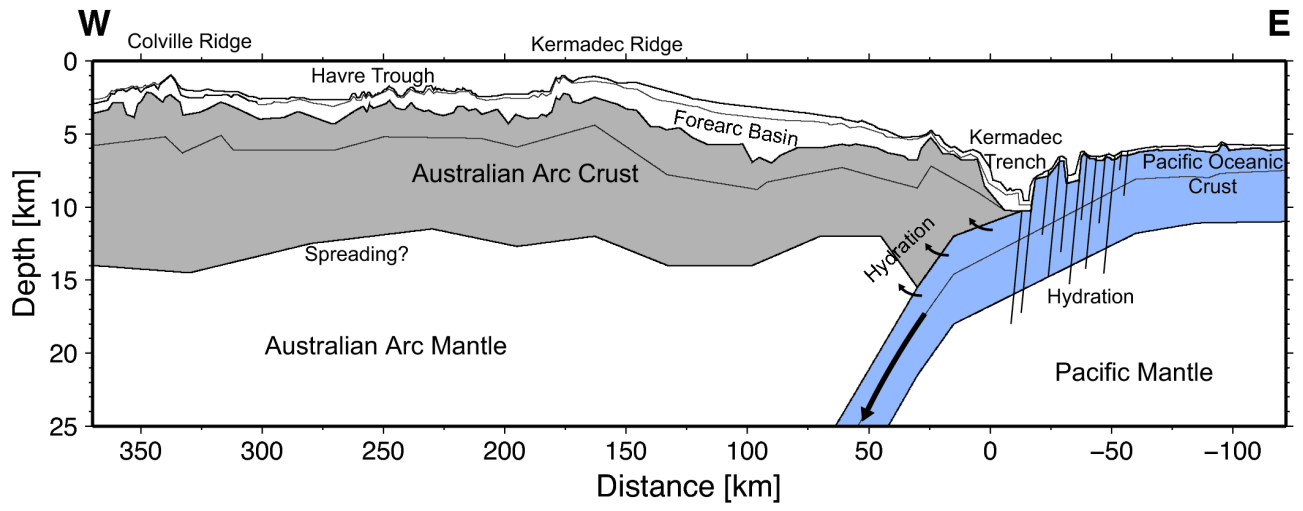


Figure 6.

Struktur der Hikurangi-Kermadec Subduktionszone vor Neuseeland

- Ergebnisse von der MANGO Ausfahrt SO-192-1

Scherwath, M.¹, Kopp, H.¹, Flüh, E.R.¹, Henrys, S.A.², Sutherland, R.²

¹ Leibniz Institute of Marine Sciences, IFM-GEOMAR, Wischhofstr. 1-3, 24148 Kiel, Germany. E-Mail: mscherwath@ifm-geomar.de

² GNS Science, 1 Fairway Drive, Avalon, PO Box 30-368, Lower Hutt, New Zealand.

Einleitung und Ziele

Im März/April 2007 fand die Ausfahrt SO-192-1 des Projektes MANGO (Marine Geoscientific Investigations on the Input and Output of the Kermadec Subduction Zone) im Gebiet nördlich der Nordinsel von Neuseeland statt, zwischen 28° und 38° Süd (Abb. 1). Hier befindet sich das Hikurangi-Kermadec Subduktionssystem, wo sich die pazifische Platte unter die australische Lithosphäre schiebt. Ziel der Ausfahrt war es, geophysikalische Daten zu sammeln, die die lithosphärischen Strukturen dieser Subduktionszone auflösen. Hierzu wurden in erster Linie seismische Weitwinkeldaten gesammelt, die tief in die Kruste und den oberen Mantel der beiden tektonischen Platten eindringen, um die genaue Plattengeometrie zu entschlüsseln. Zusätzlich wurde ein kurzer seismischer Mehrkanal-Streamer geschleppt, um die flachen Sedimentstrukturen aufzulösen. Ferner wurden magnetische Daten zur Altersbestimmung der ozeanischen Platte bzw. zum Erfassen von magnetischen Anomalien subduzierender Seamounts gesammelt. Abgerundet wurde die Datenakquisition durch Fächerecholotdaten, die ein genaues Abbild der Meeresbodenmorphologie liefern. Die Projektziele umfassen die Aufschlüsselung der Subduktionsstrukturen sowie die Übergänge zwischen den verschiedenen Subduktionssystemen (Hikurangi Plateau im Süden, "normale" ozeanische Kruste im Norden). Die Zusammenhänge zwischen den tektonischen Strukturen sowie der nach Norden hin zunehmenden Seismizität und den Stratovulkanen spiegeln sich im Materialtransfer (Input und Output) wieder (Flüh und Kopp, 2007).

Seismische Daten

Seismische Weitwinkeldaten wurden entlang von vier Profilen senkrecht zum Tiefseegraben erhoben (Abb. 1). Insgesamt wurden 147 Stationen entlang dieser Profile mit Ozeanbodenseismometern und -hydrophonen (OBS/H) erfolgreich

abgedeckt. Als seismische Quelle diente ein 64 I Airguncluster. Die Datenqualität der seismischen Stationen ist insgesamt gut; nur die OBS/H-Signale auf dem Hikurangi Plateau und dem East Cape Ridge gehen kaum weiter als 40 km Offset. Ein Vergleich mit anderen seismischen Daten aus diesem Bereich zeigt jedoch, dass hier

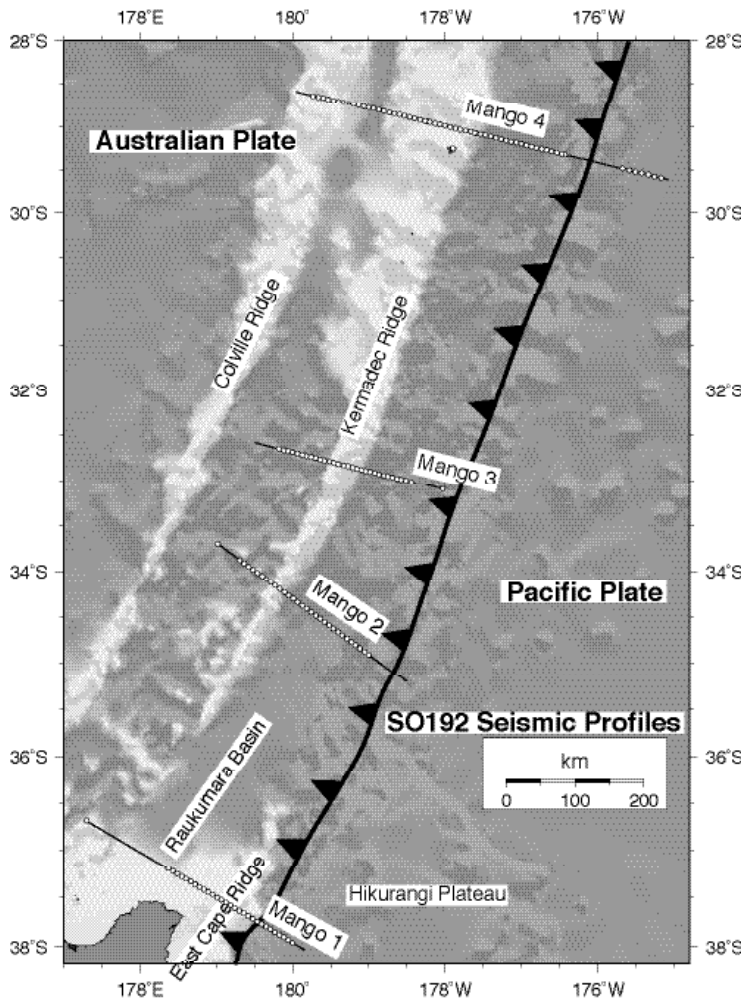


Abb. 1: Übersichtskarte des Arbeitsgebietes MANGO

allgemein eine hohe Signaldämpfung vorhanden ist, was auf eine hohe interne Deformation dieser Strukturen hindeutet. Die Stationen des dahinter liegenden Raukumara Fore-Arc Beckens zeichneten hingegen klare Signale auf, mit Arc-Mantel-Phasen bis über 70 km Offset. Die nördlichen Profile sind von deutlich besserer Qualität, mit klaren Signalen häufig über 80 km bis hin zu einem Maximum von 200 km Offset.

Ergebnisse

Das südliche Profil Mango-1 um 37°S erfasst das Hikurangi Plateau, das East Cape Ridge und das Raukumara Fore-Arc Becken (Abb. 2). Das Hikurangi Plateau besteht unter den Sedimenten aus einer Schicht Volcanoclastics/Limestone/Chert (Davy et al., 2008) über Plateau-Kruste. Die Mächtigkeit des Plateaus wurde mit

Gravimetriemodellierung abgeleitet, da keine Mantelphasen gemessen wurden. Jenseits des Tiefseegrabens scheint Crustal Underplating für die Erhebung des East Cape Ridges verantwortlich zu sein. Hier verdickt sich das reinkommende Plateau unterhalb der Fore-Arc-Hochs. Anomal hohe seismische Geschwindigkeiten unterhalb des East Cape Ridge zusammen mit einer starken magnetischen Anomalie

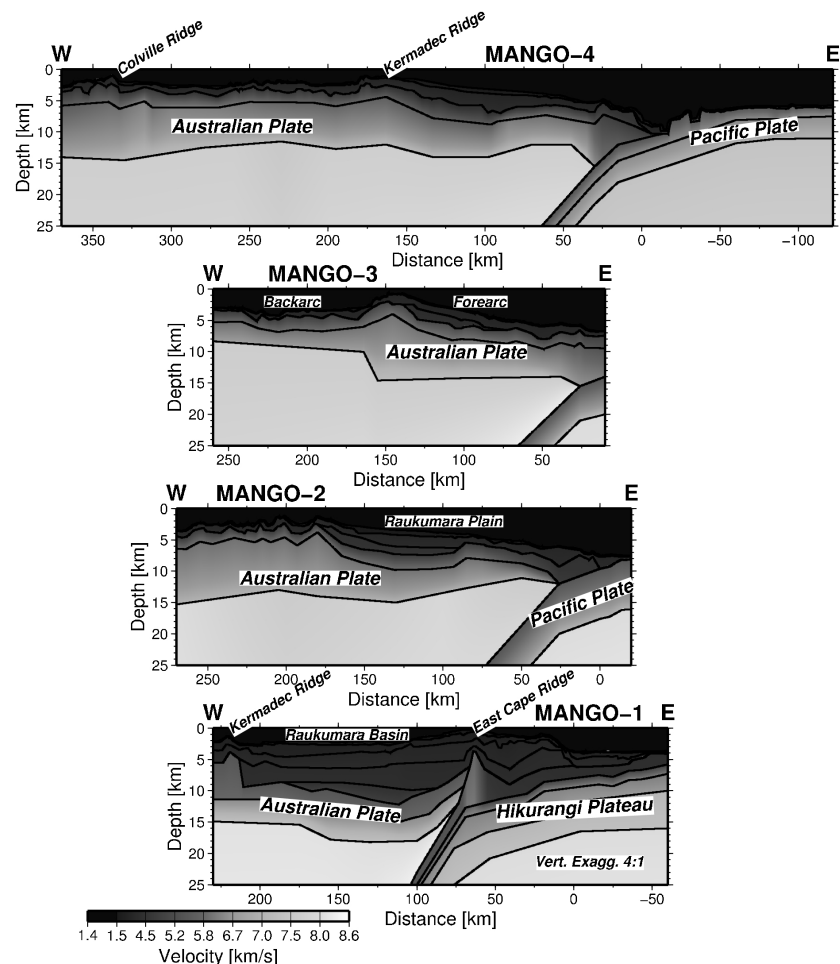


Abb. 2: Strukturmodelle entlang der vier MANGO Profile.

deuten entweder auf einen subduzierten Seamount oder auf sogenannte Allochthon Basaltic Volcanics hin, wie sie auch 60 km weiter südwestlich an Land gefunden werden. Seismische Reflexionsdaten vom Raukumara Becken zeigen hochaufgelöste Sedimentstrukuren, die wahrscheinlich bis zu einer Zeit von vor 85 Millionen Jahren zurück gehen, als hier schon einmal Subduktion unter Gondwana stattfand (Davey et al., 1997, Sutherland et al., 2008).

Knapp 400 bzw. 600 km weiter nördlich befinden sich Mango-2 und Mango-3 (Abb. 2). Diese beiden mittleren Profile decken den australischen Arc zu beiden Seiten des Kermadec Ridge ab. Trotz der relativen Nähe der beiden Profile zeigen

unsere Ergebnisse Unterschiede auf. Im Back-Arc-Bereich ist die Kruste am nördlichen Mango-3 Profil deutlich verdünnt, was auf eine durch Rifting gestreckte Kruste schließen lässt. Auch die Wassertiefen sind größer als bei Mango-2, wo auch die Back-Arc-Kruste deutlich mächtiger ist. Dieser südlichere Teil weist auch erniedrigte seismische Geschwindigkeiten im oberen Mantel auf (7.6 km/s statt 7.9 km/s wie im Fore-Arc-Bereich), was eventuell auf thermische Streckung hinweist, die mit einer Veränderung des Arc-Vulkanismus einhergeht (de Ronde et al., 2006).

Das nördlichste und längste Profil Mango-4 (Abb. 2) befindet sich auf Höhe des aktiven Vulkan Raoul Island bei 29°S. Charakteristisch für dieses Profil sind relativ deutlich reduzierte seismischen Geschwindigkeiten sowohl im pazifischen als auch im australischen Mantel. Die pazifische Mantelanomalie ist vielleicht ein kombinierter Effekt von seismischer Anisotropie und Plattenbiegungseffekten. Der Arc-Mantel hingegen ist vermutlich thermisch beeinflusst, ähnlich wie bei Mango-2.

Danksagung

Wir bedanken uns bei Kapitän Mallon, den Offizieren und der Crew der FS Sonne für die reibungslose Datenakquisition.

Davey, F.J., Henrys, S.A. und Lodolo, E., 1997. A seismic crustal section across the East Cape convergent margin, New Zealand.: Tectonophysics, v. 269, p. 199-215.

Davy, B., Hoernle, K. und Werner, R., 2008. Hikurangi Plateau: Crustal structure, rifted formation, and Gondwana subduction history, Geochem. Geophys. Geosyst., 9, Q07004, doi:10.1029/2007GC001855.

De Ronde, C.E.J., Baker, E.T., Massoth, G.J., Lupton, J.E., Wright, I.C., Sparks, R.J., Bannister, S.C., Reyners, M.E., Walker, S.L., Green, R.R., Ishibashi, J., Faure, K., Resins, J.A. und Lebon, G.T., 2007. Submarine hydrothermal activity along the mid-Kermadec Arc, New Zealand: Large-scale effects on venting, Geochem. Geophys. Geosyst., 8, Q07007, doi:10.1029/2006GC001495.

Flüh, E.R. und Kopp, H., 2007. FS Sonne Fahrtbericht / Cruise Report SO192-1 MANGO, IFM-GEOMAR Report 11, pp. 118.

Sutherland, R., Stagpoole, V., Uruski, C., Henrys, S., Field, B., Toulmin, S., Barker, D., Bannister, S., Davey, F., Kennedy, C., Basset, D., Stern, T., Scherwath, M., Flueh, E., Kopp, H., submitted to Tectonics in 2008. Reactivation of forearc tectonics, crustal underplating, and uplift after 60 Myr of passive subsidence: Raukumara Basin, Hikurangi-Kermadec plate boundary, northeastern New Zealand.